Combined measurements of Higgs boson production and decay using up to 80 fb⁻¹ of proton-proton collision data at $\sqrt{s} = 13$ TeV collected with the ATLAS experiment

G. Aad *et al.*[*]

(ATLAS Collaboration)

Combined measurements of Higgs boson production cross sections and branching fractions are presented. The combination is based on the analyses of the Higgs boson decay modes $H \to \gamma\gamma$, ZZ^*, WW^*, $\tau\tau$, $b\bar{b}$, $\mu\mu$, searches for decays into invisible final states, and on measurements of off-shell Higgs boson production. Up to 79.8 fb⁻¹ of proton–proton collision data collected at $\sqrt{s} = 13$ TeV with the ATLAS detector are used. Results are presented for the gluon–gluon fusion and vector-boson fusion processes, and for associated production with vector bosons or top-quarks. The global signal strength is determined to be $\mu = 1.11^{+0.09}_{-0.08}$. The combined measurement yields an observed (expected) significance for the vector-boson fusion production process of 6.5σ (5.3σ). Measurements in kinematic regions defined within the simplified template cross section framework are also shown. The results are interpreted in terms of modifiers applied to the Standard Model couplings of the Higgs boson to other particles, and are used to set exclusion limits on parameters in two-Higgs-doublet models and in the simplified minimal supersymmetric Standard Model. No significant deviations from Standard Model predictions are observed.

I. INTRODUCTION

Following the discovery of the Higgs boson H [1–6] by the ATLAS [7] and CMS [8] experiments, its properties have been probed using proton–proton (pp) collision data produced by the Large Hadron Collider (LHC) at CERN. The coupling properties of the Higgs boson to other Standard Model (SM) particles, such as its production cross sections in pp collisions and decay branching fractions, can be precisely computed within the SM, given the value of the Higgs boson mass. Measurements of these properties can therefore provide stringent tests of the validity of the SM.

Higgs boson production and decay rates have been determined using the Run 1 dataset collected in the years 2011 and 2012, through the combination of ATLAS and CMS measurements [9]. More recently, these measurements have been extended using the Run 2 dataset recorded by the ATLAS detector in 2015, 2016 and 2017, using up to 79.8 fb⁻¹ of pp collision data produced by the LHC. The analyses target several production and decay modes, including: the $H \to \gamma\gamma$ and $H \to ZZ^* \to 4\ell$[1] decay channels

following the same methodologies as those presented in Ref. [10] and Ref. [11] respectively, with improved selections for Higgs boson production in association with a top–antitop pair, described in Ref. [12]; the $H \to WW^*$ [13] and $H \to \tau\tau$ [14] decay channels; $H \to b\bar{b}$ in associated production with a weak vector boson $V = W$ or Z (VH) [15,16] and in the weak vector-boson fusion (VBF) production process [17]; associated production with a top–antitop pair ($t\bar{t}H$) [12,18,19]; the $H \to \mu\mu$ decay channel following the same methodology as presented in Ref. [20], applied to the larger 2015–2017 input dataset; Higgs decays into invisible final states [21–24]; and off-shell production of Higgs bosons [25]. This paper presents measurements of Higgs boson properties at $\sqrt{s} = 13$ TeV obtained from the combination of these results, using techniques similar to those in Ref. [9]. A Higgs boson mass value of $m_H = 125.09$ GeV, corresponding to the central value of the combination of ATLAS and CMS measurements in Run 1 [26], is used for SM predictions. The uncertainty in the measured Higgs boson mass is considered in the $H \to \gamma\gamma$ and $H \to ZZ^* \to 4\ell$ analyses. Similar measurements [27–33], as well as their combination [34], have been reported by the CMS Collaboration.

All the input analyses except those for the $H \to \mu\mu$ and the VBF, $H \to b\bar{b}$ processes use a parametrization of the Higgs boson signal yields based on the Stage 1 simplified template cross section (STXS) framework [35,36] described in Sec. VI A. These cross sections are

---

[*]Full author list given at the end of the article.
[1]Throughout the paper ℓ denotes the light leptons e and μ.

TABLE I.   Dataset and integrated luminosity ($\mathcal{L}$) used for each input analysis to the combination. The last column provides the references for published analyses. The references in parentheses indicate analyses similar to the ones used in the combination but using a smaller dataset, in the cases where the analyses were not published separately.

Analysis	Dataset	$\mathcal{L}$ [fb^{-1}]	Reference
$H \to \gamma\gamma$ (including $t\bar{t}H$, $H \to \gamma\gamma$)	2015–2017	79.8	([10]), [12]
$H \to ZZ^* \to 4\ell$ (including $t\bar{t}H$, $H \to ZZ^* \to 4\ell$)		79.8	([11]), [12]
VH, $H \to b\bar{b}$		79.8	[15,16]
$H \to \mu\mu$		79.8	([20])
$H \to WW^* \to e\nu\mu\nu$	2015–2016	36.1	[13]
$H \to \tau\tau$		36.1	[14]
VBF, $H \to b\bar{b}$		24.5–30.6	[17]
$t\bar{t}H$, $H \to b\bar{b}$ and $t\bar{t}H$ multilepton		36.1	[12,18,19]
$H \to$ invisible		36.1	[21–24]
Off-shell $H \to ZZ^* \to 4\ell$ and $H \to ZZ^* \to 2\ell 2\nu$		36.1	[25]

defined in the fiducial region $|y_H| < 2.5$, where y_H is the Higgs boson rapidity, partitioned within each Higgs boson production process into multiple kinematic regions based on the transverse momentum of the Higgs boson, the number of associated jets, and the transverse momentum of associated W or Z bosons. The $H \to \mu\mu$ and VBF, $H \to b\bar{b}$ analyses use a coarser description based on the Higgs boson production mode only.

The paper is structured as follows: Section II describes the data and simulation samples and Sec. III presents the analyses in individual decay channels which are used as inputs to the combination. Section IV provides a short description of the statistical procedures. The measurement of the signal strength μ, defined as the ratio of the total Higgs boson signal yield to its SM prediction, is presented in Sec. V A. Measurements of the cross sections of the main production processes within $|y_H| < 2.5$, assuming SM predictions for the branching fractions, are then shown in Sec. V B. The production modes considered are gluon–gluon fusion (ggF), VBF, VH, $t\bar{t}H$ and associated production with a single top quark (tH). Measurements of cross sections times branching fractions for Higgs boson production and decay processes are shown in Sec. V C. Section V D presents a parametrization where the measured quantities are the cross section times branching fraction of the process $gg \to H \to ZZ^*$, together with ratios of production cross sections and ratios of branching fractions. Common systematic uncertainties and modeling assumptions partially cancel out in these ratios, reducing the model dependence of the result. Section VI presents results in the STXS framework. Potential deviations from SM predictions are then probed in a framework of multiplicative modifiers κ applied to the SM values of Higgs boson couplings [37], presented in Sec. VII. Finally, Sec. VIII presents an interpretation of the data within two benchmark models of beyond-the-SM (BSM) phenomena. Indirect limits on model parameters are set following a methodology similar to that of Ref. [38]. Section IX summarizes the results.

II. DATA AND SIMULATED EVENT SAMPLES

The results of this paper are based on pp collision data collected by the ATLAS experiment[2] [39–41] in the years 2015, 2016 and 2017, with the LHC operating at a center-of-mass energy of 13 TeV. The integrated luminosities of the datasets used in each analysis are shown in Table I. The uncertainty in the combined 2015–2016 integrated luminosity is 2.1% and 2.0% in the combined 2015–2017 integrated luminosity [42], obtained using the LUCID-2 detector [43] for the primary luminosity measurements.

Most analyses use a consistent set of simulated Higgs boson samples to describe the signal processes, which is detailed in the following paragraphs. Exceptions are the VBF, $H \to b\bar{b}$ and off-shell production analyses, described in Secs. III E and III I respectively, and the measurements targeting decays of the Higgs boson into invisible final states described in Sec. III H. The samples used for these analyses are described separately at the end of this section. For each Higgs boson decay mode, the branching fraction used corresponds to higher-order state-of-the-art theoretical calculations [35]. The simulated background samples vary channel by channel and are described in the individual references for the input analyses.

Higgs boson production via gluon–gluon fusion was simulated using the POWHEG BOX [44–47] NNLOPS implementation [48,49]. The event generator uses the HNNLO formalism [50] to reweight the inclusive Higgs boson rapidity distribution produced by the next-to-leading order (NLO) generation of $pp \to H +$ parton, with the scale of each parton emission determined using the MINLO procedure

---

[2]ATLAS uses a right-handed coordinate system with its origin at the nominal interaction point (IP) in the center of the detector and the z-axis along the beam pipe. The x-axis points from the IP to the center of the LHC ring, and the y-axis points upwards. Cylindrical coordinates (r, ϕ) are used in the transverse plane, ϕ being the azimuthal angle around the z-axis. The pseudorapidity is defined in terms of the polar angle θ as $\eta = -\ln\tan(\theta/2)$. Angular distance is measured in units of $\Delta R \equiv \sqrt{(\Delta\eta)^2 + (\Delta\phi)^2}$.

[51–53]. The PDF4LHC15 [54] parton distribution functions (PDFs) were used for the central prediction and uncertainty. The sample is normalized such that it reproduces the total cross section predicted by a next-to-next-to-next-to-leading-order (N³LO) QCD calculation with NLO electroweak corrections applied [35,55–64]. The NNLOPS generator reproduces the Higgs boson p_T distribution predicted by the next-to-next-to-leading-order (NNLO) plus next-to-next-to-leading-logarithm (NNLL) calculation of HRES2.3 [65–67], which includes the effects of top- and bottom-quark masses and uses dynamical renormalization and factorization scales.

The VBF production process was simulated to NLO accuracy in QCD using the POWHEG BOX [68] generator with the PDF4LHC15 set of PDFs. The sample is normalized to an approximate-NNLO QCD cross section with NLO electroweak corrections applied [35,69–71].

The $qq \to VH$ production processes were simulated to NLO accuracy in QCD using the POWHEG BOX, GOSAM [72] and MINLO [51,73] generators with the PDF4LHC15 set of PDFs. The samples are normalized to cross sections calculated at NNLO in QCD with NLO electroweak corrections [74–83]. The $gg \to ZH$ process was generated only at leading order (LO), using POWHEG BOX and NLO PDFs and normalized to an NLO computation with next-to-leading-logarithm (NLL) corrections [35,84].

Higgs boson production in association with a top–antitop pair was simulated at NLO accuracy in QCD using the POWHEG BOX [85] generator with the PDF4LHC15 set of PDFs for the $H \to \gamma\gamma$ and $H \to ZZ^* \to 4\ell$ decay processes. For other Higgs boson decays, the MADGRAPH5_AMC@NLO [86,87] generator was used with the NNPDF3.0 [88] set of PDFs. In both cases the sample is normalized to a calculation with NLO QCD and electroweak corrections [35,89–92].

In addition to the primary Higgs boson processes, separate samples are used to model lower-rate processes. Higgs boson production in association with a $b\bar{b}$ pair ($b\bar{b}H$) was simulated using MADGRAPH5_AMC@NLO [93] with NNPDF2.3LO PDFs [94] and is normalized to a cross section calculated to NNLO in QCD [35,95–97]. The sample includes the effect of interference with the ggF production mechanism. Higgs boson production in association with a single top quark and a W boson (tHW) was produced at LO accuracy using MADGRAPH5_AMC@NLO with the CTEQ6L1 PDF set [98]. Finally, Higgs boson production in association with a single top quark in the t-channel (tHq) was generated at LO accuracy using MADGRAPH5_AMC@NLO with CT10 [99] PDFs. The tH samples are normalized to NLO QCD calculations [35,100,101].

The parton-level events were input to PYTHIA8 [102] or HERWIG++ [103] to model the Higgs boson decay, parton showering, hadronization, and multiple parton interaction (MPI) effects. The generators were interfaced to PYTHIA8 for all samples except tHW. For PYTHIA8 the AZNLO [104] and A14 [105] parameter sets were used, and for HERWIG++ its UEEE5 parameter set was used.

Higgs boson decay branching fractions were computed using HDECAY [106–108] and PROPHECY4F [109–111].

In the all-hadronic channel of the VBF, $H \to b\bar{b}$ analysis, the POWHEG BOX generator with the CT10 [99] set of PDFs was used to simulate the ggF [112] and VBF production processes, and interfaced with PYTHIA8 for parton shower. In the photon channel of the VBF, $H \to b\bar{b}$ analysis, VBF and ggF production in association with a photon was simulated using the MADGRAPH5_AMC@NLO generator with the PDF4LHC15 set of PDFs, and also using PYTHIA8 for parton shower. For both channels, contributions from VH and $t\bar{t}H$ production were generated using the PYTHIA8 generator with the NNPDF3.0 set of PDFs, and using the MADGRAPH5_AMC@NLO generator interfaced with HERWIG++ and the NLO CT10 set of PDFs, respectively.

In the analyses targeting Higgs boson decays into invisible final states, the ggF, VBF and ZH signals were simulated in a similar way to the general procedure described above, but for the VBF production process the NNPDF3.0 PDF set was used instead of PDF4LHC15, while for the ZH process the CT10 PDF set was used.

In the off-shell production analysis, the $gg \to H^* \to ZZ$ process was generated together with the corresponding irreducible continuum production, using the SHERPA2.2.2 + OPENLOOPS [113–116] generator and the NNPDF3.0 PDF set. The generation was performed at leading order with up to one additional jet in the final state, and interfaced with the SHERPA parton shower [117]. The cross section calculations take into account K-factors following the methodology described in Ref. [25].

The particle-level Higgs boson events were passed through a GEANT 4 [118] simulation of the ATLAS detector [119] and reconstructed using the same analysis software as used for the data. Event pileup is included in the simulation by overlaying inelastic pp collisions, such that the average number of interactions per bunch crossing reproduces that observed in the data. The inelastic pp collisions were simulated with PYTHIA8 using the MSTW2008LO [120] set of PDFs with the A2 [121] set of tuned parameters or using the NNPDF2.3LO set of PDFs with the A3 [122] set of tuned parameters.

III. INDIVIDUAL CHANNEL MEASUREMENTS

Brief descriptions of the input analyses to the combination are given below. More details can be found in the individual analysis references listed in each section. The categorization is summarized in Table II. The overlap between the event selections of the analyses included in the combination is found to be negligible.

A. $H \to \gamma\gamma$

The $H \to \gamma\gamma$ analysis [10,12] requires the presence of two isolated photons [123] within the pseudorapidity range $|\eta| < 2.37$, excluding the region $1.37 < |\eta| < 1.52$

TABLE II. Summary of the signal regions entering the combined measurements. "Leptonic" and "hadronic" refers to $t\bar{t}H$ and VH processes where the associated $t\bar{t}$ pair or vector boson decays to final states with respectively at least one lepton or no leptons. "Resolved" and "boosted" refers to configurations in which hadronic Higgs boson decay products are reconstructed respectively as two or more jets, or a single jet. In the VBF, $H \to \gamma\gamma$ analysis, $p_T^{\ell+E_T^{miss}}$ is the transverse momentum of the system composed of the leading lepton and the missing transverse momentum. Other notations are defined in Sec. III. Each 0-jet and 1-jet $H \to WW^*$ entry corresponds to two categories for a leading lepton flavor of either e or μ. For $H \to \tau\tau$, each entry corresponds to three categories for $\tau_{lep}\tau_{lep}$, $\tau_{lep}\tau_{had}$ and $\tau_{had}\tau_{had}$, unless otherwise specified. "Multilepton" refers to decays of the Higgs boson with one or more leptons, and encompasses $H \to WW^*$, $H \to \tau\tau$, and $H \to ZZ^*$ excluding $H \to ZZ^* \to 4\ell$. The selections targeting $H \to \mu\mu$, $H \to$ invisible and off-shell Higgs boson production are not included this table.

	$H \to \gamma\gamma$	$H \to ZZ^*$	$H \to WW^*$	$H \to \tau\tau$	$H \to b\bar{b}$
$t\bar{t}H$	$t\bar{t}H$ leptonic (3 categories) $t\bar{t}H$ hadronic (4 categories)	$t\bar{t}H$ multilepton $1\ell + 2\tau_{had}$ $t\bar{t}H$ multilepton 2 opposite-sign $\ell + 1\tau_{had}$ $t\bar{t}H$ multilepton 2 same-sign ℓ (categories for 0 or 1 τ_{had}) $t\bar{t}H$ multilepton 3ℓ (categories for 0 or 1 τ_{had}) $t\bar{t}H$ multilepton 4ℓ (except $H \to ZZ^* \to 4\ell$) $t\bar{t}H$ leptonic, $H \to ZZ^* \to 4\ell$ $t\bar{t}H$ hadronic, $H \to ZZ^* \to 4\ell$			$t\bar{t}H$ 1ℓ, boosted $t\bar{t}H$ 1ℓ, resolved (11 categories) $t\bar{t}H$ 2ℓ (7 categories)
VH	VH 2ℓ VH 1ℓ, $p_T^{\ell+E_T^{miss}} \geq 150$ GeV VH 1ℓ, $p_T^{\ell+E_T^{miss}} < 150$ GeV VH E_T^{miss}, $E_T^{miss} \geq 150$ GeV VH E_T^{miss}, $E_T^{miss} < 150$ GeV VH + VBF $p_T^{j1} \geq 200$ GeV VH hadronic (2 categories)	VH leptonic 0-jet, $p_T^{4\ell} \geq 100$ GeV 2-jet, $m_{jj} < 120$ GeV	VH leptonic		2ℓ, $75 \leq p_T^V < 150$ GeV, $N_{jets} = 2$ 2ℓ, $75 \leq p_T^V < 150$ GeV, $N_{jets} \geq 3$ 2ℓ, $p_T^V \geq 150$ GeV, $N_{jets} = 2$ 2ℓ, $p_T^V \geq 150$ GeV, $N_{jets} \geq 3$ 1ℓ, $p_T^V \geq 150$ GeV, $N_{jets} = 2$ 1ℓ, $p_T^V \geq 150$ GeV, $N_{jets} = 3$ 0ℓ, $p_T^V \geq 150$ GeV, $N_{jets} = 2$ 0ℓ, $p_T^V \geq 150$ GeV, $N_{jets} = 3$
VBF	VBF, $p_T^{\gamma\gamma jj} \geq 25$ GeV (2 categories) VBF, $p_T^{\gamma\gamma jj} < 25$ GeV (2 categories)	2-jet VBF, $p_T^{j1} \geq 200$ GeV 2-jet VBF, $p_T^{j1} < 200$ GeV	2-jet VBF	VBF $p_T^{\tau\tau} > 140$ GeV ($\tau_{had}\tau_{had}$ only) VBF high-m_{jj} VBF low-m_{jj}	VBF, two central jets VBF, four central jets VBF + γ
ggF	2-jet, $p_T^{\gamma\gamma} \geq 200$ GeV 2-jet, 120 GeV $\leq p_T^{\gamma\gamma} < 200$ GeV 2-jet, 60 GeV $\leq p_T^{\gamma\gamma} < 120$ GeV 2-jet, $p_T^{\gamma\gamma} < 60$ GeV 1-jet, $p_T^{\gamma\gamma} \geq 200$ GeV 1-jet, 120 GeV $\leq p_T^{\gamma\gamma} < 200$ GeV 1-jet, 60 GeV $\leq p_T^{\gamma\gamma} < 120$ GeV 1-jet, $p_T^{\gamma\gamma} < 60$ GeV 0-jet (2 categories)	1-jet, $p_T^{4\ell} \geq 120$ GeV 1-jet, 60 GeV $\leq p_T^{4\ell} < 120$ GeV 1-jet, $p_T^{4\ell} < 60$ GeV 0-jet, $p_T^{4\ell} < 100$ GeV	1-jet, $m_{\ell\ell} < 30$ GeV, $p_T^{\ell 2} < 20$ GeV 1-jet, $m_{\ell\ell} < 30$ GeV, $p_T^{\ell 2} \geq 20$ GeV 1-jet, $m_{\ell\ell} \geq 30$ GeV, $p_T^{\ell 2} < 20$ GeV 1-jet, $m_{\ell\ell} \geq 30$ GeV, $p_T^{\ell 2} \geq 20$ GeV 0-jet, $m_{\ell\ell} < 30$ GeV, $p_T^{\ell 2} < 20$ GeV 0-jet, $m_{\ell\ell} < 30$ GeV, $p_T^{\ell 2} \geq 20$ GeV 0-jet, $m_{\ell\ell} \geq 30$ GeV, $p_T^{\ell 2} < 20$ GeV 0-jet, $m_{\ell\ell} \geq 30$ GeV, $p_T^{\ell 2} \geq 20$ GeV	Boosted, $p_T^{\tau\tau} > 140$ GeV Boosted, $p_T^{\tau\tau} \leq 140$ GeV	

corresponding to the transition between the barrel and endcap sections of the electromagnetic calorimeter. The transverse momenta of the leading and subleading photons are required to be greater than $0.35m_{\gamma\gamma}$ and $0.25m_{\gamma\gamma}$ respectively, where $m_{\gamma\gamma}$ is the invariant mass of the diphoton system. The event reconstruction and selection procedures are largely unchanged from the ones described in Ref. [10]. The only significant change concerns the reconstruction of the calorimeter energy clusters associated with the photons; a dynamical, topological cell clustering-based algorithm [124,125] is now used instead of a sliding-window technique [123,126].

Selected events are separated into 29 mutually exclusive categories based on the kinematics of the diphoton system and associated particles, chosen to approximately match those of the Stage 1 STXS regions described in Sec. VI A. Seven categories are defined to select $t\bar{t}H$ production, including both semileptonic and hadronic top-quark decay processes through various selections on the multiplicities and kinematics of leptons [127–129], jets [130], and jets tagged as containing b-hadrons [131]. These categories are described in Ref. [12]. The remaining events are classified into categories targeting the VH, VBF and ggF production modes, described in Ref. [10]. Five categories are defined to select WH and ZH production with leptonic decays of the W or Z, based on the presence of leptons and missing transverse momentum $E_{\mathrm{T}}^{\mathrm{miss}}$ [132]. Seven categories cover the VBF and VH processes: one category requires the presence of two jets, with the leading jet transverse momentum $p_{\mathrm{T}}^{j1} > 200$ GeV; two categories select hadronic vector-boson decays by requiring two jets with an invariant mass compatible with the W or Z boson mass; and four categories enrich VBF production by requiring forward jets in a VBF-like topology. The requirement of a second jet for the $p_{\mathrm{T}}^{j1} > 200$ GeV category is a change compared to Ref. [10] where only one jet was required, and helps to reduce contamination from ggF production. The remaining events are split into 10 categories, separating events with 0, 1, and $\geq$2-jets and classifying them further according to the pseudorapidity of the two photons (for 0-jet events) or the transverse momentum of the diphoton system $p_{\mathrm{T}}^{\gamma\gamma}$ (for 1 and $\geq$2-jet events). The distribution of $m_{\gamma\gamma}$ is used to separate the Higgs boson signal from continuum background processes in each category.

B. $H \to ZZ^* \to 4\ell$

The $H \to ZZ^* \to 4\ell$ analysis requires the presence of at least two same-flavor and opposite-charge light-lepton pairs, with a four-lepton invariant mass $m_{4\ell}$ in the range 115 GeV $< m_{4\ell} < 130$ GeV. The analysis follows the strategy described in the previous publication [11], but employs improved event reconstruction and electron reconstruction [125] techniques, and defines additional event categories to enhance sensitivity to the production

of the SM Higgs boson associated with a vector boson (VH, $V \to \ell\nu/\nu\nu$) and with a top-quark pair [12].

To distinguish the $t\bar{t}H$, VH, VBF, and ggF production modes and to enhance the purity of each kinematic selection, 11 mutually exclusive reconstructed event categories based on the presence of jets and additional leptons in the final state are defined. Candidate events with at least one b-tagged jet and three or more additional jets, or one additional lepton and at least two additional jets are classified into categories enriched in $t\bar{t}H$ production with fully hadronic or semileptonic top-quark decays respectively [12]. Events failing these requirements but containing at least one additional lepton are assigned to a VH-enriched category with leptonic vector boson decays. The remaining events are classified according to their jet multiplicity (0-jet, 1-jet, and $\geq$ 2-jet). Events with at least two jets are divided into a VBF-enriched region, for which the dijet invariant mass m_{jj} is required to be above 120 GeV, and a region enriched in VH events with a hadronically decaying vector boson for $m_{jj} < 120$ GeV. The VBF-enriched region is further split into two categories, in which the transverse momentum of the leading jet p_{T}^{j1} is required to be either above or below 200 GeV. The selected 0-jet and 1-jet events are further separated according to the transverse momentum $p_{\mathrm{T}}^{4\ell}$ of the four-lepton system: the 0-jet events are split into two categories with a boundary at $p_{\mathrm{T}}^{4\ell} = 100$ GeV, with the lower $p_{\mathrm{T}}^{4\ell}$ selection being enriched in Higgs boson events produced via ggF and the higher $p_{\mathrm{T}}^{4\ell}$ selection being enriched in Higgs boson events produced in association with a weak vector boson. The 1-jet events are split into three categories, each containing predominantly Higgs boson events produced via ggF, with boundaries at $p_{\mathrm{T}}^{4\ell} = 60$ and 120 GeV to match the STXS selections described in Sec. VI A. Boosted decision trees (BDTs) are employed to separate the signal from the background processes and to enhance the sensitivity to the various Higgs boson production modes.

C. $H \to WW^* \to e\nu\mu\nu$

The $H \to WW^* \to e\nu\mu\nu$ analysis [13] included in the combination targets the ggF and VBF production modes. Signal candidates are selected by requiring the presence of an isolated $e^{\pm}\mu^{\mp}$ pair, with transverse momentum thresholds at 22 and 15 GeV for the leading and subleading lepton. Events with jets tagged as containing b-hadrons are rejected to suppress background contributions originating from top-quark production. Contributions from $W \to \tau\nu$ decays in which the τ-leptons subsequently decay into electrons or muons are also included.

Selected events are classified according to the number of associated jets (N_{jets}). Exclusive $N_{\mathrm{jets}} = 0$ and $N_{\mathrm{jets}} = 1$ selections are enriched in signal events produced via ggF. To isolate regions with higher sensitivity, they are each further split into eight categories apiece, based on the flavor

of the leading lepton (e or μ), two bins of the invariant mass of the dilepton system $m_{\ell\ell}$ and two bins of the transverse momentum of the subleading lepton $p_T^{\ell_2}$. The distribution of the transverse mass of the dilepton plus E_T^{miss} system is used to separate the Higgs boson signal from background in each category. The $N_{\text{jets}} \geq 2$ category is naturally sensitive to the VBF process. A central-jet veto is applied to suppress the multijet background and the contribution from ggF production. The output of a BDT exploiting the kinematic properties of the two leading jets and the two leptons is used to separate VBF Higgs boson production from background processes, including Higgs boson production via ggF.

D. $H \to \tau\tau$

The $H \to \tau\tau$ analysis [14] measures the Higgs boson production cross section in the VBF production process or in ggF production with large Higgs boson transverse momentum p_T^H. Final states with both leptonic (τ_{lep}) and hadronic (τ_{had}) decays of the τ-lepton are considered. Selected lepton candidates are required to be of opposite charge, meet identification and isolation criteria and satisfy the p_T thresholds of the triggers used. Three mutually exclusive analysis channels, $\tau_{\text{lep}}\tau_{\text{lep}}$, $\tau_{\text{lep}}\tau_{\text{had}}$, and $\tau_{\text{had}}\tau_{\text{had}}$, are defined according to the number of selected electron, muon and τ_{had} candidates. All channels require the presence of at least one jet with high transverse momentum.

To exploit signal-sensitive event topologies, candidate events are divided into three categories targeting the VBF process and two categories for high-p_T^H Higgs production. The VBF categories collect events with two jets with a large pseudorapidity separation and a high invariant mass (m_{jj}). The Higgs boson decay products are required to be in the central rapidity region. One VBF category is defined by requiring the transverse momentum of the $\tau\tau$ system $p_T^{\tau\tau}$ to be above 140 GeV, for $\tau_{\text{had}}\tau_{\text{had}}$ events only. The two remaining VBF categories are defined for lower and higher values of m_{jj}, with definitions that differ between the $\tau_{\text{lep}}\tau_{\text{lep}}$, $\tau_{\text{lep}}\tau_{\text{had}}$, and $\tau_{\text{had}}\tau_{\text{had}}$ channels. The high-p_T^H categories select events with large values of $p_T^{\tau\tau}$, with contributions mainly from the ggF process. Events failing the VBF selection and with $p_T^{\tau\tau} > 100$ GeV are selected. In order to improve the sensitivity of the analysis, two categories are defined for $p_T^{\tau\tau} > 140$ GeV and $p_T^{\tau\tau} \leq 140$ GeV, with additional selections on the angular separation between the τ-leptons. The distribution of the invariant mass of the $\tau\tau$ system is used to separate the Higgs boson signal from background in each category.

E. $H \to b\bar{b}$

The $H \to b\bar{b}$ decay channel is used to measure the production cross section in the VH, VBF and $t\bar{t}H$ production modes, the latter described in Sec. III G.

The search for $H \to b\bar{b}$ in the VH production mode [15,16] considers final states containing at least two jets,

of which exactly two must be tagged as containing b-hadrons. Either zero, one or two charged leptons are also required, exploring the associated production of a Higgs boson with a W or Z boson decaying leptonically as $Z \to \nu\nu$, $W \to \ell\nu$, or $Z \to \ell\ell$. Contributions from $W \to \tau\nu$ and $Z \to \tau\tau$ decays in which the τ-leptons subsequently decay into electrons or muons are also included.

To enhance the signal sensitivity, selected candidate events are classified according to the charged-lepton multiplicity, the vector-boson transverse momentum p_T^V, and the jet multiplicity. For final states with zero or one lepton, $p_T^V > 150$ GeV is required. In two-lepton final states, two regions are considered, 75 GeV $< p_T^V < 150$ GeV and $p_T^V > 150$ GeV. The p_T^V thresholds are chosen to select regions with strong experimental sensitivity, and match the STXS definitions described in Sec. VI A. Each of these regions is finally separated into a category with exactly two reconstructed jets and another with three or more. In the zero- and one-lepton channel, events with four or more jets are rejected. Topological and kinematic selection criteria are applied within each of the resulting categories. BDTs incorporating the event kinematics and topology, in addition to the dijet invariant mass, are employed in each lepton channel and analysis region to separate the signal process from the sum of the expected background processes.

The $H \to b\bar{b}$ mode is also used to measure the VBF production process [17]. Three orthogonal selections are employed, targeting two all-hadronic channels and a photon-associated channel. Each selection requires the presence of at least two jets tagged as containing b-hadrons in the central pseudorapidity region $|\eta| < 2.5$ as well as at least two additional jets used to identify the VBF topology.

The first of the two all-hadronic selections requires the b-tagged jets to have transverse momenta larger than 95 GeV and 70 GeV, while one of the additional jets is required to be in the forward region $3.2 < |\eta| < 4.4$ and have a transverse momentum larger than 60 GeV and another must satisfy $p_T > 20$ GeV and $|\eta| < 4.4$. The transverse momentum p_T^{bb} of the system composed of the two b-tagged jets must be larger than 160 GeV.

The second all-hadronic selection with four central jets is defined by the presence of two jets with $|\eta| < 2.8$ in addition to the b-tagged jets with $|\eta| < 2.5$. All selected jets must pass a common threshold requirement of 55 GeV on their transverse momenta. The p_T of the $b\bar{b}$-system is required to be larger than 150 GeV. Events containing at least one forward jet satisfying the selection criteria of the first all-hadronic channel are removed.

A VBF $+ \gamma$ selection is defined by the presence of a photon with transverse momentum $p_T > 30$ GeV and $|\eta| < 2.37$, excluding the region $1.37 < |\eta| < 1.52$, which suppresses the dominant background from nonresonant $b\bar{b}jj$ production. Events must have at least four jets, all satisfying $p_T > 40$ GeV and $|\eta| < 4.4$, with at least two jets in $|\eta| < 2.5$ passing the b-tag requirements.

The invariant mass of the VBF jets is required to be higher than 800 GeV, and $p_T^{bb} > 80$ GeV.

In all three selections a BDT built from variables describing jet and photon kinematics is used to enhance the sensitivity, and the distribution of the invariant mass m_{bb} of the two b-tagged jets is used to separate the Higgs boson signal from background.

The VBF, $H \to b\bar{b}$ channels are included in all the measurements except for those presented in Sec. VI.

F. $H \to \mu\mu$

The $H \to \mu\mu$ search uses a similar technique to the $H \to \gamma\gamma$ analysis, requiring a pair of opposite-charge muons. The analysis closely follows the $H \to \mu\mu$ search described in Ref. [20], which used a smaller dataset collected in the years 2015 and 2016 only.

Events are classified into eight categories. The output of a BDT exploiting the kinematic properties of the two leading jets and the two muons is used to define two categories targeting the VBF process. In order to enhance the sensitivity of the analysis, the remaining events are classified into three ranges of the transverse momentum $p_T^{\mu\mu}$ of the dimuon system ($p_T^{\mu\mu} < 15$ GeV, 15 GeV $\leq p_T^{\mu\mu} < 50$ GeV and $p_T^{\mu\mu} \geq 50$ GeV) and two ranges of the muon pseudorapidities η^μ (both muons within $|\eta^\mu| \leq 1$, or at least one muon outside this range), for a total of six categories. The distribution of the invariant mass $m_{\mu\mu}$ of the two muons is used to separate signal from background in each category.

The analysis is not sensitive at the level of the Higgs boson signal expected in the SM, and is only included in the results presented in Section VII D.

G. $t\bar{t}H$, $H \to b\bar{b}$ and $t\bar{t}H$ multilepton analyses

Searches for the associated production of the Higgs boson with a $t\bar{t}$ pair have been performed using Higgs boson decays into $b\bar{b}$ [19] and in multilepton final states, targeting Higgs boson decays into WW^*, ZZ^* and $\tau\tau$ [12,18]. These analyses complement the selections sensitive to $t\bar{t}H$ production defined in the analyses of the $H \to \gamma\gamma$ and $H \to ZZ^* \to 4\ell$ decay channels, described in Secs. III A and III B.

The search for $t\bar{t}H$ production with $H \to b\bar{b}$ employs two selections, optimized for single-lepton and dilepton final states of $t\bar{t}$ decays. In the single-lepton channel, events are required to have one isolated electron or muon and at least five jets, of which at least two must be identified as containing b-hadrons. In the dilepton channel, events are required to have two opposite-charge leptons and at least three jets, of which at least two must be identified as containing b-hadrons. Candidate events are classified into 11 (7) orthogonal categories in the single-lepton (dilepton) channel, according to the jet multiplicity and the values of the b-tagging discriminant for the jets. In the single-lepton channel, an additional category, referred to as *boosted*, is designed to select events with large transverse momenta

for the Higgs candidate ($p_T^H > 200$ GeV) and one of the top-quark candidates ($p_T^t > 250$ GeV). In each region, a BDT exploiting kinematic information of the events is employed to separate $t\bar{t}H$ production from background processes.

The $t\bar{t}H$ search with Higgs boson decays into WW^*, ZZ^* and $\tau\tau$ exploits several multilepton signatures resulting from leptonic decays of vector bosons and/or the presence of τ_{had} candidates. Seven final states, categorized by the number and flavor of reconstructed charged-lepton candidates, are examined. They are: one lepton with two τ_{had} candidates, two same-charge leptons with zero or one τ_{had} candidates, two opposite-charge leptons with one τ_{had} candidate, three leptons with zero or one τ_{had} candidates, and four leptons, excluding events from $H \to ZZ^* \to 4\ell$ decays. Events in all channels are required to have at least two jets, at least one of which must be b-tagged. Additional requirements are employed for each final state. Multivariate analysis techniques exploiting the kinematic properties and topologies of the selected events are applied in most channels to improve the discrimination between the signal and the background.

H. Searches for invisible Higgs boson decays

Searches for decays of the Higgs boson into invisible final states select events with large missing transverse momentum; backgrounds are suppressed by requiring in addition either jets with a VBF topology [21], an associated Z boson decaying into charged leptons [22] or an associated W or Z boson decaying into hadronic final states [23].

Production in the VBF topology is identified by requiring two jets with a pseudorapidity difference $|\Delta\eta_{jj}| > 4.8$ and invariant mass $m_{jj} > 1$ TeV. The missing transverse momentum is required to be larger than 180 GeV. Events with isolated lepton candidates or additional jets are rejected. Three signal regions are defined for $1 < m_{jj} < 1.5$ TeV, $1.5 < m_{jj} < 2$ TeV and $m_{jj} > 2$ TeV.

Production in association with a leptonically decaying Z boson is identified by requiring the presence of a pair of isolated electrons or muons with an invariant mass close to m_Z. The missing transverse momentum is required to be larger than 90 GeV. It must also be larger than 60% of the scalar sum of the transverse momenta of the identified leptons and jets, and must be oriented back-to-back with the dilepton system in the transverse plane.

Two event topologies are considered in order to identify production in association with a hadronically decaying W and Z boson. The *resolved* topology is defined by the presence of two jets compatible with originating from the hadronic decay of a W or Z boson, reconstructed using the anti-k_t algorithm [133] with a radius parameter of 0.4. The *merged* topology identifies W or Z bosons with large transverse momentum through the presence of a single jet, reconstructed using the anti-k_t algorithm with a radius parameter of 1. The missing transverse momentum is

required to be larger than 150 GeV and 250 GeV for the resolved and boosted topologies respectively. In both cases, events are categorized according to the multiplicity of jets tagged as containing *b*-quarks. A separate category is also defined for events in which the mass of the jet system, defined as the dijet mass in the resolved topology and the mass of the large-radius jet in the merged topology, is compatible with a hadronic *W* or *Z* decay.

The statistical combination of these analyses [24] yields an observed (expected) upper limit on the branching fraction for Higgs boson decays into invisible final states of $B_{\mathrm{inv}} < 0.38$ (0.21) at 95% confidence level. In this paper, these analyses are only included in the coupling measurements presented in Secs. VII C and VII E.

I. Off-shell Higgs boson production

Measurements of the $H^* \to ZZ$ final state in the mass range above the $2m_Z$ threshold (off-shell region) provide an opportunity to measure the off-shell coupling strength of the observed Higgs boson, as discussed in Refs. [134–137]. The $ZZ \to 4\ell$ and $ZZ \to 2\ell 2\nu$ decay channels, detailed in Ref. [25], are used in these measurements.

Assuming that the coupling modifiers are identical for on-shell and off-shell production, the total width of the Higgs boson can be constrained from a combination with the on-shell measurements. It is also assumed that the coupling modifiers are independent of the momentum transfer of the Higgs boson production mechanism considered in the analysis, and that any new physics which modifies the off-shell signal strength and the off-shell couplings does not modify the relative phase of the interfering signal and background processes. Further, it is assumed that there are neither sizable kinematic modifications to the off-shell signal nor new sizable signals in the search region of this analysis unrelated to an enhanced off-shell signal strength [138,139].

The analysis in the $ZZ \to 4\ell$ final state closely follows the Higgs boson measurements in the same final state, described in Sec. III B, with the same event reconstruction, trigger and event selections and background estimation methods. The off-peak region is defined to cover the range 220 GeV $< m_{4\ell} < 2000$ GeV. The distribution of a matrix-element-based discriminant constructed to enhance the $gg \to H^* \to ZZ$ is used to separate the Higgs boson signal from background processes.

The analysis in the $ZZ \to 2\ell 2\nu$ channel is similar to the one designed to search for heavy ZZ resonances [140] with the same object definitions. The analysis is performed inclusively in the number of final-state jets and kinematic selections are optimized accordingly. Sensitivity to the off-shell Higgs boson signal is obtained through the distribution of the transverse mass m_{T}^{ZZ} reconstructed from the momentum of the dilepton system and the missing transverse momentum [25], within the range 250 GeV $< m_{\mathrm{T}}^{ZZ} < 2000$ GeV.

These off-shell analyses are only included in the coupling measurements presented in Sec. VII E.

IV. STATISTICAL MODEL

The statistical methods used in this paper follow those of Ref. [9]. The results of the combination are obtained from a likelihood function defined as the product of the likelihoods of each input analysis. These are themselves products of likelihoods computed in mutually exclusive regions selected in the analysis, referred to as analysis categories.

The number of signal events in each analysis category k is expressed as

$$n_k^{\mathrm{signal}} = \mathcal{L}_k \sum_i \sum_f (\sigma \times B)_{if} (A \times \epsilon)_{if,k} \qquad (1)$$

where the sum runs over production modes i ($i =$ ggF, VBF, WH, ZH, $t\bar{t}H$, …) and decay final states f ($f = \gamma\gamma$, ZZ^*, WW^*, $\tau\tau$, $b\bar{b}$, $\mu\mu$), $\mathcal{L}_k$ is the integrated luminosity of the dataset used in category k, and $(A \times \epsilon)_{if,k}$ is the acceptance times efficiency factor in category k for production mode i and final state f. The cross section times branching fraction $(\sigma \times B)_{if}$ for each relevant pair (i, f) are the parameters of interest of the model. The measurements presented in this paper are obtained from fits in which these products are free parameters (Sec. V C), or in which they are re-expressed in terms of smaller sets of parameters: of a single signal-strength parameter μ (Sec. V A), of the cross sections σ_i in each of the main production modes (Sec. V B), of ratios of cross sections and branching fractions (Secs. V D and VI B) or of coupling modifiers (Sec. VII). Additional parameters, referred to as nuisance parameters, are used to describe systematic uncertainties and background quantities that are constrained by sidebands or control regions in data.

Systematic uncertainties that affect multiple analyses are modeled with common nuisance parameters to propagate the effects of these uncertainties coherently to all measurements. The assessment of the associated uncertainties varies between data samples, reconstruction algorithms and software releases, leading to differences particularly between analyses performed using the 2017 dataset and those using 2015 and 2016 data only. Between these two sets of analyses, components of systematic uncertainties in the luminosity, the jet energy scale, the electron/photon resolution and energy scale, and in the electron reconstruction and identification efficiencies are also treated as correlated. Uncertainties due to the limited number of simulated events used to estimate expected signal and background yields are included using the simplified version of the Beeston–Barlow technique [141] implemented in the HISTFACTORY tool [142]. They are counted among the systematic uncertainties.

Theory uncertainties in the signal, such as missing higher-order QCD corrections and PDF-induced uncertainties, affect the expected signal yields of each production and decay process, as well as the signal acceptance in each category. These uncertainties are modeled by a common set of nuisance parameters in most channels. For the signal-strength (Sec. V A) and coupling modifier (Sec. VII) results and constraints on new phenomena (Sec. VIII), which rely on the comparison of measured and SM-expected yields, both the acceptance and signal yield uncertainties are included. For the cross section and branching fraction results of Secs. V B and VI, only acceptance uncertainties are considered. The effects of correlations between Higgs boson branching fractions are modeled using the correlation model specified in Ref. [35]. Uncertainties due to dependencies on SM parameter values and missing higher-order effects are applied to the partial decay widths and propagated to the branching fractions. The uncertainties due to modeling of background processes are typically treated as uncorrelated between analyses.

The measurement of the parameters of interest is carried out using a statistical test based on the profile likelihood ratio [143],

$$\Lambda(\boldsymbol{\alpha}) = \frac{L(\boldsymbol{\alpha}, \hat{\hat{\boldsymbol{\theta}}}(\boldsymbol{\alpha}))}{L(\hat{\boldsymbol{\alpha}}, \hat{\boldsymbol{\theta}})},$$

where $\boldsymbol{\alpha}$ and $\boldsymbol{\theta}$ are respectively the parameters of interest and the nuisance parameters. In the numerator, the nuisance parameters are set to their profiled values $\hat{\hat{\boldsymbol{\theta}}}(\boldsymbol{\alpha})$, which maximize the likelihood function for fixed values of the parameters of interest $\boldsymbol{\alpha}$. In the denominator, both the parameters of interest and the nuisance parameters are set to the values $\hat{\boldsymbol{\alpha}}$ and $\hat{\boldsymbol{\theta}}$ respectively which jointly maximize the likelihood.

In the asymptotic regime, in which the likelihood is approximately Gaussian, the value of $-2 \ln \Lambda(\boldsymbol{\alpha})$ follows a χ^2 distribution with a number of degrees of freedom (d.o.f.) n equal to the dimensionality of the vector $\boldsymbol{\alpha}$ [143]. This property is assumed to hold for all the results presented in the following sections. Confidence intervals for a confidence level (CL) $1 - p$ are then defined as the regions with values of $-2 \ln \Lambda(\boldsymbol{\alpha})$ below a threshold $F_{\chi_n^2}^{-1}(1 - p)$, where $F_{\chi_n^2}^{-1}$ is the quantile function of the χ^2 distribution with n d.o.f.

The CL_s prescription [144] is applied when setting an upper limits on a single parameter directly related to measured event rates, for instance a production cross section. When setting limits in more than one dimension, the CL_s procedure is not applied.

For relevant parameters of interest, a physical bound on the parameter values is included in the statistical interpretation. For example, branching fraction parameters cannot conceptually be smaller than zero. The 95% confidence interval quoted for such parameters is then based on the

profile likelihood ratio restricted to the allowed region of parameter space, using the $\tilde{t}_\mu$ test statistic of Ref. [143]. The confidence interval is defined by the standard χ^2 cutoff, which leads to some overcoverage near the boundaries.

Uncertainties in the measurement parameters are in some cases broken down into separate components for theory uncertainties affecting the background processes, theory uncertainties affecting the Higgs boson signal production, experimental uncertainties including Monte Carlo (MC) statistical uncertainties, and statistical uncertainties. Each component is derived by fixing the associated nuisance parameters to their best-fit values $\hat{\theta}$ in both the numerator and denominator of Λ, and computing again the uncertainty in the measurement parameters. This is done for each component in turn, following the order in which they are listed above. The uncertainty obtained at each step is then subtracted in quadrature from the uncertainty obtained in the previous step (in the first step, from the total uncertainty) to obtain the corresponding uncertainty component. The statistical uncertainty component is obtained in the last step, with all nuisance parameters fixed except for the ones that are only constrained by data, such as parameters used to describe data-driven background estimates.

For the systematic uncertainties reported in the detailed breakdowns shown for instance in Table III, a simpler procedure is used: in each case the corresponding nuisance parameters are fixed to their best-fit values, while other nuisance parameters are left free, and the resulting uncertainty is subtracted in quadrature from the total uncertainty.

The probability of compatibility with the Standard Model is quantified using the test statistic $\lambda_{SM} = -2 \ln \Lambda(\boldsymbol{\alpha} = \boldsymbol{\alpha}_{SM})$, where $\boldsymbol{\alpha}_{SM}$ are the Standard Model values of the parameters of interest. A p-value[3] p_{SM} for the probability of compatibility is computed in the asymptotic approximation as $p_{SM} = 1 - F_{\chi_n^2}(\lambda_{SM})$, with n equal to the number of free parameters of interest. For the cross section and branching fraction measurements reported in this paper, this definition does not account for the uncertainties in the SM values used as reference and may therefore lead to an underestimate of the probability of compatibility with the SM.

Results for expected significances and limits are obtained using the Asimov dataset technique [143].

The correlation coefficients presented in this paper are constructed to be symmetric around the observed best-fit values of the parameters of interest using the second derivatives of the negative log-likelihood ratio. Hence, the correlation matrices shown are not fully representative of the observed asymmetric uncertainties in the measurements. While the reported information is sufficient to reinterpret the measurements in terms of other

---

[3]The p-value is defined as the probability to obtain a value of the test statistic that is at least as high as the observed value under the hypothesis that is being tested.

parameterizations of the parameters of interest, this provides only an approximation to the information contained in the full likelihood function. For this reason, results for a number of commonly used parameterizations are also provided in Secs. V–VII.

V. COMBINED MEASUREMENTS OF SIGNAL STRENGTH, PRODUCTION CROSS SECTIONS, AND BRANCHING RATIOS

A. Global signal strength

The global signal strength μ is determined following the procedures used for the measurements performed at $\sqrt{s} = 7$ and 8 TeV [9]. For a specific production mode i and decay final state f, the signal yield is expressed in terms of a single modifier μ_{if}, as the production cross section σ_i and the branching fraction B_f cannot be separately measured without further assumptions. The modifiers are defined as the ratios of the measured Higgs boson yields and their SM expectations, denoted by the superscript "SM",

$$\mu_{if} = \frac{\sigma_i}{\sigma_i^{\mathrm{SM}}} \times \frac{B_f}{B_f^{\mathrm{SM}}}. \qquad (2)$$

The SM expectation by definition corresponds to $\mu_{if} = 1$. The uncertainties in the SM predictions are included as nuisance parameters in the measurement of the signal strength modifiers, following the methodology introduced in Sec. IV, where the procedures to decompose the uncertainties are also described.

In the model used in this section, all the μ_{if} are set to a global signal strength μ, describing a common scaling of the expected Higgs boson yield in all categories. Its combined measurement is

$$\mu = 1.11^{+0.09}_{-0.08} = 1.11 \pm 0.05(\mathrm{stat})^{+0.05}_{-0.04}(\mathrm{exp})^{+0.05}_{-0.04}(\mathrm{sig\ th})$$
$$\pm 0.03(\mathrm{bkg\ th})$$

where the total uncertainty is decomposed into components for statistical uncertainties, experimental systematic uncertainties, and theory uncertainties in signal and background modeling. The signal theory component includes uncertainties due to missing higher-order perturbative QCD and electroweak corrections in the MC simulation, uncertainties in PDF and α_s values, the treatment of the underlying event, the matching between the hard-scattering process and the parton shower, choice of hadronization models, and branching fraction uncertainties. The measurement is consistent with the SM prediction with a p-value of $p_{\mathrm{SM}} = 18\%$, computed using the procedure defined in Sec. IV with one d.o.f. The value of $-2 \ln \Lambda(\mu)$ as a function of μ is shown in Fig. 1, for the full likelihood and the versions with sets of nuisance parameters fixed to their best-fit values to obtain the components of the uncertainty.
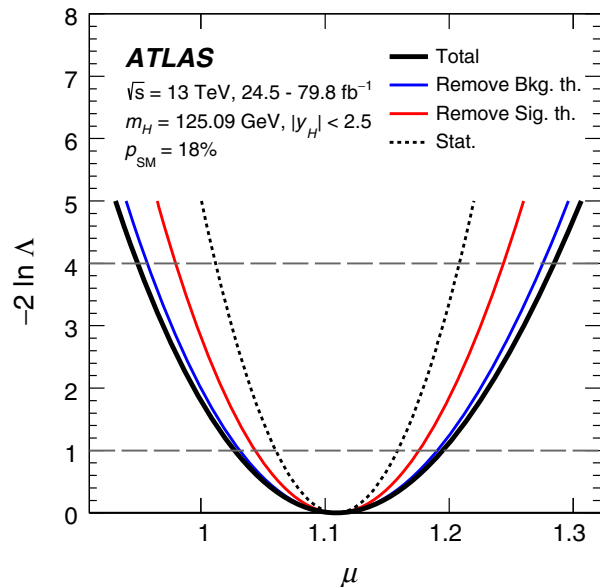

FIG. 1. Variations of $-2 \ln \Lambda(\mu)$ as a function of μ with all systematic uncertainties included (solid black line), with parameters describing theory uncertainties in background processes fixed to their best-fit values (solid blue line), with the same procedure also applied to theory uncertainties in the signal process (solid red line) and to all systematic uncertainties, so that only statistical uncertainties remain (dotted black line). The dashed horizontal lines show the levels $-2 \ln \Lambda(\mu) = 1$ and $-2 \ln \Lambda(\mu) = 4$ which are used to define, respectively, the 1σ and 2σ confidence intervals for μ.

Table III shows a summary of the leading uncertainties in the combined measurement of the global signal strength. The dominant uncertainties arise from the theory modeling of the signal and background processes in simulation. Further important uncertainties relate to the luminosity measurement; the selection efficiencies, energy scale and energy resolution of electrons and photons; the estimate of lepton yields from heavy-flavor decays, photon conversions or misidentified hadronic jets (classified as *background modeling* in the table); the jet energy scale and resolution, and the identification of heavy-flavor jets.

B. Production cross sections

Higgs boson production is studied in each of its main production modes. The production mechanisms considered are ggF, VBF, WH, ZH (including $gg \rightarrow ZH$), and the combination of $t\bar{t}H$ and tH ($t\bar{t}H + tH$). In cases where several processes are combined, the combination assumes the relative fractions of each component to be as in the SM, with theory uncertainties assigned. The small contribution from $b\bar{b}H$ is grouped with ggF. Cross sections are reported in the region $|y_H| < 2.5$ of the Higgs boson rapidity y_H. Results are obtained in a simultaneous fit to the data, with the cross sections of each production mechanism as parameters of interest. Higgs boson decay branching

TABLE III. Summary of the relative uncertainties $\Delta\mu/\mu$ affecting the measurement of the combined global signal strength μ. "Other" refers to the combined effect of the sources of experimental systematic uncertainty not explicitly listed in the table. The sum in quadrature of systematic uncertainties from individual sources differs from the uncertainty evaluated for the corresponding group in general, due to the presence of small correlations between nuisance parameters describing the different sources and other effects which are not taken into account in the procedure described in Sec. IV.

Uncertainty source	$\Delta\mu/\mu$ [%]
Statistical uncertainty	4.4
Systematic uncertainties	6.2
Theory uncertainties	4.8
Signal	4.2
Background	2.6
Experimental uncertainties (excl. MC stat.)	4.1
Luminosity	2.0
Background modeling	1.6
Jets, E_T^{miss}	1.4
Flavor tagging	1.1
Electrons, photons	2.2
Muons	0.2
τ-lepton	0.4
Other	1.6
MC statistical uncertainty	1.7
Total uncertainty	7.6

fractions are set to their SM values, within the uncertainties specified in Ref. [35].

The results are shown in Fig. 2 and Table IV. The leading sources of uncertainty in the production cross section measurements are summarized in Table V, with uncertainties

computed as described in Sec. IV. The measured $t\bar{t}H + tH$ production cross section differs from the $t\bar{t}H$ cross section reported in Ref. [12], even after accounting for the difference between the $|y_H| < 2.5$ region used in this paper and the inclusive phase space considered in Ref. [12]. This is due in part to the inclusion of tH, which in Ref. [12] is fixed to the SM expectation and not included in the reported $t\bar{t}H$ cross section, as well as to better control of systematic effects, especially those related to photon energy scale and resolution, due to the $H \to \gamma\gamma$ categories targeting other processes which are included in this combination, as described in Sec. III A. The correlations between the measured cross sections, shown in Figure 3, are significantly reduced relative to previous analyses [9,145].

A modest correlation of -15% between the ggF and VBF processes remains, however, because of contributions from ggF production in the VBF-enriched selections. The probability of compatibility between the measurement and the SM prediction corresponds to a p-value of $p_{\text{SM}} = 76\%$, computed using the procedure outlined in Sec. IV with five d.o.f.

Figure 4 shows the observed likelihood contours in the plane of σ_{ggF} versus σ_{VBF} from individual channels and the combined fit, together with the SM prediction. The cross sections for the other production modes are profiled.

Significances above 5σ are observed for the combined measurements of the ggF, VBF, VH and $t\bar{t}H + tH$ production processes. For the VBF process, the observed (expected) significance is 6.5σ (5.3σ). For the WH and ZH modes, these are respectively 3.5σ (2.7σ) and 3.6σ (3.6σ). Combining WH and ZH production into a single VH process, with the ratio of WH to ZH production set to its SM value leads to an observed (expected) significance for
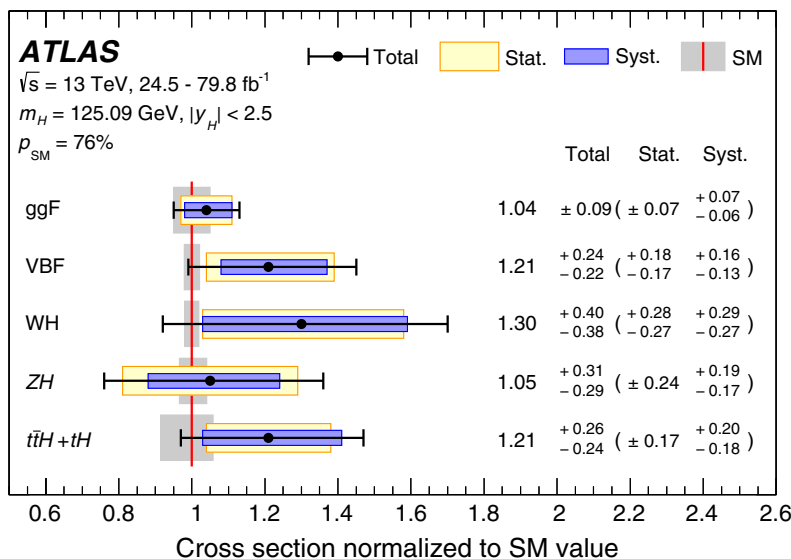

FIG. 2. Cross sections for ggF, VBF, WH, ZH and $t\bar{t}H + tH$ normalized to their SM predictions, measured with the assumption of SM branching fractions. The black error bars, blue boxes and yellow boxes show the total, systematic, and statistical uncertainties in the measurements, respectively. The gray bands indicate the theory uncertainties in the cross section predictions.

TABLE IV. Best-fit values and uncertainties for the production cross sections of the Higgs boson, assuming SM values for its decay branching fractions. The total uncertainties are decomposed into components for data statistics (Stat.), experimental systematic uncertainties (Exp.), and theory uncertainties in the modeling of the signal (Sig. th.) and background (Bkg. th.) processes. SM predictions are shown for the cross section of each production process. They are obtained from the inclusive cross sections and associated uncertainties reported in Ref. [35], multiplied by an acceptance factor for the region $|y_H| < 2.5$ computed using the Higgs boson simulation samples described in Sec. II. The observed (obs.) and expected (exp.) significances of the observed signals relative to the no-signal hypothesis are also shown for all processes except ggF, which was observed in Run 1. For the WH and ZH modes, a combined VH significance is reported assuming the SM value of the ratio of WH to ZH production.

| | | Uncertainty [pb] | | | | | | Significance |
Process ($\|y_H\| < 2.5$)	Value [pb]	Total	Data statistics	Experimental systematic uncertainties	Signal theory	Background theory	SM prediction [pb]	Observed (Expected)
ggF	46.5	± 4.0	± 3.1	± 2.2	± 0.9	± 1.3	44.7 ± 2.2	$\cdots$
VBF	4.25	$^{+0.84}_{-0.77}$	$^{+0.63}_{-0.60}$	$^{+0.35}_{-0.32}$	$^{+0.42}_{-0.32}$	$^{+0.14}_{-0.11}$	3.515 ± 0.075	6.5 (5.3)
WH	1.57	$^{+0.48}_{-0.46}$	$^{+0.34}_{-0.33}$	$^{+0.25}_{-0.24}$	$^{+0.11}_{-0.07}$	± 0.20	1.204 ± 0.024	3.5 (2.7)
ZH	0.84	$^{+0.25}_{-0.23}$	± 0.19	± 0.09	$^{+0.07}_{-0.04}$	± 0.10	$0.797^{+0.033}_{-0.026}$	3.6 (3.6)
$t\bar{t}H + tH$	0.71	$^{+0.15}_{-0.14}$	± 0.10	$^{+0.07}_{-0.06}$	$^{+0.05}_{-0.04}$	$^{+0.08}_{-0.07}$	$0.586^{+0.034}_{-0.049}$	5.8 (5.4)

(WH and ZH combined: 5.3 (4.7))

this process of 5.3σ (4.7σ). For the combination of $t\bar{t}H$ and tH production, the observed (expected) significance is 5.8σ (5.4σ).

C. Products of production cross sections and branching fractions

A description of both the production and decay mechanisms of the Higgs boson is obtained by considering the products $(\sigma \times B)_{if}$ of the cross section in production process i and branching fraction to final state f. The production processes are defined as in Sec. V B except for the fact that the WH and ZH processes, which cannot be reliably determined in all decay channels except $H \to b\bar{b}$, are considered together as a single VH process, with the ratio of WH to ZH cross sections fixed to its SM value within uncertainties. The decay modes considered are $H \to \gamma\gamma$, $H \to ZZ^*$, $H \to WW^*$, $H \to \tau\tau$ and $H \to b\bar{b}$. There are in total 20 such independent products, but the analyses included in the combination provide little sensitivity to ggF production in the $H \to b\bar{b}$ decay mode, and to VH production in the $H \to WW^*$ and $H \to \tau\tau$ decay modes. The corresponding products are therefore fixed to their SM

TABLE V. Summary of the uncertainties affecting the production cross section measurements. "Other" refers to the combined effect of the sources of experimental systematic uncertainty not explicitly listed in the table. The sum in quadrature of systematic uncertainties from individual sources differs from the uncertainty evaluated for the corresponding group in general, due to the presence of small correlations between nuisance parameters describing the different sources and other effects which are not taken into account in the procedure described in Sec. IV.

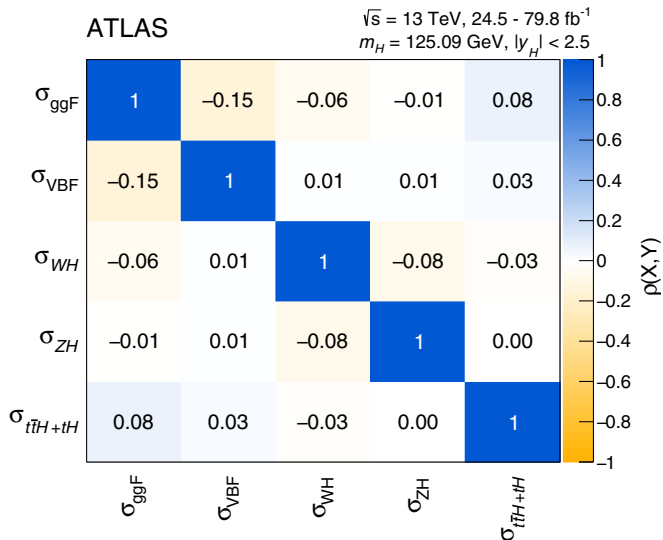| Uncertainty source	$\frac{\Delta\sigma_{ggF}}{\sigma_{ggF}}$ [%]	$\frac{\Delta\sigma_{VBF}}{\sigma_{VBF}}$ [%]	$\frac{\Delta\sigma_{WH}}{\sigma_{WH}}$ [%]	$\frac{\Delta\sigma_{ZH}}{\sigma_{ZH}}$ [%]	$\frac{\Delta\sigma_{t\bar{t}H+tH}}{\sigma_{t\bar{t}H+tH}}$ [%]
Statistical uncertainties	6.4	15	21	23	14
Systematic uncertainties	6.2	12	22	17	15
Theory uncertainties	3.4	9.2	14	14	12
Signal	2.0	8.7	5.8	6.7	6.3
Background	2.7	3.0	13	12	10
Experimental uncertainties (excl. MC stat.)	5.0	6.5	9.9	9.6	9.2
Luminosity	2.1	1.8	1.8	1.8	3.1
Background modeling	2.5	2.2	4.7	2.9	5.7
Jets, E_T^{miss}	0.9	5.4	3.0	3.3	4.0
Flavor tagging	0.9	1.3	7.9	8.0	1.8
Electrons, photons	2.5	1.7	1.8	1.5	3.8
Muons	0.4	0.3	0.1	0.2	0.5
τ-lepton	0.2	1.3	0.3	0.1	2.4
Other	2.5	1.2	0.3	1.1	0.8
MC statistical uncertainties	1.6	4.8	8.8	7.9	4.4
Total uncertainties	8.9	19	30	29	21

FIG. 3. Correlation matrix for the measurement of production cross sections of the Higgs boson, assuming SM values for its decay branching fractions.

FIG. 5. Cross sections times branching fraction for ggF, VBF, VH and $t\bar{t}H + tH$ production in each relevant decay mode, normalized to their SM predictions. The values are obtained from a simultaneous fit to all channels. The cross sections of the ggF, $H \to b\bar{b}$, VH, $H \to WW^*$ and VH, $H \to \tau\tau$ processes are fixed to their SM predictions. Combined results for each production mode are also shown, assuming SM values for the branching fractions into each decay mode. The black error bars, blue boxes and yellow boxes show the total, systematic, and statistical uncertainties in the measurements, respectively. The gray bands show the theory uncertainties in the predictions.

values within uncertainties. For the same reason, in $t\bar{t}H$ production the $H \to ZZ^*$ decay mode is considered together with $H \to WW^*$ as a single $H \to VV^*$ process, with the ratio of $H \to ZZ^*$ to $H \to WW^*$ fixed to its SM value. The results are obtained from a simultaneous fit of all input analyses, with the 16 independent $(\sigma \times B)$ products defined above as
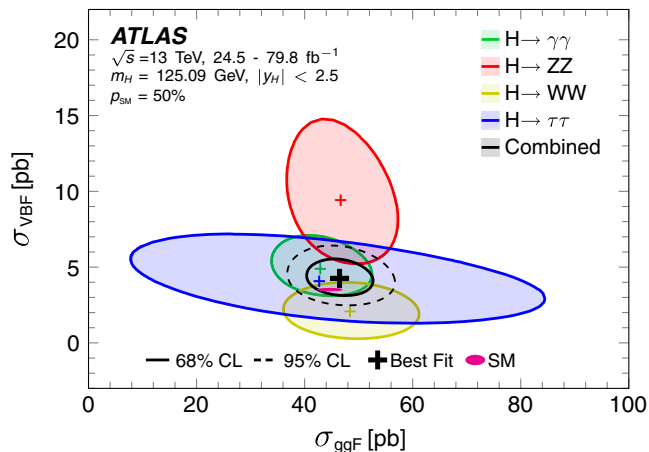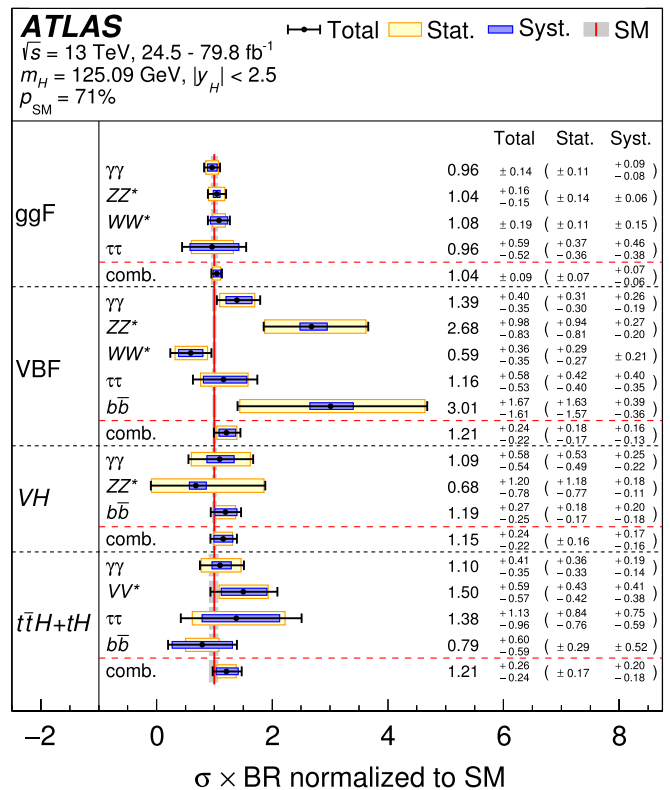

FIG. 4. Observed likelihood contours in the plane of σ_{VBF} versus σ_{ggF} from individual channels and the combined fit. Contours for 68% CL, defined in the asymptotic approximation by $-2 \ln \Lambda = 2.28$, are shown as solid lines. The 95% CL contour for the combined fit, corresponding to $-2 \ln \Lambda = 5.99$, is also shown as a dashed line. The crosses indicate the best-fit values, and the solid ellipse the SM prediction. Higgs boson branching fractions are fixed to their SM values within theory uncertainties. The probability of compatibility between the combined measurement and the SM prediction, estimated using the procedure outlined in the text with two d.o.f., corresponds to a p-value of $p_{\mathrm{SM}} = 50\%$.

parameters of interest. They are shown in Figure 5 and Table VI. The correlation matrix of the measurements is shown in Figure 6. The largest terms in absolute value are between the $t\bar{t}H, H \to VV^*$ and $t\bar{t}H, H \to \tau\tau$ processes, and between the ggF, $H \to \tau\tau$ and VBF, $H \to \tau\tau$ processes. In both cases, this is due to cross-contamination between these processes in the analyses providing the most sensitive measurements. The probability of compatibility between the measurement and the SM prediction corresponds to a p-value of $p_{\mathrm{SM}} = 71\%$, computed using the procedure outlined in Sec. IV with 16 d.o.f.

D. Ratios of cross sections and branching fractions

The products $(\sigma \times B)_{if}$ described in Sec. V C can be expressed as

$$(\sigma \times B)_{if} = \sigma_{\mathrm{ggF}}^{ZZ} \cdot \left(\frac{\sigma_i}{\sigma_{\mathrm{ggF}}}\right) \cdot \left(\frac{B_f}{B_{ZZ}}\right),$$

TABLE VI. Best-fit values and uncertainties for the production cross sections times branching fractions of the Higgs boson, for the combinations in which sufficient sensitivity is provided by the input analyses. Combinations not shown in the table are fixed to their SM values within uncertainties. For $t\bar{t}H + tH$ production, $H \to VV^*$ refers to the combination of $H \to WW^*$ and $H \to ZZ^*$, with a relative weight fixed by their respective SM branching fractions. The total uncertainties are decomposed into components for data statistics (Stat.), experimental systematic uncertainties (Exp.), and theory uncertainties in the modeling of the signal (Sig. th.) and background (Bkg. th.) processes. SM predictions [35] are shown for each process.

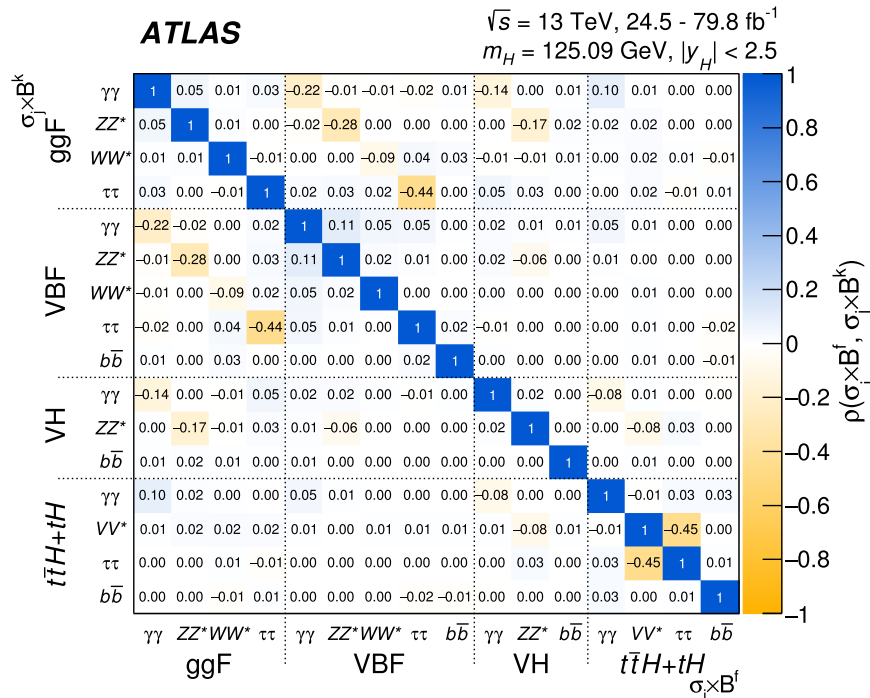| Process ($\|y_H\| < 2.5$)	Value [fb]	Uncertainty [fb]					SM prediction [fb]
		Total	Data statistics	Experimental systematic uncertainties	Signal theory	Background theory	
ggF, $H \to \gamma\gamma$	97	± 14	± 11	± 8	± 2	$^{+2}_{-1}$	101.5 ± 5.3
ggF, $H \to ZZ^*$	1230	$^{+190}_{-180}$	± 170	± 60	± 20	± 20	1181 ± 61
ggF, $H \to WW^*$	10400	± 1800	± 1100	± 1100	± 400	$^{+1000}_{-900}$	9600 ± 500
ggF, $H \to \tau\tau$	2700	$^{+1700}_{-1500}$	± 1000	± 900	$^{+800}_{-300}$	± 400	2800 ± 140
VBF, $H \to \gamma\gamma$	11.1	$^{+3.2}_{-2.8}$	$^{+2.5}_{-2.4}$	$^{+1.4}_{-1.0}$	$^{+1.5}_{-1.1}$	$^{+0.3}_{-0.2}$	7.98 ± 0.21
VBF, $H \to ZZ^*$	249	$^{+91}_{-77}$	$^{+87}_{-75}$	$^{+16}_{-11}$	$^{+17}_{-12}$	$^{+9}_{-7}$	92.8 ± 2.3
VBF, $H \to WW^*$	450	$^{+270}_{-260}$	$^{+220}_{-200}$	$^{+120}_{-130}$	$^{+80}_{-70}$	$^{+70}_{-80}$	756 ± 19
VBF, $H \to \tau\tau$	260	$^{+130}_{-120}$	± 90	$^{+80}_{-70}$	$^{+30}_{-10}$	$^{+30}_{-20}$	220 ± 6
VBF, $H \to b\bar{b}$	6100	$^{+3400}_{-3300}$	$^{+3300}_{-3200}$	$^{+700}_{-600}$	± 300	± 300	2040 ± 50
VH, $H \to \gamma\gamma$	5.0	$^{+2.6}_{-2.5}$	$^{+2.4}_{-2.2}$	$^{+1.0}_{-0.9}$	± 0.5	± 0.1	$4.54^{+0.13}_{-0.12}$
VH, $H \to ZZ^*$	36	$^{+63}_{-41}$	$^{+62}_{-41}$	$^{+5}_{-4}$	$^{+6}_{-4}$	$^{+4}_{-2}$	52.8 ± 1.4
VH, $H \to b\bar{b}$	1380	$^{+310}_{-290}$	$^{+210}_{-200}$	± 150	$^{+120}_{-80}$	± 140	1162^{+31}_{-29}
$t\bar{t}H + tH$, $H \to \gamma\gamma$	1.46	$^{+0.55}_{-0.47}$	$^{+0.48}_{-0.44}$	$^{+0.19}_{-0.15}$	$^{+0.17}_{-0.11}$	± 0.03	$1.33^{+0.08}_{-0.11}$
$t\bar{t}H + tH$, $H \to VV^*$	212	$^{+84}_{-81}$	$^{+61}_{-59}$	$^{+47}_{-44}$	$^{+17}_{-10}$	$^{+31}_{-30}$	142^{+8}_{-12}
$t\bar{t}H + tH$, $H \to \tau\tau$	51	$^{+41}_{-35}$	$^{+31}_{-28}$	$^{+26}_{-21}$	$^{+6}_{-4}$	$^{+8}_{-6}$	$36.7^{+2.2}_{-3.1}$
$t\bar{t}H + tH$, $H \to b\bar{b}$	270	± 200	± 100	± 80	$^{+40}_{-10}$	$^{+150}_{-160}$	341^{+20}_{-29}

FIG. 6. Correlation matrix for the measured values of the production cross sections times branching fractions of the Higgs boson, for the combinations in which sufficient sensitivity is provided by the input analyses.
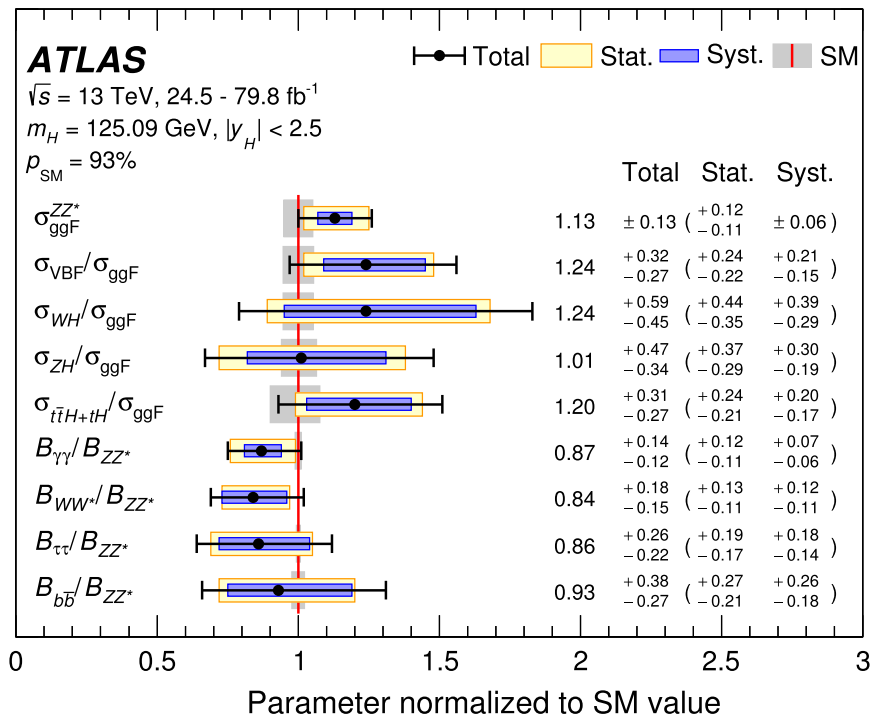
FIG. 7. Results of a simultaneous fit for $\sigma_{\mathrm{ggF}}^{ZZ}$, $\sigma_{\mathrm{VBF}}/\sigma_{\mathrm{ggF}}$, $\sigma_{WH}/\sigma_{\mathrm{ggF}}$, $\sigma_{ZH}/\sigma_{\mathrm{ggF}}$, $\sigma_{t\bar{t}H+tH}/\sigma_{\mathrm{ggF}}$, $B_{\gamma\gamma}/B_{ZZ}$, B_{WW}/B_{ZZ}, $B_{\tau\tau}/B_{ZZ}$, and B_{bb}/B_{ZZ}. The fit results are normalized to the SM predictions. The black error bars, blue boxes and yellow boxes show the total, systematic, and statistical uncertainties in the measurements, respectively. The gray bands show the theory uncertainties in the predictions.

in terms of the cross section times branching fraction $\sigma_{\mathrm{ggF}}^{ZZ}$ for the reference process $gg \to H \to ZZ^*$, which is precisely measured and exhibits small systematic uncertainties, ratios of production cross sections to that of ggF, $\sigma_i/\sigma_{\mathrm{ggF}}$, and ratios of branching fractions to that of $H \to ZZ^*$, B_f/B_{ZZ}.

Results are shown in Fig. 7 and Table VII. The probability of compatibility between the measurements and the SM predictions corresponds to a p-value of $p_{\mathrm{SM}} = 93\%$, computed using the procedure outlined in Sec. IV with nine d.o.f.

TABLE VII. Best-fit values and uncertainties for $\sigma_{\mathrm{ggF}}^{ZZ}$, together with ratios of production cross sections normalized to σ_{ggF}, and ratios of branching fractions normalized to B_{ZZ}. The total uncertainties are decomposed into components for data statistics (Stat.), experimental systematic uncertainties (Exp.), and theory uncertainties in the modeling of the signal (Sig. th.) and background (Bkg. th.) processes. The SM predictions [35] are also shown with their total uncertainties.

Quantity	Value [pb]	Uncertainty					SM prediction
		Total	Data statistics	Experimental systematic uncertainties	Signal theory	Background theory	
$\sigma_{\mathrm{ggF}}^{ZZ}$	1.33	± 0.15	$+0.14$ -0.13	± 0.06	$+0.02$ -0.01	$+0.04$ -0.02	1.181 ± 0.061
$\sigma_{\mathrm{VBF}}/\sigma_{\mathrm{ggF}}$	0.097	$+0.025$ -0.021	$+0.019$ -0.017	$+0.010$ -0.008	$+0.011$ -0.008	$+0.006$ -0.005	0.0786 ± 0.0043
$\sigma_{WH}/\sigma_{\mathrm{ggF}}$	0.033	$+0.016$ -0.012	$+0.012$ -0.009	$+0.007$ -0.006	$+0.003$ -0.002	$+0.007$ -0.005	$0.0269 ^{+0.0014}_{-0.0015}$
$\sigma_{ZH}/\sigma_{\mathrm{ggF}}$	0.0180	$+0.0084$ -0.0061	$+0.0066$ -0.0052	$+0.0034$ -0.0021	$+0.0016$ -0.0009	$+0.0037$ -0.0025	$0.0178 ^{+0.0011}_{-0.0010}$
$\sigma_{t\bar{t}H+tH}/\sigma_{\mathrm{ggF}}$	0.0157	$+0.0041$ -0.0035	$+0.0031$ -0.0028	$+0.0020$ -0.0017	$+0.0012$ -0.0008	$+0.0013$ -0.0012	$0.0131 ^{+0.0010}_{-0.0013}$
$B_{\gamma\gamma}/B_{ZZ}$	0.075	$+0.012$ -0.010	$+0.010$ -0.009	$+0.006$ -0.005	± 0.001	± 0.002	0.0860 ± 0.0010
B_{WW}/B_{ZZ}	6.8	$+1.5$ -1.2	$+1.1$ -0.9	$+0.8$ -0.7	± 0.2	$+0.6$ -0.5	$8.15 \pm {<}0.01$
$B_{\tau\tau}/B_{ZZ}$	2.04	$+0.62$ -0.52	$+0.45$ -0.40	$+0.36$ -0.31	$+0.17$ -0.09	$+0.12$ -0.09	2.369 ± 0.017
B_{bb}/B_{ZZ}	20.5	$+8.4$ -5.9	$+5.9$ -4.6	$+3.7$ -2.4	$+1.3$ -0.9	$+4.2$ -2.9	22.00 ± 0.51

VI. COMBINED MEASUREMENTS OF SIMPLIFIED TEMPLATE CROSS SECTIONS

A. Simplified template cross section framework

Simplified template cross sections [35,36] are defined through a partition of the phase space of the SM Higgs production process into a set of nonoverlapping regions. These regions are defined in terms of the kinematics of the Higgs boson and, when they are present, of associated jets and W and Z bosons, independently of the Higgs boson decay process. They are chosen according to three criteria: sensitivity to deviations from the SM expectation, avoidance of large theory uncertainties in the corresponding SM predictions, and to approximately match experimental selections so as to minimize model-dependent extrapolations. Analysis selections do not, however, necessarily correspond exactly to the STXS regions.

All regions are defined for a Higgs boson rapidity y_H satisfying $|y_H| < 2.5$, corresponding approximately to the region of experimental sensitivity. Jets are reconstructed from all stable particles with a lifetime greater than 10 ps, excluding the decay products of the Higgs boson and leptons from W and Z boson decays, using the anti-k_t algorithm with a jet radius parameter $R = 0.4$, and must have a transverse momentum $p_{\mathrm{T,jet}} > 30$ GeV.

The measurements presented in this paper are based on the Stage 1 splitting of the STXS framework [35]. Higgs boson production is first classified according to the nature of the initial state and of associated particles, the latter including the decay products of W and Z bosons if they are present. These categories are, by order of decreasing selection priority: $t\bar{t}H$ and tH processes; $qq \to Hqq$ processes, with contributions from both VBF production and quark-initiated VH production with a hadronic decay of the gauge boson; $gg \to ZH$ with $Z \to q\bar{q}$; VH production with a leptonic decay of the vector boson ($V(\mathrm{lep})H$), including $gg \to ZH$ production; and finally the gluon–gluon fusion process. The last is considered together with $gg \to ZH$, $Z \to q\bar{q}$ production, as a single $gg \to H$ process. The $b\bar{b}H$ production mode is modeled as a 1% [35] increase of the $gg \to H$ yield in each STXS bin, since the acceptances for both processes are similar for all input analyses [35]. The $t\bar{t}H$ and tH processes are also combined in a single $t\bar{t}H + tH$ category, assuming the relative fraction of each component to be as in the SM, within uncertainties.

The analyses included in this paper provide only limited sensitivity to the cross section in some bins of the Stage 1 scheme, mainly due to limited data statistics in some regions. In other cases, they only provide sensitivity to a combination of bins, leading to strongly correlated measurements. To mitigate these effects, the results are presented in terms of a reduced splitting, with the measurement bins defined as merged groups of Stage 1 bins (and in the case of $V(\mathrm{lep})H$ with an additional splitting not
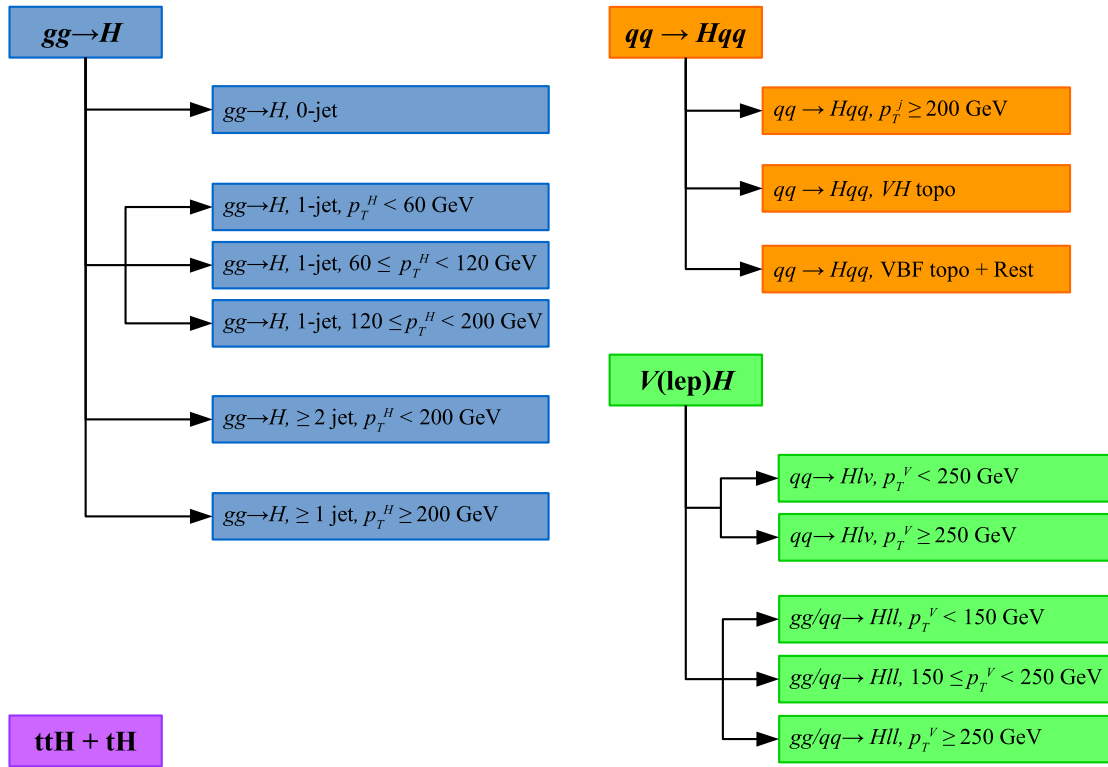

FIG. 8. Definition of the STXS measurement regions used in this paper. For each Higgs boson production process, the regions are defined starting from the top of the corresponding schematic, with regions nearer the top taking precedence if the selections overlap. The $b\bar{b}H$ production mode is considered as part of $gg \to H$.
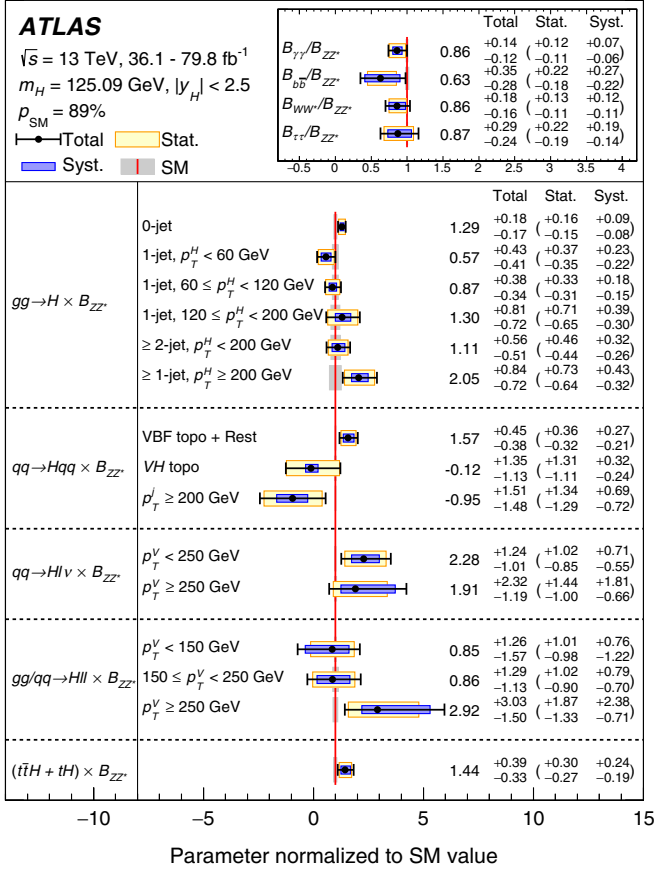
FIG. 9. Best-fit values and uncertainties for the cross sections in each measurement region and of the ratios of branching fractions B_f/B_{ZZ}, normalized to the SM predictions for the various parameters. The parameters directly extracted from the fit are the products $(\sigma_i \times B_{ZZ})$ and the ratios B_f/B_{ZZ}. The black error bar shows the total uncertainty in each measurement.

FIG. 10. Best-fit values and uncertainties for the cross sections in each measurement region and of the ratios of branching fractions B_f/B_{ZZ}. The parameters directly extracted from the fit are the products $(\sigma_i \times B_{ZZ})$ and the ratios B_f/B_{ZZ}; the former are shown divided by the SM value of B_{ZZ}. The black error bar shows the total uncertainty in each measurement.

present in the original Stage 1 scheme, as described below). These measurement bins are defined as follows for each process:

(i) $gg \to H$ is separated into regions defined by the jet multiplicity and the Higgs boson transverse momentum p_T^H. A region is defined for events with one or more jets and $p_T^H \geq 200$ GeV, providing sensitivity to deviations from the SM at high momentum transfer. The remaining events are separated into classes with 0, 1 and ≥ 2 jets in the final state. The one-jet category is further split in bins of p_T^H, probing perturbative QCD predictions and providing sensitivity to deviations from the SM. Three bins are defined with $p_T^H < 60$ GeV, 60 GeV $\leq p_T^H <$ 120 GeV and 120 GeV $\leq p_T^H < 200$ GeV.

(ii) $qq \to Hqq$ is separated into three regions. The first selects events in which the transverse momentum of the leading jet p_T^j is ≥ 200 GeV. A second region, denoted by *VH topo*, is defined by $p_T^j < 200$ GeV and the presence of two jets with an invariant mass

m_{jj} in the range $60 \leq m_{jj} < 120$ GeV, selecting events originating from VH production in particular. The remaining events are grouped into a third bin, denoted by *VBF topo+Rest*, which includes mainly the VBF-topology region (*VBF topo*) defined by the presence of two jets with $m_{jj} \geq 400$ GeV and a pseudorapidity difference $|\Delta\eta_{jj}| \geq 2.8$, as well as events that fall in none of the above selections (*Rest*). The measurement sensitivity for the corresponding cross section is provided mainly by the VBF-topology region, within which the cross section is measured precisely by the analyses targeting VBF production.

(iii) $V(\mathbf{lep})H$ is split into the two processes $qq \to WH$ and $pp \to ZH$, the latter including both quark-initiated and gluon-initiated production. These regions are further split according to p_T^V, the transverse momentum of the W or Z boson. For the $qq \to WH$ process two bins are defined for $p_T^V < 250$ GeV and $p_T^V \geq 250$ GeV, while for $pp \to ZH$ three bins are

defined for $p_T^V < 150$ GeV, 150 GeV $\leq p_T^V <$ 250 GeV and $p_T^V \geq 250$ GeV. This definition deviates from the one given in Ref. [35], where the $qq \to ZH$ and $gg \to ZH$ processes are measured separately and no splitting is performed at $p_T^V = 250$ GeV for $gg \to ZH$, given the limited sensitivity of the current measurements to separating the $qq \to ZH$ and $gg \to ZH$ processes.

The above merging scheme of Stage 1 bins is summarized in Figure 8.

Sensitivity to the 0-jet and 1-jet, $p_T^H < 60$ GeV regions of the $gg \to H$ process is provided mainly by the $H \to ZZ^* \to 4\ell$, $H \to \gamma\gamma$ and $H \to WW^* \to e\nu\mu\nu$ analyses, with the leading contribution in each region coming from $H \to WW^* \to e\nu\mu\nu$ and $H \to \gamma\gamma$ respectively. For the 1-jet, $60 \leq p_T^H < 120$ GeV region, the main contributions to the sensitivity are from $H \to ZZ^* \to 4\ell$ and $H \to \gamma\gamma$, dominated by the latter. The $H \to \gamma\gamma$ analysis also provides the largest sensitivity in the rest of the $gg \to H$ regions as

well as in the $qq \to Hqq$ sector, apart from the $p_T^j > 200$ GeV region for which $H \to \tau\tau$ dominates the sensitivity. The VH, $H \to b\bar{b}$ analysis provides the most sensitive measurements in the $V(\text{lep})H$ regions. Finally, the $H \to \gamma\gamma$ and $t\bar{t}H$ multilepton analyses provide the leading contributions to the measurement of the $t\bar{t}H + tH$ region.

The measured event yields are described by Eq. (1), with parameters of interest of the form $(\sigma \times B)_{if}$ denoting the cross section times branching fraction in STXS region i and decay channel f. The acceptance factors $(\epsilon \times A)_{if}^k$ for each analysis category k are determined from SM Higgs boson production processes, modeled using the samples described in Sec. II, and act as templates in the fits of the STXS cross sections to the data. The dependence on the theory assumptions is less than in the measurement of the total cross sections in each production mode, since the $(\epsilon \times A)_{if}^k$ are computed over smaller regions. Assumptions about the kinematics within a given STXS region lead to some

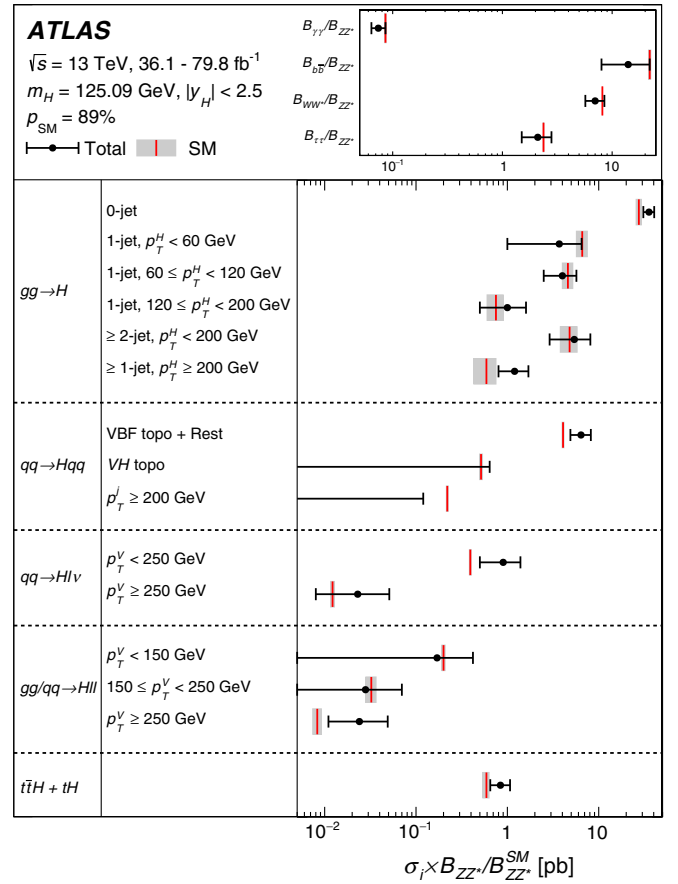TABLE VIII. Best-fit values and uncertainties for the cross sections in each measurement region, and of the ratios of branching fractions B_f/B_{ZZ}. The total uncertainties are decomposed into components for data statistics (Stat.) and systematic uncertainties (Syst.). The SM predictions [35] are also shown for each quantity with their total uncertainties. The parameters directly extracted from the fit are the products $(\sigma_i \times B_{ZZ})$ and the ratios B_f/B_{ZZ}; the former are shown divided by the SM value of B_{ZZ}.

Measurement region $((\sigma_i \times B_{ZZ})/B_{ZZ}^{SM})$	Value [pb]	Uncertainty [pb]			SM prediction [pb]
		Total	Data statistics	Systematic uncertainties	
$gg \to H, 0\text{-jet}$	35.5	$+5.0$ -4.7	$+4.4$ -4.1	$+2.5$ -2.2	27.5 ± 1.8
$gg \to H, 1\text{-jet}, p_T^H < 60$ GeV	3.7	$+2.8$ -2.7	$+2.4$ -2.3	$+1.5$ -1.4	6.6 ± 0.9
$gg \to H, 1\text{-jet}, 60 \leq p_T^H < 120$ GeV	4.0	$+1.7$ -1.5	$+1.5$ -1.4	$+0.8$ -0.7	4.6 ± 0.6
$gg \to H, 1\text{-jet}, 120 \leq p_T^H < 200$ GeV	1.0	$+0.6$ -0.5	± 0.5	$+0.3$ -0.2	0.75 ± 0.15
$gg \to H, \geq 1-\text{jet}, p_T^H \geq 200$ GeV	1.2	$+0.5$ -0.4	± 0.4	$+0.3$ -0.2	0.59 ± 0.16
$gg \to H, \geq 2\text{-jet}, p_T^H < 200$ GeV	5.4	$+2.7$ -2.5	$+2.2$ -2.1	$+1.5$ -1.3	4.8 ± 1.0
$qq \to Hqq, \text{VBF topo} + \text{Rest}$	6.4	$+1.8$ -1.5	$+1.5$ -1.3	$+1.1$ -0.9	4.07 ± 0.09
$qq \to Hqq, VH \text{ topo}$	-0.06	$+0.70$ -0.58	$+0.68$ -0.57	$+0.16$ -0.12	0.515 ± 0.019
$qq \to Hqq, p_T^j \geq 200$ GeV	-0.21	± 0.33	$+0.29$ -0.28	$+0.15$ -0.16	0.220 ± 0.005
$qq \to H\ell\nu, p_T^V < 250$ GeV	0.90	$+0.49$ -0.40	$+0.40$ -0.33	$+0.28$ -0.22	0.393 ± 0.009
$qq \to H\ell\nu, p_T^V \geq 250$ GeV	0.023	$+0.028$ -0.015	$+0.018$ -0.012	$+0.022$ -0.008	0.0122 ± 0.0006
$gg/qq \to H\ell\ell, p_T^V < 150$ GeV	0.17	$+0.25$ -0.31	± 0.20	$+0.15$ -0.24	0.200 ± 0.008
$gg/qq \to H\ell\ell, 150 \leq p_T^V < 250$ GeV	0.028	$+0.042$ -0.037	$+0.033$ -0.029	$+0.026$ -0.023	0.0324 ± 0.0041
$gg/qq \to H\ell\ell, p_T^V \geq 250$ GeV	0.024	$+0.025$ -0.013	$+0.016$ -0.011	$+0.020$ -0.006	0.0083 ± 0.0009
$t\bar{t}H + tH$	0.84	$+0.23$ -0.19	$+0.18$ -0.16	$+0.14$ -0.11	$0.59^{+0.04}_{-0.05}$

Branching fraction ratio	Value	Uncertainty			SM prediction
		Total	Data statistics	Systematic uncertainties	
$B_{\gamma\gamma}/B_{ZZ}$	0.074	$+0.012$ -0.010	$+0.010$ -0.009	$+0.006$ -0.005	0.0860 ± 0.0010
$B_{b\bar{b}}/B_{ZZ}$	14	$+8$ -6	$+5$ -4	$+6$ -5	22.0 ± 0.5
B_{WW}/B_{ZZ}	7.0	$+1.5$ -1.3	$+1.1$ -0.9	$+1.0$ -0.9	$8.15 \pm <0.01$
$B_{\tau\tau}/B_{ZZ}$	2.1	$+0.7$ -0.6	± 0.5	$+0.5$ -0.3	2.37 ± 0.02

model-dependence, which can be reduced further by using a finer splitting of the phase space, as allowed by experimental precision. Results using a splitting finer than the one described in this section are presented in Appendix.

Theory uncertainties for the $gg \to H$ and $qq \to Hqq$ processes are defined as in Ref. [10], while those of the $V(\text{lep})H$ process follow the scheme described in Ref. [146]. For the measurement bins defined by merging several bins of the STXS Stage-1 framework, the $(\epsilon \times A)$ factors are determined assuming that the relative fractions of each Stage-1 bin are as in the SM, and SM uncertainties in these fractions are taken into account.

B. Results

The fit parameters chosen for the combined STXS measurements are the cross sections for Higgs boson production in STXS region i times the branching fraction for the $H \to ZZ^*$ decay, $(\sigma \times B)_{i,ZZ}$, and the ratios of branching fractions B_f/B_{ZZ} for the other final states f. Similarly to the ratio model in Sec. V D, the cross sections times branching fractions for final states other than ZZ are parametrized as

$$(\sigma \times B)_{if} = (\sigma \times B)_{i,ZZ} \cdot \left(\frac{B_f}{B_{ZZ}}\right).$$

The results are shown in Figs. 9 and 10 and in Table VIII. The observed upper limits at 95% CL on the cross sections

in the $qq \to Hqq, VH$ topo and $qq \to Hqq, p_T^j \geq 200$ GeV bins are found to be 1.45 pb and 0.59 pb, respectively, taking into account the physical bound on the parameter values as discussed in Sec. IV. The corresponding expected upper limits are 1.53 pb and 0.80 pb, respectively.

The correlations between the measured parameters are shown in Fig. 11. The largest anticorrelations are between $B_{b\bar{b}}/B_{ZZ}$ and the cross section measurements in the $V(\text{lep})H$ region, since the $VH, H \to b\bar{b}$ analysis is sensitive to products of these quantities; between the cross section measurement in the $gg \to H$ 0-jet region and both $B_{\gamma\gamma}/B_{ZZ}$ and B_{WW}/B_{ZZ}, since the $H \to \gamma\gamma$, $H \to ZZ^* \to 4\ell$ and $H \to WW^* \to e\nu\mu\nu$ decay channels provide the most precise measurements in this region; between $B_{\gamma\gamma}/B_{ZZ}$ and the cross section measurement in the $qq \to Hqq$, VBF topo + Rest region, since there is a tension between the $H \to \gamma\gamma$ and $H \to ZZ^* \to 4\ell$ measurements in this region; between $B_{\tau\tau}/B_{ZZ}$ and the cross section measurement in the $p_T^H > 200$ GeV region, since the high-p_T^H channels of the $H \to \tau\tau$ analysis are sensitive to their product; and between the cross section measurements in the $qq \to Hqq, p_T^j \geq 200$ GeV and $gg \to H$, $\geq$1-jet, $p_T^H \geq 200$ GeV regions on the one hand, and the $qq \to Hqq, p_T^j \geq 200$ GeV and $gg \to H$, 1-jet, $120 \leq p_T^H < 200$ GeV regions on the other hand, since in both cases there is cross contamination between these processes in the experimental selections.

ATLAS $\sqrt{s}$ = 13 TeV, 36.1 - 79.8 fb^{-1}
m_H = 125.09 GeV, $|y_H| < 2.5$

	(1)	(2)	(3)	(4)	(5)	(6)	(7)	(8)	(9)	(10)	(11)	(12)	(13)	(14)	(15)	(16)	(17)	(18)	(19)
(1) 0-jet	1	−0.27	0.18	0.18	0.00	0.22	0.32	0.03	−0.01	0.15	0.12	0.03	0.08	0.12	0.33	−0.52	−0.17	−0.50	−0.25
(2) 1-jet, $p_T^H < 60$ GeV	−0.27	1	−0.17	−0.08	0.07	−0.01	−0.02	−0.01	0.04	0.00	0.01	0.01	0.00	0.02	0.04	−0.06	−0.02	−0.05	−0.01
(3) 1-jet, $60 \leq p_T^H < 120$ GeV	0.18	−0.17	1	0.09	−0.22	0.05	−0.04	0.05	0.07	0.02	0.03	−0.01	0.02	0.02	0.06	−0.10	−0.03	−0.13	−0.01
(4) 1-jet, $120 \leq p_T^H < 200$ GeV	0.18	−0.08	0.09	1	−0.17	0.01	−0.01	0.05	0.08	0.03	0.04	−0.01	0.02	0.04	0.11	−0.13	−0.05	−0.11	−0.18
(5) $\geq$ 2-jet, $p_T^H < 200$ GeV	0.00	0.07	−0.22	−0.17	1	−0.03	−0.26	−0.42	−0.01	0.04	0.03	0.02	0.01	0.04	0.08	−0.21	−0.05	0.03	−0.07
(6) $\geq$ 1-jet, $p_T^H \geq 200$ GeV	0.22	−0.01	0.05	0.01	−0.03	1	0.31	−0.15	−0.55	0.08	0.06	0.03	0.04	0.07	0.20	−0.35	−0.09	−0.15	−0.41
(7) VBF topo + Rest	0.32	−0.02	−0.04	−0.01	−0.26	0.31	1	0.13	−0.30	0.12	0.10	0.05	0.05	0.10	0.29	−0.42	−0.14	−0.45	−0.26
(8) VH topo	0.03	−0.01	0.05	0.05	−0.42	−0.15	0.13	1	0.09	0.00	0.00	−0.01	0.00	0.00	0.01	0.03	0.00	−0.05	−0.01
(9) $p_T^j \geq 200$ GeV	−0.01	0.04	0.07	0.08	−0.01	−0.55	−0.30	0.09	1	−0.02	−0.01	−0.02	−0.01	−0.01	−0.03	0.07	0.02	−0.05	−0.06
(10) $p_T^V < 250$ GeV	0.15	0.00	0.02	0.03	0.04	0.08	0.12	0.00	−0.02	1	0.12	−0.15	0.05	0.39	0.17	−0.24	−0.45	−0.13	−0.10
(11) $p_T^V \geq 250$ GeV	0.12	0.01	0.03	0.04	0.03	0.06	0.10	0.00	−0.01	0.12	1	0.19	0.21	0.47	0.22	−0.18	−0.72	−0.12	−0.10
(12) $p_T^V < 150$ GeV	0.03	0.01	−0.01	−0.01	0.02	0.03	0.05	−0.01	−0.02	−0.15	0.19	1	−0.05	−0.19	−0.01	−0.09	0.26	−0.03	−0.02
(13) $150 \leq p_T^V < 250$ GeV	0.08	0.00	0.02	0.02	0.01	0.04	0.05	0.00	−0.01	0.05	0.21	−0.05	1	−0.20	0.09	−0.11	−0.23	−0.06	−0.05
(14) $p_T^V \geq 250$ GeV	0.12	0.02	0.02	0.04	0.04	0.07	0.10	0.00	−0.01	0.39	0.47	−0.19	−0.20	1	0.23	−0.19	−0.73	−0.12	−0.10
(15) $(t\bar{t}H + tH) \times B_{ZZ^*}$	0.33	0.04	0.06	0.11	0.08	0.20	0.29	0.01	−0.03	0.17	0.22	−0.01	0.09	0.23	1	−0.45	−0.31	−0.39	−0.33
(16) $B_{\gamma\gamma}/B_{ZZ^*}$	−0.52	−0.06	−0.10	−0.13	−0.21	−0.35	−0.42	0.03	0.07	−0.24	−0.18	−0.09	−0.11	−0.19	−0.45	1	0.26	0.45	0.39
(17) $B_{b\bar{b}}/B_{ZZ^*}$	−0.17	−0.02	−0.03	−0.05	−0.05	−0.09	−0.14	0.00	0.02	0.45	−0.72	0.26	−0.23	−0.73	−0.31	0.26	1	0.17	0.14
(18) B_{WW}/B_{ZZ^*}	−0.50	−0.05	−0.13	−0.11	0.03	−0.15	−0.45	−0.05	−0.05	−0.13	−0.12	−0.03	−0.06	−0.12	−0.39	0.45	0.17	1	0.25
(19) $B_{\tau\tau}/B_{ZZ^*}$	−0.25	−0.01	−0.01	−0.18	−0.07	−0.41	−0.26	−0.01	−0.06	−0.10	−0.10	−0.02	−0.05	−0.10	−0.33	0.39	0.14	0.25	1

Row/column groups: (1)–(6) $gg \to H \times B_{ZZ^*}$; (7)–(9) $qq \to Hqq \times B_{ZZ^*}$; (10)–(11) $qq \to Hl\nu \times B_{ZZ^*}$; (12)–(14) $gg/qq \to Hll \times B_{ZZ^*}$; (15) $(t\bar{t}H + tH) \times B_{ZZ^*}$; (16)–(19) branching-fraction ratios.
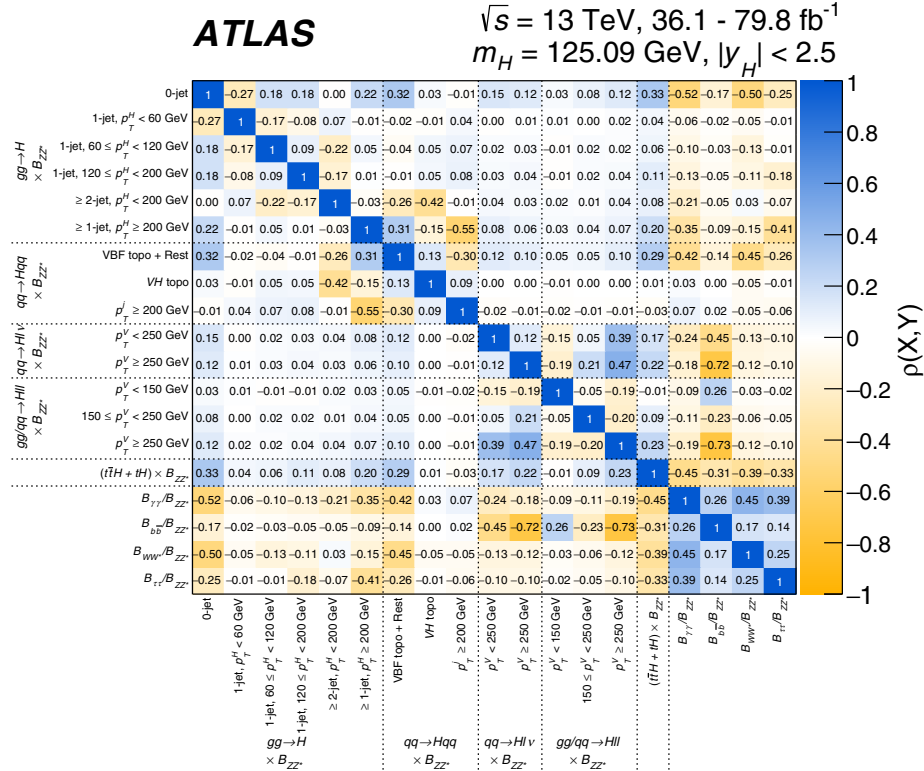
FIG. 11. Correlation matrix for the measured values of the simplified template cross sections and ratios of branching fractions. The fit parameters are the products $(\sigma_i \times B_{ZZ})$ and the ratios B_f/B_{ZZ}.

The largest positive correlations are between the $(W \to \ell\nu)H$ and $(Z \to \ell\ell)H$ measurement regions, related to their strong anticorrelation with $B_{b\bar{b}}/B_{ZZ}$; and between $B_{\gamma\gamma}/B_{ZZ}$ and B_{WW}/B_{ZZ}, due to their strong anticorrelation with the cross section measurement in the 0-jet region.

The results show good overall agreement with the SM predictions in a range of kinematic regions of Higgs boson production processes. The probability of compatibility between the measurement and the SM prediction corresponds to a p-value of $p_{\text{SM}} = 89\%$, computed using the procedure outlined in Sec. IV with 19 d.o.f.

VII. INTERPRETATION OF RESULTS IN THE κ FRAMEWORK

When testing the Higgs boson coupling strengths, the production cross sections σ_i, decay branching fractions B_f and the signal-strength parameters μ_{if} defined in Eq. (2) cannot be treated independently, as each observed process involves at least two Higgs boson coupling strengths. Scenarios with a consistent treatment of coupling strengths in Higgs boson production and decay modes are presented in this section.

A. Framework for coupling-strength measurements

Coupling-strength modifiers κ are introduced to study modifications of the Higgs boson couplings related to BSM physics, within a framework [37] (κ-framework) based on the leading-order contributions to each production and decay process. Within the assumptions made in this framework, the Higgs boson production and decay can be factorized, such that the cross section times branching fraction of an individual channel $\sigma(i \to H \to f)$ contributing to a measured signal yield is parametrized as

$$\sigma_i \times B_f = \frac{\sigma_i(\kappa) \times \Gamma_f(\kappa)}{\Gamma_H}, \quad (3)$$

where Γ_H is the total width of the Higgs boson and Γ_f is the partial width for Higgs boson decay into the final state f. For a given production process or decay mode j, the corresponding coupling-strength modifier κ_j is defined by

$$\kappa_j^2 = \frac{\sigma_j}{\sigma_j^{\text{SM}}} \quad \text{or} \quad \kappa_j^2 = \frac{\Gamma_j}{\Gamma_j^{\text{SM}}}.$$

The SM expectation, denoted by the label "SM," by definition corresponds to $\kappa_j = 1$.

The total width of the Higgs boson is affected both by modifications of the κ_j, and contributions from two additional classes of Higgs boson decays: invisible decays, which are identified through an E_T^{miss} signature in the analyses described in Sec. III H; and undetected decays, to which none of the analyses included in this combination are sensitive (the latter includes for instance Higgs boson decays into light quarks, or to BSM particles to which none

of the input analyses provide appreciable sensitivity). In the SM, the branching fraction for decays into invisible final states is $\sim 0.1\%$, from the $H \to ZZ^* \to 4\nu$ process. BSM contributions to this branching fraction and to the branching fraction to undetected final states are denoted by B_{inv} and B_{undet} respectively, with the SM corresponding to $B_{\text{inv}} = B_{\text{undet}} = 0$. The Higgs boson total width is then expressed as $\Gamma_H(\kappa, B_{\text{inv}}, B_{\text{undet}}) = \kappa_H^2(\kappa, B_{\text{inv}}, B_{\text{undet}})\Gamma_H^{\text{SM}}$ with

$$\kappa_H^2(\kappa, B_{\text{inv}}, B_{\text{undet}}) = \frac{\sum_j B_f^{\text{SM}} \kappa_j^2}{(1 - B_{\text{inv}} - B_{\text{undet}})}. \quad (4)$$

Constraints on B_{inv} are provided by the analyses described in Sec. III H, but no direct constraints are included for B_{undet}. Since its value scales all observed cross sections of on-shell Higgs boson production $\sigma(i \to H \to f)$ through Eqs. (3) and (4), further assumptions about undetected decays must be included in order to interpret these measurements in terms of absolute coupling-strength scale factors κ_j. The simplest assumption is that there are no undetected Higgs boson decays and the invisible branching fraction is as predicted by the SM. An alternative, weaker assumption, is to require $\kappa_W \leq 1$ and $\kappa_Z \leq 1$ [37]. A second alternative uses the assumption that the signal strength of off-shell Higgs boson production only depends on the coupling-strength scale factors and not on the total width [134,135], $\sigma^{\text{off}}(i \to H^* \to f) \sim \kappa_{i,\text{off}}^2 \times \kappa_{f,\text{off}}^2$. If the coupling strengths in off-shell Higgs boson production are furthermore assumed to be identical to those for on-shell Higgs boson production, $\kappa_{j,\text{off}} = \kappa_{j,\text{on}}$, and under the assumptions given in Sec. III I, the Higgs boson total width can be determined from the ratio of off-shell to on-shell signal strengths [25,147]. These assumptions can also be extended to apply to B_{inv} as well as B_{undet}, as an alternative to the measurements of Sec. III H.

An alternative approach is to rely on measurements of ratios of coupling-strength scale factors, which can be measured without assumptions about the Higgs boson total width, since the dependence on Γ_H of each coupling strength cancels in their ratios.

The current LHC data are insensitive to the coupling-strength modifiers κ_c and κ_s. Thus, in the following it is assumed that κ_c varies as κ_t and κ_s varies as κ_b. Other coupling modifiers (κ_u, κ_d, and κ_e) are irrelevant for the combination provided they are of order unity. The $gg \to H$, $H \to gg$, $gg \to ZH$, $H \to \gamma\gamma$ and $H \to Z\gamma$ processes are loop-induced in the SM. The ggH vertex and the $H \to \gamma\gamma$ process are treated either using effective scale factors κ_g and κ_γ, respectively, or expressed in terms of the more fundamental coupling-strength scale factors corresponding to the particles that contribute to the loop, including all interference effects. The $gg \to ZH$ process is never described using an effective scale factor and always resolved in terms of modifications of the SM Higgs boson couplings to the

TABLE IX. Parametrizations of Higgs boson production cross sections σ_i, partial decay widths Γ^f, and the total width Γ_H, normalized to their SM values, as functions of the coupling-strength modifiers κ. The effect of invisible and undetected decays is not considered in the expression for Γ_H. For effective κ parameters associated with loop processes, the resolved scaling in terms of the modifications of the Higgs boson couplings to the fundamental SM particles is given. The coefficients are derived following the methodology in Ref. [37].

Production	Loops	Interference	Effective modifier	Resolved modifier
$\sigma(\text{ggF})$	✓	$t\text{–}b$	κ_g^2	$1.04\kappa_t^2 + 0.002\kappa_b^2 - 0.04\kappa_t\kappa_b$
$\sigma(\text{VBF})$	...	...	...	$0.73\kappa_W^2 + 0.27\kappa_Z^2$
$\sigma(qq/qg \to ZH)$	...	...	...	κ_Z^2
$\sigma(gg \to ZH)$	✓	$t\text{–}Z$	$\kappa_{(ggZH)}$	$2.46\kappa_Z^2 + 0.46\kappa_t^2 - 1.90\kappa_Z\kappa_t$
$\sigma(WH)$	...	...	...	κ_W^2
$\sigma(t\bar{t}H)$	...	...	...	κ_t^2
$\sigma(tHW)$	...	$t\text{–}W$	...	$2.91\kappa_t^2 + 2.31\kappa_W^2 - 4.22\kappa_t\kappa_W$
$\sigma(tHq)$	...	$t\text{–}W$	...	$2.63\kappa_t^2 + 3.58\kappa_W^2 - 5.21\kappa_t\kappa_W$
$\sigma(b\bar{b}H)$	...	...	...	κ_b^2
Partial decay width				
Γ^{bb}	...	...	...	κ_b^2
Γ^{WW}	...	...	...	κ_W^2
Γ^{gg}	✓	$t\text{–}b$	κ_g^2	$1.11\kappa_t^2 + 0.01\kappa_b^2 - 0.12\kappa_t\kappa_b$
$\Gamma^{\tau\tau}$	...	...	...	κ_τ^2
Γ^{ZZ}	...	...	...	κ_Z^2
Γ^{cc}	...	...	...	$\kappa_c^2 (= \kappa_t^2)$
$\Gamma^{\gamma\gamma}$	✓	$t\text{–}W$	κ_γ^2	$1.59\kappa_W^2 + 0.07\kappa_t^2 - 0.67\kappa_W\kappa_t$
$\Gamma^{Z\gamma}$	✓	$t\text{–}W$	$\kappa_{(Z\gamma)}^2$	$1.12\kappa_W^2 - 0.12\kappa_W\kappa_t$
Γ^{ss}	...	...	...	$\kappa_s^2 (= \kappa_b^2)$
$\Gamma^{\mu\mu}$	...	...	...	κ_μ^2
Total width ($B_{\text{inv}} = B_{\text{undet}} = 0$)				
Γ_H	✓	...	κ_H^2	$0.58\kappa_b^2 + 0.22\kappa_W^2$ $+0.08\kappa_g^2 + 0.06\kappa_\tau^2$ $+0.03\kappa_Z^2 + 0.03\kappa_c^2$ $+0.0023\kappa_\gamma^2 + 0.0015\kappa_{(Z\gamma)}^2$ $+0.0004\kappa_s^2 + 0.00022\kappa_\mu^2$

top quark and the Z boson. This assumption impacts the description of BSM effects in $gg \to ZH$, since these lead to modified production kinematics [148]. However, the effect of introducing an explicit dependence on the transverse momentum of the Z boson in the parametrization was found to have a negligible impact on the results at the current level of experimental precision. Similarly, the $H \to Z\gamma$ decay is always expressed in terms of the Higgs boson couplings to the W boson and the t-quark as no analysis targeting this decay mode is included in the combination. These relations are summarized in Table IX. All uncertainties in the best-fit values shown in the following take into account both the experimental and theoretical systematic uncertainties, following the procedures outlined in Sec. IV.

B. Fermion and gauge boson couplings

The model studied in this section probes the universal coupling-strength scale factors $\kappa_V = \kappa_W = \kappa_Z$ for all vector bosons and $\kappa_F = \kappa_t = \kappa_b = \kappa_\tau = \kappa_\mu$ for all fermions.

The effective couplings corresponding to the ggH and $H \to \gamma\gamma$ vertex loops are resolved in terms of the fundamental SM couplings. It is assumed that there are no invisible or undetected Higgs boson decays, i.e., $B_{\text{inv}} = B_{\text{undet}} = 0$. Only the relative sign between κ_V and κ_F is physical. As a negative relative sign has been excluded [9], $\kappa_V \geq 0$ and $\kappa_F \geq 0$ are assumed. These definitions can be applied either globally, yielding two parameters, or separately for each of the five major decay channels, yielding ten parameters, κ_V^f and κ_F^f with the superscript f indicating the decay mode. The best-fit values and uncertainties from a combined fit are

$$\kappa_V = 1.05 \pm 0.04$$
$$\kappa_F = 1.05 \pm 0.09.$$

Figure 12 shows the results of the combined fit in the (κ_V, κ_F) plane as well as those of the individual decay modes in this benchmark model. Both κ_V and κ_F are
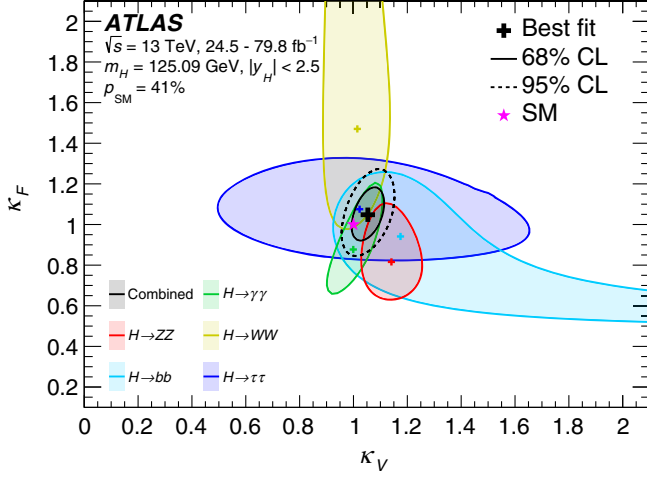
FIG. 12. Negative log-likelihood contours at 68% and 95% CL in the (κ_V^f, κ_F^f) plane for the individual decay modes and their combination (κ_F versus κ_V shown in black) assuming the coupling strengths to fermions and vector bosons to be positive. No contributions from invisible or undetected Higgs boson decays are assumed. The best-fit value for each measurement is indicated by a cross while the SM hypothesis is indicated by a star.

measured to be compatible with the SM expectation. The probability of compatibility between the SM hypothesis with the best-fit point corresponds to a *p*-value of $p_{\rm SM} = 41\%$, computed using the procedure outlined in Sec. IV with two d.o.f. In the combined measurement a linear correlation of 44% between κ_V and κ_F is observed.

C. Probing BSM contributions in loops and decays

To probe contributions of new particles either though loops or new final states, the effective coupling strengths to photons and gluons κ_γ and κ_g are measured. These parameters are defined to be positive as there is by construction no sensitivity to the sign of these coupling strengths. The modifiers corresponding to other loop-induced processes are resolved. The potential new particles contributing to these vertex loops may or may not contribute to the total width of the Higgs boson through direct invisible or undetected decays. In the former case, the total width is parameterized in terms of the branching fractions $B_{\rm inv}$ and $B_{\rm undet}$ defined in Sec. VII A. Furthermore, the benchmark models studied in this section assume that all coupling-strength modifiers of known SM particles are unity, i.e., they follow the SM predictions, and that the kinematics of the Higgs boson decay products are not altered significantly.

Assuming $B_{\rm inv} = B_{\rm undet} = 0$, the best-fit values and uncertainties from a combined fit are

$$\kappa_\gamma = 1.00 \pm 0.06$$
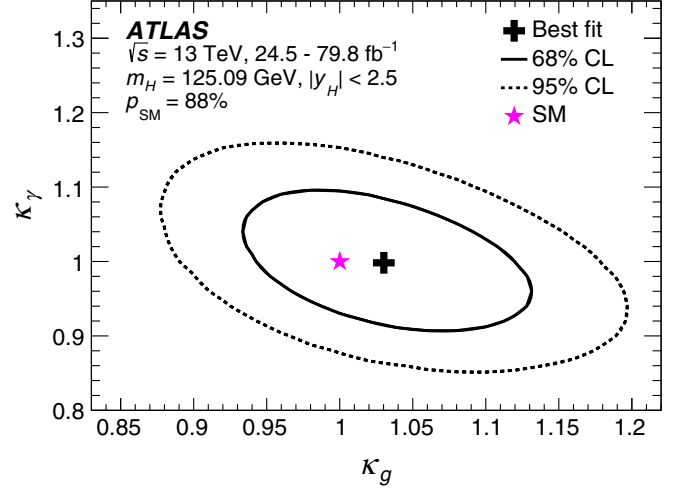$$\kappa_g = 1.03^{+0.07}_{-0.06}.$$

FIG. 13. Negative log-likelihood contours at 68% and 95% CL in the $(\kappa_\gamma, \kappa_g)$ plane obtained from a combined fit, constraining all other coupling-strength modifiers to their SM values and assuming no contributions from invisible or undetected Higgs boson decays. The best-fit value for each measurement is indicated by a cross while the SM hypothesis is indicated by a star.

Figure 13 shows negative log-likelihood contours obtained from the combined fit in the $(\kappa_\gamma, \kappa_g)$ plane. Both κ_γ and κ_g are measured to be compatible with the SM expectation. The probability of compatibility between the SM hypothesis with the best-fit point corresponds to a *p*-value of $p_{\rm SM} = 88\%$, computed using the procedure outlined in Sec. IV with two d.o.f. A linear correlation of -44% between κ_γ and κ_g is observed, in part due to the constraint on their product from the rate of $H \to \gamma\gamma$ decays in the ggF channel.

To also consider additional contributions to the total width of the Higgs boson, the assumption of no invisible or undetected decays is dropped and $B_{\rm inv}$ and $B_{\rm undet}$ are included as independent parameters in the model. The measurements sensitive to Higgs boson decays into invisible final states described in Sec. III H are included in the combination and used to constrain $B_{\rm inv}$. The $B_{\rm undet}$ parameter is constrained by decay modes that do not involve a loop process. The results from this model are

$$\kappa_\gamma = 0.97 \pm 0.06$$
$$\kappa_g = 0.95 \pm 0.08$$
$$B_{\rm inv} < 0.43 \text{ at } 95\% \text{ CL}$$
$$B_{\rm undet} < 0.12 \text{ at } 95\% \text{ CL.}$$

Limits on $B_{\rm inv}$ and $B_{\rm undet}$ are set using the $\tilde{t}_\mu$ prescription presented in Sec. IV. The expected upper limits at 95% CL on $B_{\rm inv}$ and $B_{\rm undet}$ are 0.20 and 0.31 respectively. The probability of compatibility between the SM hypothesis with the best-fit point corresponds to a *p*-value of
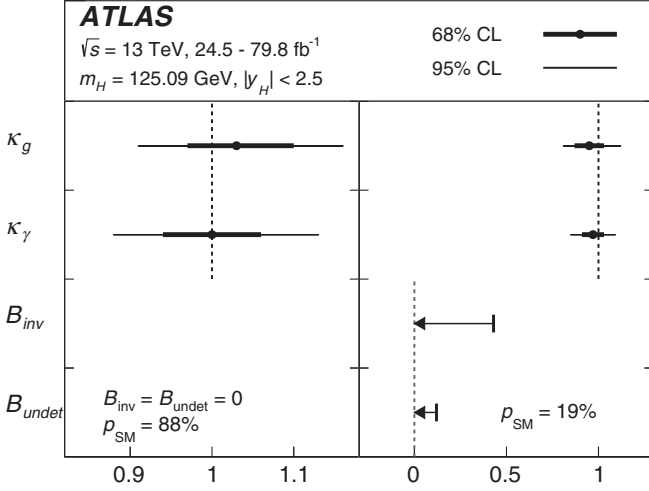
FIG. 14.   Best-fit values and uncertainties for effective modifiers to the photon and gluon couplings of the Higgs boson, with either $B_{\mathrm{inv}} = B_{\mathrm{undet}} = 0$ (left), or B_{inv} and B_{undet} included as free parameters (right). In the latter case, the measurements of the Higgs boson decay rate into invisible final states are included in the combination. The SM corresponds to $\kappa_\gamma = \kappa_g = 1$ and $B_{\mathrm{inv}} = B_{\mathrm{undet}} = 0$. All coupling-strength modifiers of known SM particles are assumed to be unity, i.e., they follow the SM predictions.

TABLE X.   Fit results for κ_Z, κ_W, κ_b, κ_t, κ_τ and κ_μ, all assumed to be positive. In this benchmark model BSM contributions to Higgs boson decays are assumed not to exist and Higgs boson vertices involving loops are resolved in terms of their SM content. The upper limit on κ_μ is set using the CL_s prescription.

Parameter	Result
κ_Z	1.10 ± 0.08
κ_W	1.05 ± 0.08
κ_b	$1.06\,^{+0.19}_{-0.18}$
κ_t	$1.02\,^{+0.11}_{-0.10}$
κ_τ	1.07 ± 0.15
κ_μ	<1.53 at $95\%\,CL$

$$y_V = \sqrt{\kappa_V \frac{g_V}{2v}} = \sqrt{\kappa_V}\,\frac{m_V}{v}$$

for weak bosons with a mass m_V, where g_V is the absolute Higgs boson coupling strength and $v = 246$ GeV is the vacuum expectation value of the Higgs field, and

$$y_F = \kappa_F \frac{g_F}{\sqrt{2}} = \kappa_F \frac{m_F}{v}$$

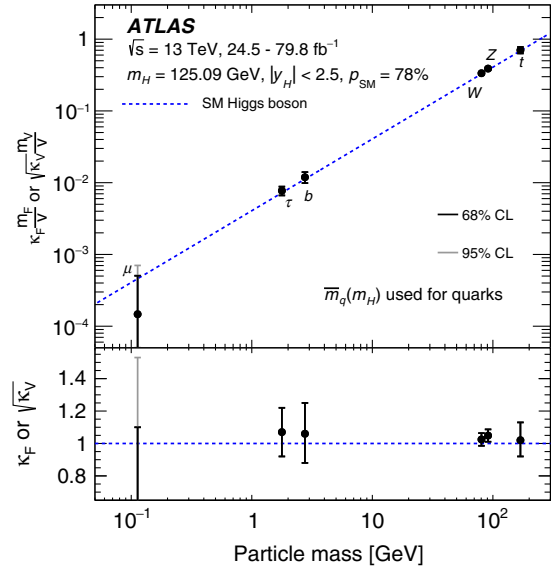$p_{\mathrm{SM}} = 19\%$, computed using the procedure outlined in Sec. IV with four d.o.f.

The results for both models are summarized in Fig. 14.

D. Generic parametrization assuming no new particles in loops and decays

In this model the scale factors for the coupling strengths to W, Z, t, b, τ and μ are treated independently. The Higgs boson couplings to second-generation quarks are assumed to scale as the couplings to the third-generation quarks. SM values are assumed for the couplings to first-generation fermions. Furthermore, it is assumed that only SM particles contribute to Higgs boson vertices involving loops, and modifications of the coupling-strength scale factors for fermions and vector bosons are propagated through the loop calculations. Invisible or undetected Higgs boson decays are assumed not to exist. All coupling-strength scale factors are assumed to be positive. The results of the $H \to \mu\mu$ analysis are included for this specific benchmark model. The results are shown in Table X. The expected 95% CL upper limit on κ_μ is 1.79. All measured coupling-strength scale factors in this generic model are found to be compatible with their SM expectation. The probability of compatibility between the SM hypothesis with the best-fit point corresponds to a p-value of $p_{\mathrm{SM}} = 78\%$, computed using the procedure outlined in Sec. IV with six d.o.f. Figure 15 shows the results of this benchmark model in terms of reduced coupling-strength scale factors, defined as

FIG. 15.   Reduced coupling-strength modifiers $\kappa_F \frac{m_F}{v}$ for fermions ($F = t$, b, τ, μ) and $\sqrt{\kappa_V}\frac{m_V}{v}$ for weak gauge bosons ($V = W$, Z) as a function of their masses m_F and m_V, respectively, and the vacuum expectation value of the Higgs field $v = 246$ GeV. The SM prediction for both cases is also shown (dotted line). The black error bars represent 68% CL intervals for the measured parameters. For κ_μ the light error bars indicate the 95% CL interval. The coupling modifiers κ_F and κ_V are measured assuming no BSM contributions to the Higgs boson decays, and the SM structure of loop processes such as ggF, $H \to \gamma\gamma$ and $H \to gg$. The lower inset shows the ratios of the values to their SM predictions.

TABLE XI. Fit results for Higgs boson coupling modifiers per particle type with effective photon and gluon couplings and either (a) $B_{\rm inv} = B_{\rm undet} = 0$, (b) $B_{\rm inv}$ and $B_{\rm undet}$ included as free parameters, the conditions $\kappa_{W,Z} \leq 1$ applied and the measurement of the Higgs boson decay rate into invisible final states included in the combination, or (c) $B_{\rm BSM} = B_{\rm inv} + B_{\rm undet}$ included as a free parameter, the measurement of off-shell Higgs boson production included in the combination, and the assumptions described in the text applied to the off-shell coupling-strength scale factors. The SM corresponds to $B_{\rm inv} = B_{\rm undet} = B_{\rm BSM} = 0$ and all κ parameters set to unity. All parameters except κ_t are assumed to be positive.

Parameter	(a) $B_{\rm inv} = B_{\rm undet} = 0$	(b) $B_{\rm inv}$ free, $B_{\rm undet} \geq 0$, $\kappa_{W,Z} \leq 1$	(c) $B_{\rm BSM} \geq 0$, $\kappa_{\rm off} = \kappa_{\rm on}$
κ_Z	1.11 ± 0.08	>0.88 at 95% CL	$1.20 ^{+0.18}_{-0.17}$
κ_W	1.05 ± 0.09	>0.85 at 95% CL	1.15 ± 0.18
κ_b	$1.03 ^{+0.19}_{-0.17}$	$0.85 ^{+0.15}_{-0.13}$	$1.14 ^{+0.21}_{-0.25}$
κ_t	$1.09 ^{+0.15}_{-0.14}$	$[-1.08, -0.77] \cup [0.96, 1.23]$ at 68% CL	1.18 ± 0.23
κ_τ	$1.05 ^{+0.16}_{-0.15}$	0.99 ± 0.14	$1.16 ^{+0.22}_{-0.24}$
κ_γ	1.05 ± 0.09	$0.96 ^{+0.08}_{-0.06}$	$1.16 ^{+0.17}_{-0.18}$
κ_g	$0.99 ^{+0.11}_{-0.10}$	$1.05 ^{+0.12}_{-0.14}$	$1.08 ^{+0.17}_{-0.18}$
$B_{\rm inv}$	$\cdots$	<0.30 at 95% CL	$\cdots$
$B_{\rm undet}$	$\cdots$	<0.21 at 95% CL	$\cdots$
$B_{\rm BSM}$	$\cdots$	$\cdots$	< 0.49 at 95% CL

for fermions with a mass m_F. For the b quark and the top quark, the $\overline{\rm MS}$ running mass evaluated at a scale of 125.09 GeV is used.

E. Generic parametrization including effective photon and gluon couplings with and without BSM contributions in decays

The models considered in this section are based on the same parametrization as the one in Sec. VII D but the ggF, $H \to gg$ and $H \to \gamma\gamma$ loop processes are parametrized using the effective coupling-strength modifiers κ_g and κ_γ, similar to the benchmark model probed in Sec. VII C.

The measured parameters include κ_Z, κ_W, κ_b, κ_t, κ_τ, κ_γ and κ_g. The sign of κ_t can be either positive or negative, while κ_Z is assumed to be positive without loss of generality. All other model parameters are also assumed to be positive. Furthermore it is assumed that the probed for BSM effects do not affect the kinematics of the Higgs boson decay products significantly. Three alternative scenarios are considered for the total width of the Higgs boson:

(a) No BSM contributions to the total width ($B_{\rm inv} = B_{\rm undet} = 0$).

(b) Both $B_{\rm inv}$ and $B_{\rm undet}$ are added as free parameters to the model. The measurements of Higgs boson decays into invisible final states described in Sec. III H are included in the combination, for these results only, and used to provide a constraint on $B_{\rm inv}$. The conditions $\kappa_W \leq 1$ and $\kappa_Z \leq 1$ are used to provide a constraint on $B_{\rm undet}$ as discussed in Sec. VII A.

(c) A single free parameter $B_{\rm BSM} = B_{\rm inv} + B_{\rm undet}$ is added to the model. The measurements of off-shell production described in Sec. III I are included in the combination, for these results only, and used to provide a constraint on $B_{\rm BSM}$ under the assumptions listed in Sec. VII A.

The numerical results for the various scenarios are summarized in Table XI and illustrated in Fig. 16. Limits on $B_{\rm inv}$, $B_{\rm undet}$ and $B_{\rm BSM}$ are set using the $\tilde{t}_\mu$ prescription presented in Sec. IV. All probed fundamental coupling-strength scale factors, as well as the probed loop-induced coupling scale factors are measured to be compatible with their SM expectation for all explored assumptions. Upper limits are set on the fraction of Higgs boson decays into invisible or undetected decays. In scenario (b) the observed (expected) 95% CL upper limits on the branching fractions are $B_{\rm inv} < 0.30$ (0.16) and $B_{\rm undet} < 0.21$ (0.36), and the lower limits on the couplings to vector bosons are $\kappa_Z > 0.88$ (0.76) and $\kappa_W > 0.85$ (0.77). In scenario (c), the observed (expected) upper limit on $B_{\rm BSM}$ is 0.49 (0.51). The probability of compatibility between the SM hypothesis with the best-fit point in scenario (a) corresponds to a p-value of $p_{\rm SM} = 88\%$, computed using the procedure outlined in Sec. IV with seven d.o.f.

F. Generic parametrization using ratios of coupling modifiers

The five absolute coupling-strength scale factors and two effective loop-coupling scale factors measured in the previous benchmark model are expressed as ratios of scale factors that can be measured independent of any assumptions about the Higgs boson total width. The model parameters are defined in Table XII. All parameters are assumed to be positive. This parametrization represents the most model-independent determination of coupling-strength scale factors that is currently possible in the κ-framework. The numerical results from the fit to this benchmark model are summarized in Table XII and visualized in Fig. 17. All model parameters are measured to be compatible with their SM expectation. The probability of compatibility between the SM hypothesis with the best-fit
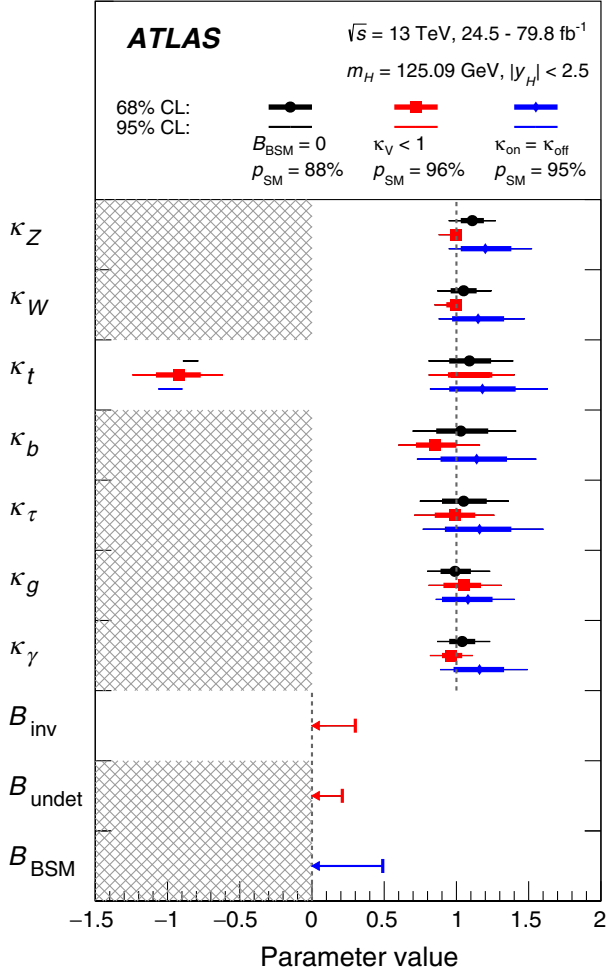
FIG. 16. Best-fit values and uncertainties for Higgs boson coupling modifiers per particle type with effective photon and gluon couplings and either $B_{\text{inv}} = B_{\text{undet}} = 0$ (black); B_{inv} and B_{undet} included as free parameters, the conditions $\kappa_{W,Z} \leq 1$ applied and the measurement of the Higgs boson decay rate into invisible final states included in the combination (red); or $B_{\text{BSM}} = B_{\text{inv}} + B_{\text{undet}}$ included as a free parameter, the measurement of off-shell Higgs boson production included in the combination, and the assumptions described in the text applied to the off-shell coupling-strength scale factors (blue). The SM corresponds to $B_{\text{inv}} = B_{\text{undet}} = 0$ and all κ parameters set to unity. All parameters except κ_t are assumed to be positive.

point corresponds to a p-value of $p_{\text{SM}} = 85\%$, computed using the procedure outlined in Sec. IV with seven d.o.f.

The parameter λ_{WZ} in this model is of particular interest: identical coupling-strength scale factors for the W and Z bosons are required within tight bounds by the SU(2) custodial symmetry and the ρ parameter measurements at LEP and at the Tevatron [149]. The ratio $\lambda_{\gamma Z}$ is sensitive to new charged particles contributing to the $H \to \gamma\gamma$ loop unlike in $H \to ZZ^*$ decays. Similarly, the ratio λ_{tg} is sensitive to new colored particles contributing through the ggF loop unlike in $t\bar{t}H$ events. The observed values are in agreement with the SM expectation.

TABLE XII. Best-fit values and uncertainties for ratios of coupling modifiers. The second column provides the expression of the measured parameters in terms of the coupling modifiers defined in previous sections. All parameters are defined to be unity in the SM.

Parameter	Definition in terms of κ modifiers	Result
κ_{gZ}	$\kappa_g \kappa_Z / \kappa_H$	1.06 ± 0.07
λ_{tg}	κ_t / κ_g	$1.10^{+0.15}_{-0.14}$
λ_{Zg}	κ_Z / κ_g	$1.12^{+0.15}_{-0.13}$
λ_{WZ}	κ_W / κ_Z	0.95 ± 0.08
$\lambda_{\gamma Z}$	κ_γ / κ_Z	0.94 ± 0.07
$\lambda_{\tau Z}$	κ_τ / κ_Z	0.95 ± 0.13
λ_{bZ}	κ_b / κ_Z	$0.93^{+0.15}_{-0.13}$

VIII. CONSTRAINTS ON NEW PHENOMENA

Two-Higgs-doublet models (2HDMs) [37,150–152] and supersymmetry [153–158] are promising extensions of the SM. The measurements are interpreted in these benchmark models, providing indirect limits on their parameters that are complementary to those obtained by direct searches for new particles. The interpretations presented in this section follow the procedure discussed in Ref. [38].

A. Two-Higgs-doublet model

In 2HDMs, the SM Higgs sector is extended by introducing an additional complex isodoublet scalar field with weak hypercharge one. Four types of 2HDMs satisfy the Paschos–Glashow–Weinberg condition [159,160], which prevents the appearance of tree-level flavor-changing neutral currents:

(i) Type I: One Higgs doublet couples to vector bosons, while the other one couples to fermions. The first doublet is *fermiophobic* in the limit where the two Higgs doublets do not mix.
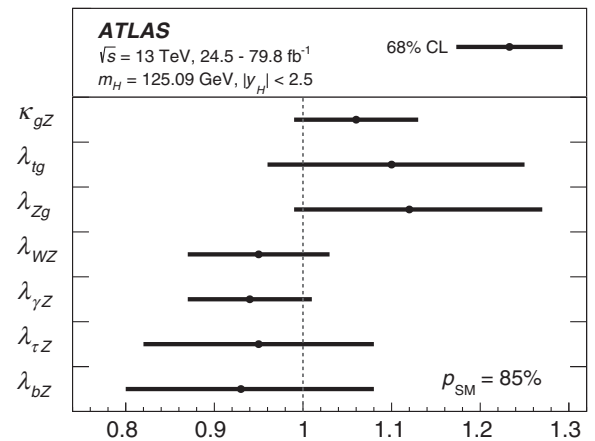

FIG. 17. Measured ratios of coupling modifiers. The dashed line indicates the SM value of unity for each parameter.

(ii) Type II: One Higgs doublet couples to up-type quarks and the other one to down-type quarks and charged leptons.

(iii) Lepton-specific: The Higgs bosons have the same couplings to quarks as in the Type I model and to charged leptons as in Type II.

(iv) Flipped: The Higgs bosons have the same couplings to quarks as in the Type II model and to charged leptons as in Type I.

The observed Higgs boson is identified with the light *CP*-even neutral scalar *h* predicted by 2HDMs, and its accessible production and decay modes are assumed to be the same as those of the SM Higgs boson. Its couplings to vector bosons, up-type quarks, down-type quarks and leptons relative to the corresponding SM predictions are expressed as functions of the mixing angle α between *h* and the heavy *CP*-even neutral scalar, and the ratio of the vacuum expectation values of the Higgs doublets, $\tan\beta$ [38].

Figure 18 shows the regions of the $(\cos(\beta - \alpha), \tan\beta)$ plane that are excluded at a confidence level of 95% or higher, for each of the four types of 2HDMs. The expected exclusion limits in the SM hypothesis are also overlaid. The data are consistent with the alignment limit [152] at $\cos(\beta - \alpha) = 0$, in which the couplings of *h* match those of the SM Higgs boson, within one standard deviation or better in each of the tested models. The allowed regions also include narrow, curved *petal* regions at positive $\cos(\beta - \alpha)$ and moderate $\tan\beta$ in the Type II, lepton-specific,

FIG. 18. Regions of the $(\cos(\beta - \alpha), \tan\beta)$ plane of four types of 2HDMs excluded by fits to the measured rates of Higgs boson production and decays. Contours at 95% CL, defined in the asymptotic approximation by $-2\ln\Lambda = 5.99$, are drawn for both the data and the expectation for the SM Higgs sector. The cross in each plot marks the observed best-fit value. The angles α and β are taken to satisfy $0 \leq \beta \leq \pi/2$ and $0 \leq \beta - \alpha \leq \pi$ without loss of generality. The alignment limit at $\cos(\beta - \alpha) = 0$, in which all Higgs boson couplings take their SM values, is indicated by the dashed red line.

and flipped models. These correspond to regions with $\cos(\beta + \alpha) \approx 0$, for which some fermion couplings have the same magnitude as in the SM, but the opposite sign.

B. Simplified minimal supersymmetric Standard Model

The scalar sector of the minimal supersymmetric Standard Model (MSSM) [161–163] is a realization of a Type II 2HDM. As a benchmark, a simplified MSSM model in which the Higgs boson is identified with the light *CP*-even scalar *h*, termed hMSSM [164–166], is studied. The assumptions made in this model are discussed in Ref. [38]. Notably, the hMSSM is a good approximation of the MSSM only for moderate values of $\tan\beta$. For $\tan\beta \gtrsim 10$ the scenario is approximate due to missing supersymmetry corrections in the Higgs boson coupling to *b*-quarks, and for $\tan\beta$ of $O(1)$ the precision of the approximation depends on m_A, the mass of the *CP*-odd scalar [35]. The production and decay modes accessible to *h* are assumed to be the same as those of the SM Higgs boson.

The Higgs boson couplings to vector bosons, up-type fermions and down-type fermions relative to the corresponding SM predictions are expressed as functions of the ratio of the vacuum expectation values of the Higgs doublets, $\tan\beta$, m_A, and the masses of the *Z* boson and of *h*.

Figure 19 shows the regions of the hMSSM parameter space that are indirectly excluded by the measurement of

FIG. 19. Regions of the $(m_A, \tan\beta)$ plane in the hMSSM excluded by fits to the measured rates of Higgs boson production and decays. Likelihood contours at 95% CL, defined in the asymptotic approximation by $-2\ln\Lambda = 5.99$, are drawn for both the data and the expectation of the SM Higgs sector. The regions to the left of the solid contour are excluded. The decoupling limit, in which all Higgs boson couplings tend to their SM value, corresponds to $m_A \to \infty$.

the Higgs boson production and decay rates. The data are consistent with the SM decoupling limit at large m_A, where the *h* couplings tend to those of the SM Higgs boson. The observed (expected) lower limit at 95% CL on the *CP*-odd Higgs boson mass is at least $m_A > 480$ GeV ($m_A > 400$ GeV) for $1 \leq \tan\beta \leq 25$, increasing to $m_A > 530$ GeV ($m_A > 450$ GeV) at $\tan\beta = 1$. The observed limit is stronger than the expected limit because the hMSSM model exhibits a physical boundary $\kappa_V \leq 1$, but the Higgs boson coupling to vector bosons is measured to be larger than the SM value, as presented in Sec. VII.

IX. CONCLUSIONS

Measurements of Higgs boson production cross sections and branching fractions have been performed using up to 79.8 fb^{-1} of *pp* collision data produced by the LHC at $\sqrt{s} = 13$ TeV and recorded by the ATLAS detector. The results presented in this paper are based on the combination of analyses of the $H \to \gamma\gamma$, $H \to ZZ^*$, $H \to WW^*$, $H \to \tau\tau$, $H \to b\bar{b}$ and $H \to \mu\mu$ decay modes, searches for decays into invisible final states, as well as on measurements of off-shell Higgs boson production.

The global signal strength is determined to be $\mu = 1.11^{+0.09}_{-0.08}$.

The Higgs boson production cross sections within the region $|y_H| < 2.5$ are measured in a combined fit for the gluon–gluon fusion process, vector-boson fusion, the associated production with a *W* or *Z* boson and the associated production with top quarks, assuming the SM Higgs boson branching fractions. The combined measurement leads to an observed (expected) significance for the vector-boson fusion production process of 6.5σ (5.3σ). For the *VH* production mode the observed (expected) significance is 5.3σ (4.7σ). The $t\bar{t}H + tH$ processes are measured with an observed (expected) significance of 5.8σ (5.3σ).

Removing the assumption of SM branching fractions, a combined fit is performed for the production cross section times branching fraction for each pair of production and decay processes to which the combined analyses are sensitive. Results are also presented for a model in which these quantities are expressed using the cross section of the $gg \to H \to ZZ^*$ process, ratios of production cross sections relative to that of ggF production, and ratios of branching fractions relative to that of $H \to ZZ^*$.

Cross sections are measured in 15 regions of Higgs boson production kinematics defined within the simplified template cross section framework, which primarily characterize the transverse momentum of the Higgs boson, the topology of associated jets and the transverse momentum of associated vector bosons. The measurements in all regions are found to be compatible with SM predictions.

The observed Higgs boson yields are used to obtain confidence intervals for κ modifiers to the couplings of the SM Higgs boson to fermions, weak vector bosons, gluons,

and photons and to the branching fraction of the Higgs boson into invisible and undetected decay modes. A variety of physics-motivated constraints on the Higgs boson total width are explored: Using searches for $H \rightarrow$ invisible and constraints on couplings to vector bosons, the branching fraction of invisible Higgs boson decays into BSM particles is constrained to be less than 30% at 95% CL, while the branching fraction of decays into undetected particles is less than 22% at 95% CL. The overall branching fraction of the Higgs boson into BSM decays is determined to be less than 47% at 95% CL using measurements of off-shell Higgs boson production in combination with measurements of SM Higgs boson production and rates. No significant deviation from the SM predictions is observed in any of the benchmark models studied.

Finally, the results are interpreted in the context of two-Higgs-doublet models and the hMSSM. Constraints are set in the $(m_A, \tan\beta)$ plane of the hMSSM and the $(\cos(\beta - \alpha), \tan\beta)$ plane in 2HDM Type-I, Type-II, lepton-specific and flipped models.

APPENDIX: SIMPLIFIED TEMPLATE CROSS SECTION MEASUREMENT RESULTS WITH FINER GRANULARITY

This section presents measurements of STXS parameters in a model that has finer granularity than the model of Sec. VI B, and is thus closer to the original proposal of Stage 1 STXS in Refs. [35,36]. The changes relative to the model of Sec. VI B are as follows: in the $gg \rightarrow H$ process, the region defined by $p_T^H \geq 200$ GeV and ≥ 1 jets is split into separate bins for 1 jet and ≥ 2 jets; a VBF-topology (*VBF topo*) region is defined for events with ≥ 2 jets using
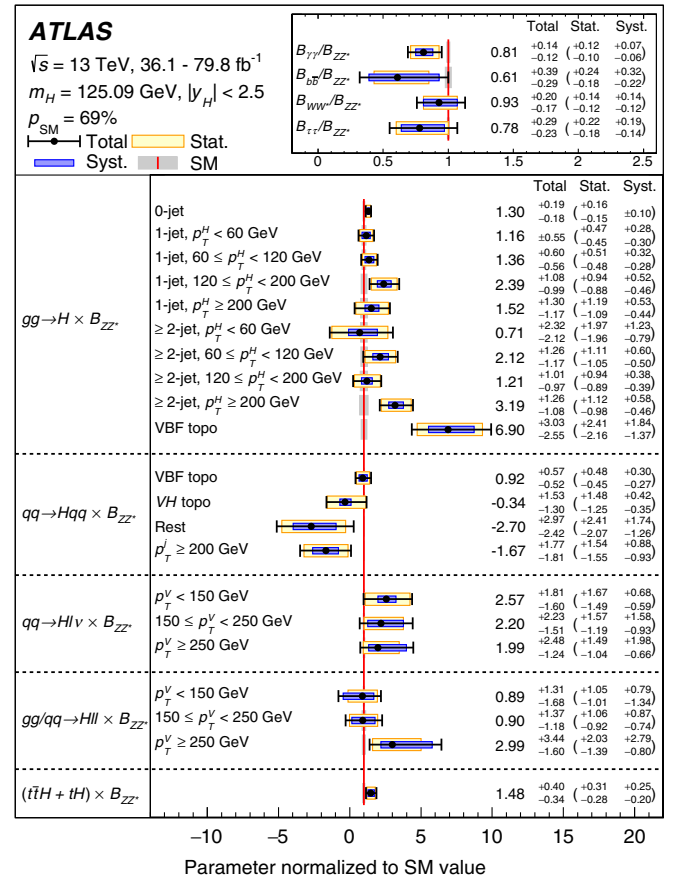

FIG. 20. Best-fit values and uncertainties for the cross sections in each measurement region times the $H \rightarrow ZZ^*$ branching fraction in a model with finer granularity. The results are shown normalized to the SM predictions for the various parameters. The black error bar shows the total uncertainty in each measurement.
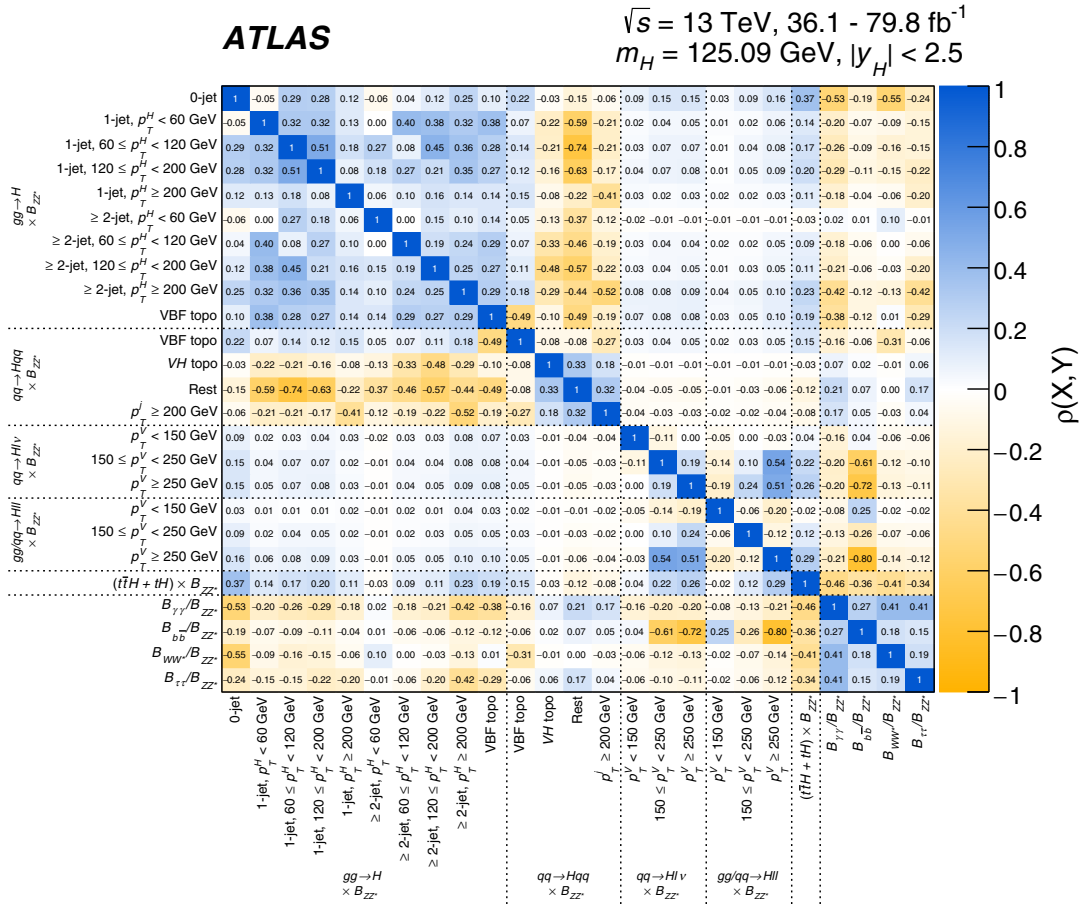
FIG. 21.　Correlation matrix for the measured values of the simplified template cross sections in each measurement region times the $H \to ZZ^*$ branching fraction in a model with finer granularity.

the same selection as in the $qq \to Hqq$ process; the remaining ≥ 2 jet events are separated into three bins of p_T^H in the same way as the 1-jet events; in the $qq \to Hqq$ process, the *VBF topo+Rest* region is split into separate bins

for *VBF topo* and *Rest*; and in the $qq \to WH$ process, the $p_T^V < 250$ GeV region is split into two bins for $p_T^V < 150$ GeV and $150 \leq p_T^V < 250$ GeV, matching the binning used in $pp \to ZH$. The results are shown in Figs. 20 and 21.

[1] F. Englert and R. Brout, Broken Symmetry and the Mass of Gauge Vector Mesons, Phys. Rev. Lett. **13**, 321 (1964).

[2] P. W. Higgs, Broken symmetries, massless particles and gauge fields, Phys. Lett. **12**, 132 (1964).

[3] P. W. Higgs, Broken Symmetries and the Masses of Gauge Bosons, Phys. Rev. Lett. **13**, 508 (1964).

[4] G. S. Guralnik, C. R. Hagen, and T. W. B. Kibble, Global Conservation Laws and Massless Particles, Phys. Rev. Lett. **13**, 585 (1964).

[5] P. W. Higgs, Spontaneous symmetry breakdown without massless bosons, Phys. Rev. **145**, 1156 (1966).

[6] T. W. B. Kibble, Symmetry breaking in non-Abelian gauge theories, Phys. Rev. **155**, 1554 (1967).

[7] ATLAS Collaboration, Observation of a new particle in the search for the Standard Model Higgs boson with the ATLAS detector at the LHC, Phys. Lett. B **716**, 1 (2012).

[8] CMS Collaboration, Observation of a new boson at a mass of 125 GeV with the CMS experiment at the LHC, Phys. Lett. B **716**, 30 (2012).

[9] ATLAS and CMS Collaborations, Measurements of the Higgs boson production and decay rates and constraints on its couplings from a combined ATLAS and CMS analysis

of the LHC pp collision data at $\sqrt{s} = 7$ and 8 TeV, J. High Energy Phys. 08 (2016) 045.

[10] ATLAS Collaboration, Measurements of Higgs boson properties in the diphoton decay channel with 36 fb^{-1} of pp collision data at $\sqrt{s} = 13$ TeV with the ATLAS detector, Phys. Rev. D **98**, 052005 (2018).

[11] ATLAS Collaboration, Measurement of the Higgs boson coupling properties in the $H \to ZZ^* \to 4\ell$ decay channel at $\sqrt{s} = 13$ TeV with the ATLAS detector, J. High Energy Phys. 03 (2018) 095.

[12] ATLAS Collaboration, Observation of Higgs boson production in association with a top quark pair at the LHC with the ATLAS detector, Phys. Lett. B **784**, 173 (2018).

[13] ATLAS Collaboration, Measurements of gluon-gluon fusion and vector-boson fusion Higgs boson production cross sections in the $H \to WW^* \to e\nu\mu\nu$ decay channel in pp collisions at $\sqrt{s} = 13$ TeV with the ATLAS detector, Phys. Lett. B **789**, 508 (2019).

[14] ATLAS Collaboration, Cross-section measurements of the Higgs boson decaying into a pair of τ-leptons in proton–proton collisions at $\sqrt{s} = 13$ TeV with the ATLAS detector, Phys. Rev. D **99**, 072001 (2019).

[15] ATLAS Collaboration, Observation of $H \to b\bar{b}$ decays and VH production with the ATLAS detector, Phys. Lett. B **786**, 59 (2018).

[16] ATLAS Collaboration, Measurement of VH, $H \to b\bar{b}$ production as a function of the vector-boson transverse momentum in 13 TeV pp collisions with the ATLAS detector, J. High Energy Phys. 05 (2019) 141.

[17] ATLAS Collaboration, Search for Higgs bosons produced via vector-boson fusion and decaying into bottom quark pairs in $\sqrt{s} = 13$ TeV pp collisions with the ATLAS detector, Phys. Rev. D **98**, 052003 (2018).

[18] ATLAS Collaboration, Evidence for the associated production of the Higgs boson and a top quark pair with the ATLAS detector, Phys. Rev. D **97**, 072003 (2018).

[19] ATLAS Collaboration, Search for the standard model Higgs boson produced in association with top quarks and decaying into a $b\bar{b}$ pair in pp collisions at $\sqrt{s} = 13$ TeV with the ATLAS detector, Phys. Rev. D **97**, 072016 (2018).

[20] ATLAS Collaboration, Search for the Dimuon Decay of the Higgs Boson in pp Collisions at $\sqrt{s} = 13$ TeV with the ATLAS Detector, Phys. Rev. Lett. **119**, 051802 (2017).

[21] ATLAS Collaboration, Search for invisible Higgs boson decays in vector boson fusion at $\sqrt{s} = 13$ TeV with the ATLAS detector, Phys. Lett. B **793**, 499 (2019).

[22] ATLAS Collaboration, Search for an invisibly decaying Higgs boson or dark matter candidates produced in association with a Z boson in pp collisions at $\sqrt{s} = 13$ TeV with the ATLAS detector, Phys. Lett. B **776**, 318 (2018).

[23] ATLAS Collaboration, Search for dark matter in events with a hadronically decaying vector boson and missing transverse momentum in pp collisions at $\sqrt{s} = 13$ TeV with the ATLAS detector, J. High Energy Phys. 10 (2018) 180.

[24] ATLAS Collaboration, Combination of Searches for Invisible Higgs Boson Decays with the ATLAS Experiment, Phys. Rev. Lett. **122**, 231801 (2019).

[25] ATLAS Collaboration, Constraints on off-shell Higgs boson production and the Higgs boson total width in $ZZ \to 4\ell$ and $ZZ \to 2\ell 2\nu$ final states with the ATLAS detector, Phys. Lett. B **786**, 223 (2018).

[26] ATLAS and CMS Collaborations, Combined Measurement of the Higgs Boson Mass in pp Collisions at $\sqrt{s} = 7$ and 8 TeV with the ATLAS and CMS Experiments, Phys. Rev. Lett. **114**, 191803 (2015).

[27] CMS Collaboration, Measurements of Higgs boson properties in the diphoton decay channel in proton–proton collisions at $\sqrt{s} = 13$ TeV, J. High Energy Phys. 11 (2018) 185.

[28] CMS Collaboration, Measurements of properties of the Higgs boson decaying to a W boson pair in pp collisions at $\sqrt{s} = 13$ TeV, Phys. Lett. B **791**, 96 (2019).

[29] CMS Collaboration, Observation of the Higgs boson decay to a pair of τ leptons, Phys. Lett. B **779**, 283 (2018).

[30] CMS Collaboration, Evidence for the Higgs boson decay to a bottom quark–antiquark pair, Phys. Lett. B **780**, 501 (2018).

[31] CMS Collaboration, Observation of $t\bar{t}H$ Production, Phys. Rev. Lett. **120**, 231801 (2018).

[32] CMS Collaboration, Observation of Higgs Boson Decay to Bottom Quarks, Phys. Rev. Lett. **121**, 121801 (2018).

[33] CMS Collaboration, Measurements of the Higgs boson width and anomalous HVV couplings from on-shell and off-shell production in the four-lepton final state, Phys. Rev. D **99**, 112003 (2019).

[34] CMS Collaboration, Combined measurements of Higgs boson couplings in proton–proton collisions at $\sqrt{s} = 13$ TeV, Eur. Phys. J. C **79**, 421 (2019).

[35] D. de Florian *et al.* (LHC Higgs Cross Section Working Group), Handbook of LHC higgs cross sections: 4. Deciphering the nature of the higgs sector, arXiv:1610.07922, https://doi.org/10.23731/CYRM-2017-002.

[36] J. R. Andersen *et al.*, Les Houches 2015: Physics at TeV colliders standard model working group report, arXiv:1605.04692.

[37] S. Heinemeyer *et al.* (LHC Higgs Cross Section Working Group), Handbook of LHC higgs cross sections: 3. Higgs properties, Report No. CERN-2013-004, 2013, https://doi.org/10.5170/CERN-2013-004.

[38] ATLAS Collaboration, Constraints on new phenomena via Higgs boson couplings and invisible decays with the ATLAS detector, J. High Energy Phys. 11 (2015) 206.

[39] ATLAS Collaboration, The ATLAS Experiment at the CERN Large Hadron Collider, J. Instrum. **3**, S08003 (2008).

[40] ATLAS Collaboration, ATLAS insertable B-layer technical design report, Report No. ATLAS-TDR-19, 2010, https://cds.cern.ch/record/1291633; Addendum, Report No. ATLAS-TDR-19-ADD-1, 2012, https://cds.cern.ch/record/1451888.

[41] B. Abbott *et al.*, Production and integration of the ATLAS insertable B-layer, J. Instrum. **13**, T05008 (2018).

[42] ATLAS Collaboration, Luminosity determination in pp collisions at $\sqrt{s} = 13$ TeV using the ATLAS detector at the LHC, Report No. ATLAS-CONF-2019-021, 2019, https://cds.cern.ch/record/2677054.

[43] G. Avoni *et al.*, The new LUCID-2 detector for luminosity measurement and monitoring in ATLAS, J. Instrum. **13,** P07017 (2018).

[44] P. Nason, A new method for combining NLO QCD with shower Monte Carlo algorithms, J. High Energy Phys. 11 (2004) 040.

[45] S. Frixione, P. Nason, and C. Oleari, Matching NLO QCD computations with parton shower simulations: The POWHEG method, J. High Energy Phys. 11 (2007) 070.

[46] S. Alioli, P. Nason, C. Oleari, and E. Re, A general framework for implementing NLO calculations in shower Monte Carlo programs: The POWHEG BOX, J. High Energy Phys. 06 (2010) 043.

[47] S. Alioli, P. Nason, C. Oleari, and E. Re, NLO Higgs boson production via gluon fusion matched with shower in POWHEG, J. High Energy Phys. 04 (2009) 002.

[48] K. Hamilton, P. Nason, E. Re, and G. Zanderighi, NNLOPS simulation of Higgs boson production, J. High Energy Phys. 10 (2013) 222.

[49] K. Hamilton, P. Nason, and G. Zanderighi, Finite quark-mass effects in the NNLOPSPOWHEG + MiNLO Higgs generator, J. High Energy Phys. 05 (2015) 140.

[50] S. Catani and M. Grazzini, Next-to-Next-to-Leading-Order Subtraction Formalism in Hadron Collisions and its Application to Higgs-Boson Production at the Large Hadron Collider, Phys. Rev. Lett. **98,** 222002 (2007).

[51] K. Hamilton, P. Nason, and G. Zanderighi, MINLO: Multi-scale improved NLO, J. High Energy Phys. 10 (2012) 155.

[52] J. M. Campbell, R. K. Ellis, R. Frederix, P. Nason, C. Oleari, and C. Williams, NLO higgs boson production plus one and two jets using the POWHEG BOX, MadGraph4 and MCFM, J. High Energy Phys. 07 (2012) 092.

[53] K. Hamilton, P. Nason, C. Oleari, and G. Zanderighi, Merging H/W/Z + 0 and 1 jet at NLO with no merging scale: A path to parton shower + NNLO matching, J. High Energy Phys. 05 (2013) 082.

[54] J. Butterworth *et al.*, PDF4LHC recommendations for LHC Run II, J. Phys. G **43,** 023001 (2016).

[55] C. Anastasiou, C. Duhr, F. Dulat, F. Herzog, and B. Mistlberger, Higgs Boson Gluon-Fusion Production in QCD at Three Loops, Phys. Rev. Lett. **114,** 212001 (2015).

[56] C. Anastasiou, C. Duhr, F. Dulat, E. Furlan, T. Gehrmann, F. Herzog, A. Lazopoulos, and B. Mistlberger, High precision determination of the gluon fusion Higgs boson cross-section at the LHC, J. High Energy Phys. 05 (2016) 058.

[57] F. Dulat, A. Lazopoulos, and B. Mistlberger, iHixs 2—Inclusive Higgs cross sections, Comput. Phys. Commun. **233,** 243 (2018).

[58] R. V. Harlander and K. J. Ozeren, Finite top mass effects for hadronic Higgs production at next-to-next-to-leading order, J. High Energy Phys. 11 (2009) 088.

[59] R. V. Harlander and K. J. Ozeren, Top mass effects in Higgs production at next-to-next-to-leading order QCD: Virtual corrections, Phys. Lett. B **679,** 467 (2009).

[60] R. V. Harlander, H. Mantler, S. Marzani, and K. J. Ozeren, Higgs production in gluon fusion at next-to-next-to-leading order QCD for finite top mass, Eur. Phys. J. C **66,** 359 (2010).

[61] S. Actis, G. Passarino, C. Sturm, and S. Uccirati, NLO electroweak corrections to Higgs boson production at hadron colliders, Phys. Lett. B **670,** 12 (2008).

[62] S. Actis, G. Passarino, C. Sturm, and S. Uccirati, NNLO computational techniques: The cases $H \to \gamma\gamma$ and $H \to gg$, Nucl. Phys. **B811,** 182 (2009).

[63] C. Anastasiou, R. Boughezal, and F. Petriello, Mixed QCD-electroweak corrections to Higgs boson production in gluon fusion, J. High Energy Phys. 04 (2009) 003.

[64] U. Aglietti, R. Bonciani, G. Degrassi, and A. Vicini, Two loop light fermion contribution to Higgs production and decays, Phys. Lett. B **595,** 432 (2004).

[65] G. Bozzi, S. Catani, D. de Florian, and M. Grazzini, Transverse-momentum resummation and the spectrum of the Higgs boson at the LHC, Nucl. Phys. **B737,** 73 (2006).

[66] D. de Florian, G. Ferrera, M. Grazzini, and D. Tommasini, Transverse-momentum resummation: Higgs boson production at the Tevatron and the LHC, J. High Energy Phys. 11 (2011) 064.

[67] M. Grazzini and H. Sargsyan, Heavy-quark mass effects in Higgs boson production at the LHC, J. High Energy Phys. 09 (2013) 129.

[68] P. Nason and C. Oleari, NLO Higgs boson production via vector-boson fusion matched with shower in POWHEG, J. High Energy Phys. 02 (2010) 037.

[69] M. Ciccolini, A. Denner, and S. Dittmaier, Strong and Electroweak Corrections to the Production of a Higgs Boson +2 Jets via Weak Interactions at the Large Hadron Collider, Phys. Rev. Lett. **99,** 161803 (2007).

[70] M. Ciccolini, A. Denner, and S. Dittmaier, Electroweak and QCD corrections to Higgs production via vector-boson fusion at the LHC, Phys. Rev. D **77,** 013002 (2008).

[71] P. Bolzoni, F. Maltoni, S.-O. Moch, and M. Zaro, Higgs Boson Production via Vector-Boson Fusion at Next-to-Next-to-Leading Order in QCD, Phys. Rev. Lett. **105,** 011801 (2010).

[72] G. Cullen, N. Greiner, G. Heinrich, G. Luisoni, P. Mastrolia, G. Ossola, T. Reiter, and F. Tramontano, Automated one-loop calculations with GoSam, Eur. Phys. J. C **72,** 1889 (2012).

[73] G. Luisoni, P. Nason, C. Oleari, and F. Tramontano, $HW^{\pm}/HZ + 0$ and 1 jet at NLO with the POWHEG BOX interfaced to GoSam and their merging within MiNLO, J. High Energy Phys. 10 (2013) 083.

[74] O. Brein, R. V. Harlander, and T. J. E. Zirke, vh@nnlo—Higgs Strahlung at hadron colliders, Comput. Phys. Commun. **184,** 998 (2013).

[75] R. V. Harlander, J. Klappert, S. Liebler, and L. Simon, vh@nnlo-v2: New physics in Higgs strahlung, J. High Energy Phys. 05 (2018) 089.

[76] O. Brein, A. Djouadi, and R. Harlander, NNLO QCD corrections to the Higgs-strahlung processes at hadron colliders, Phys. Lett. B **579,** 149 (2004).

[77] O. Brein, R. Harlander, M. Wiesemann, and T. Zirke, Top-quark mediated effects in hadronic Higgs-strahlung, Eur. Phys. J. C **72,** 1868 (2012).

[78] R. V. Harlander, A. Kulesza, V. Theeuwes, and T. Zirke, Soft gluon resummation for gluon-induced Higgs Strahlung, J. High Energy Phys. 11 (2014) 082.

[79] G. Ferrera, G. Somogyi, and F. Tramontano, Associated production of a Higgs boson decaying into bottom quarks at the LHC in full NNLO QCD, Phys. Lett. B **780,** 346 (2018).

[80] F. Caola, G. Luisoni, K. Melnikov, and R. Röntsch, NNLO QCD corrections to associated WH production and $H \to b\bar{b}$ decay, Phys. Rev. D **97,** 074022 (2018).

[81] M. L. Ciccolini, S. Dittmaier, and M. Kramer, Electroweak radiative corrections to associated WH and ZH production at hadron colliders, Phys. Rev. D **68,** 073003 (2003).

[82] A. Denner, S. Dittmaier, S. Kallweit, and A. Mück, Electroweak corrections to Higgs-strahlung off W/Z bosons at the Tevatron and the LHC with HAWK, J. High Energy Phys. 03 (2012) 075.

[83] A. Denner, S. Dittmaier, S. Kallweit, and A. Mück, HAWK 2.0: A Monte Carlo program for Higgs production in vector-boson fusion and Higgs strahlung at hadron colliders, Comput. Phys. Commun. **195,** 161 (2015).

[84] L. Altenkamp, S. Dittmaier, R. V. Harlander, H. Rzehak, and T. J. E. Zirke, Gluon-induced Higgsstrahlung at next-to-leading order QCD, J. High Energy Phys. 02 (2013) 078.

[85] H. B. Hartanto, B. Jager, L. Reina, and D. Wackeroth, Higgs boson production in association with top quarks in the POWHEG BOX, Phys. Rev. D **91,** 094003 (2015).

[86] J. Alwall, R. Frederix, S. Frixione, V. Hirschi, F. Maltoni, O. Mattelaer, H.-S. Shao, T. Stelzer, P. Torrielli, and M. Zaro, The automated computation of tree-level and next-to-leading order differential cross sections, and their matching to parton shower simulations, J. High Energy Phys. 07 (2014) 079.

[87] P. Artoisenet, R. Frederix, O. Mattelaer, and R. Rietkerk, Automatic spin-entangled decays of heavy resonances in Monte Carlo simulations, J. High Energy Phys. 03 (2013) 015.

[88] R. D. Ball *et al.*, Parton distributions for the LHC Run II, J. High Energy Phys. 04 (2015) 040.

[89] W. Beenakker, S. Dittmaier, M. Krämer, B. Plümper, M. Spira, and P. M. Zerwas, NLO QCD corrections to $t\bar{t}H$ production in hadron collisions, Nucl. Phys. **B653,** 151 (2003).

[90] S. Dawson, C. Jackson, L. Orr, L. Reina, and D. Wackeroth, Associated Higgs production with top quarks at the large hadron collider: NLO QCD corrections, Phys. Rev. D **68,** 034022 (2003).

[91] Y. Zhang, W.-G. Ma, R.-Y. Zhang, C. Chen, and L. Guo, QCD NLO and EW NLO corrections to $t\bar{t}H$ production with top quark decays at hadron collider, Phys. Lett. B **738,** 1 (2014).

[92] S. Frixione, V. Hirschi, D. Pagani, H. S. Shao, and M. Zaro, Weak corrections to Higgs hadroproduction in association with a top-quark pair, J. High Energy Phys. 09 (2014) 065.

[93] M. Wiesemann, R. Frederix, S. Frixione, V. Hirschi, F. Maltoni, and P. Torrielli, Higgs production in association with bottom quarks, J. High Energy Phys. 02 (2015) 132.

[94] R. D. Ball *et al.*, Parton distributions with LHC data, Nucl. Phys. **B867,** 244 (2013).

[95] S. Dawson, C. Jackson, L. Reina, and D. Wackeroth, Exclusive Higgs boson production with bottom quarks at hadron colliders, Phys. Rev. D **69,** 074027 (2004).

[96] S. Dittmaier, M. Krämer, and M. Spira, Higgs radiation off bottom quarks at the Tevatron and the CERN LHC, Phys. Rev. D **70,** 074010 (2004).

[97] R. V. Harlander and W. B. Kilgore, Higgs boson production in bottom quark fusion at next-to-next-to leading order, Phys. Rev. D **68,** 013001 (2003).

[98] J. Pumplin, D. R. Stump, J. Huston, H.-L. Lai, P. Nadolsky, and W.-K. Tung, New generation of parton distributions with uncertainties from global QCD analysis, J. High Energy Phys. 07 (2002) 012.

[99] H.-L. Lai, M. Guzzi, J. Huston, Z. Li, P. M. Nadolsky, J. Pumplin, and C.-P. Yuan, New parton distributions for collider physics, Phys. Rev. D **82,** 074024 (2010).

[100] F. Demartin, F. Maltoni, K. Mawatari, and M. Zaro, Higgs production in association with a single top quark at the LHC, Eur. Phys. J. C **75,** 267 (2015).

[101] F. Demartin, B. Maier, F. Maltoni, K. Mawatari, and M. Zaro, tWH associated production at the LHC, Eur. Phys. J. C **77,** 34 (2017).

[102] T. Sjöstrand, S. Mrenna, and P. Z. Skands, A brief introduction to PYTHIA 8.1, Comput. Phys. Commun. **178,** 852 (2008).

[103] S. Gieseke, A. Ribon, M. H. Seymour, P. Stephens, and B. Webber, Herwig++ 1.0: An event generator for e+e- annihilation, J. High Energy Phys. 02 (2004) 005.

[104] ATLAS Collaboration, Measurement of the Z/γ^* boson transverse momentum distribution in pp collisions at $\sqrt{s} = 7$ TeV with the ATLAS detector, J. High Energy Phys. 09 (2014) 145.

[105] ATLAS Collaboration, ATLAS Pythia 8 tunes to 7 TeV data, Report No. ATL-PHYS-PUB-2014-021, 2014, https://cds.cern.ch/record/1966419.

[106] A. Djouadi, J. Kalinowski, and M. Spira, HDECAY: A Program for Higgs boson decays in the Standard Model and its supersymmetric extension, Comput. Phys. Commun. **108,** 56 (1998).

[107] M. Spira, QCD effects in Higgs physics, Fortsch. Phys. **46,** 203 (1998).

[108] A. Djouadi, M. M. Mühlleitner, and M. Spira, Decays of supersymmetric particles: The program SUSY-HIT (SUspect-SdecaY-Hdecay-InTerface), Acta Phys. Pol. B **38,** 635 (2007).

[109] A. Bredenstein, A. Denner, S. Dittmaier, and M. Weber, Radiative corrections to the semileptonic and hadronic Higgs-boson decays $H \to WW/ZZ \to 4$ fermions, J. High Energy Phys. 02 (2007) 080.

[110] A. Bredenstein, A. Denner, S. Dittmaier, and M. Weber, Precise predictions for the Higgs-boson decay $H \to WW/ZZ \to 4$ leptons, Phys. Rev. D **74,** 013004 (2006).

[111] A. Bredenstein, A. Denner, S. Dittmaier, and M. M. Weber, Precision calculations for the Higgs decays $H \to ZZ/WW \to 4$ leptons, Nucl. Phys. B, Proc. Suppl. **160,** 131 (2006).

[112] E. Bagnaschi, G. Degrassi, P. Slavich, and A. Vicini, Higgs production via gluon fusion in the POWHEG approach in the SM and in the MSSM, J. High Energy Phys. 02 (2012) 088.

[113] F. Cascioli, S. Höche, F. Krauss, P. Maierhöfer, S. Pozzorini, and F. Siegert, Precise Higgs-background predictions: Merging NLO QCD and squared quarkloop corrections to four-lepton + 0,1 jet production, J. High Energy Phys. 01 (2014) 046.

[114] T. Gleisberg, S. Höche, F. Krauss, M. Schönherr, S. Schumann, F. Siegert, and J. Winter, Event generation with SHERPA 1.1, J. High Energy Phys. 02 (2009) 007.

[115] F. Cascioli, P. Maierhöfer, and S. Pozzorini, Scattering Amplitudes with Open Loops, Phys. Rev. Lett. **108,** 111601 (2012).

[116] A. Denner, S. Dittmaier, and L. Hofer, COLLIER—A fortran-library for one-loop integrals, Proc. Sci., LL2014 (**2014**) 071 [arXiv:1407.0087].

[117] S. Schumann and F. Krauss, A Parton shower algorithm based on Catani-Seymour dipole factorisation, J. High Energy Phys. 03 (2008) 038.

[118] S. Agostinelli et al., GEANT4—a simulation toolkit, Nucl. Instrum. Methods Phys. Res. **506,** 250 (2003).

[119] ATLAS Collaboration, The ATLAS simulation infrastructure, Eur. Phys. J. C **70,** 823 (2010).

[120] A. Martin, W. Stirling, R. Thorne, and G. Watt, Parton distributions for the LHC, Eur. Phys. J. C **63,** 189 (2009).

[121] ATLAS Collaboration, Summary of ATLAS Pythia 8 tunes, Report No. ATL-PHYS-PUB-2012-003, 2012, https://cds.cern.ch/record/1474107.

[122] ATLAS Collaboration, The Pythia 8 A3 tune description of ATLAS minimum bias and inelastic measurements incorporating the Donnachie–Landshoff diffractive model, Report No. ATL-PHYS-PUB-2016-017, 2016, https://cds.cern.ch/record/2206965.

[123] ATLAS Collaboration, Measurement of the photon identification efficiencies with the ATLAS detector using LHC Run 2 data collected in 2015 and 2016, Eur. Phys. J. C **79,** 205 (2019).

[124] ATLAS Collaboration, Topological cell clustering in the ATLAS calorimeters and its performance in LHC Run 1, Eur. Phys. J. C **77,** 490 (2017).

[125] G. Aad et al., Electron and photon performance measurements with the ATLAS detector using the 2015-2017 LHC proton-proton collision data, J. Instrum. **14,** P12006 (2019).

[126] W. Lampl et al., Calorimeter clustering algorithms: Description and performance, Report No. ATL-LARGPUB-2008-002, 2008, https://cds.cern.ch/record/1099735.

[127] ATLAS Collaboration, Electron reconstruction and identification in the ATLAS experiment using the 2015 and 2016 LHC proton–proton collision data at $\sqrt{s} = 13$ TeV, Eur. Phys. J. C **79,** 639 (2019).

[128] ATLAS Collaboration, Electron and photon energy calibration with the ATLAS detector using 2015–2016 LHC proton–proton collision data, J. Instrum. **14,** P03017 (2019).

[129] ATLAS Collaboration, Muon reconstruction performance of the ATLAS detector in proton–proton collision data at $\sqrt{s} = 13$ TeV, Eur. Phys. J. C **76,** 292 (2016).

[130] ATLAS Collaboration, Jet energy scale measurements and their systematic uncertainties in proton–proton collisions at $\sqrt{s} = 13$ TeV with the ATLAS detector, Phys. Rev. D **96,** 072002 (2017).

[131] ATLAS Collaboration, Measurements of b-jet tagging efficiency with the ATLAS detector using $t\bar{t}$ events at $\sqrt{s} = 13$ TeV, J. High Energy Phys. 08 (2018) 089.

[132] ATLAS Collaboration, Performance of missing transverse momentum reconstruction with the ATLAS detector using proton–proton collisions at $\sqrt{s} = 13$ TeV, Eur. Phys. J. C **78,** 903 (2018).

[133] M. Cacciari, G. P. Salam, and G. Soyez, The anti-k_t jet clustering algorithm, J. High Energy Phys. 04 (2008) 063.

[134] N. Kauer and G. Passarino, Inadequacy of zero-width approximation for a light Higgs boson signal, J. High Energy Phys. 08 (2012) 116.

[135] F. Caola and K. Melnikov, Constraining the Higgs boson width with ZZ production at the LHC, Phys. Rev. D **88,** 054024 (2013).

[136] J. M. Campbell, R. K. Ellis, and C. Williams, Bounding the Higgs width at the LHC using full analytic results for $gg \to e^-e^+\mu^-\mu^+$, J. High Energy Phys. 04 (2014) 060.

[137] J. M. Campbell, R. K. Ellis, and C. Williams, Bounding the Higgs width at the LHC: Complementary results from $H \to WW$, Phys. Rev. D **89,** 053011 (2014).

[138] C. Englert, Y. Soreq, and M. Spannowsky, Off-shell Higgs coupling measurements in BSM scenarios, J. High Energy Phys. 05 (2015) 145.

[139] H. E. Logan, Hiding a Higgs width enhancement from off-shell $gg(\to h*) \to ZZ$ measurements, Phys. Rev. D **92,** 075038 (2015).

[140] ATLAS Collaboration, Search for heavy ZZ resonances in the $\ell^+\ell^-\ell^+\ell^-$ and $\ell^+\ell^-\nu\bar{\nu}$ final states using proton–proton collisions at $\sqrt{s} = 13$ TeV with the ATLAS detector, Eur. Phys. J. C **78,** 293 (2018).

[141] R. J. Barlow and C. Beeston, Fitting using finite Monte Carlo samples, Comput. Phys. Commun. **77,** 219 (1993).

[142] K. Cranmer, G. Lewis, L. Moneta, A. Shibata, and W. Verkerke, HistFactory: A tool for creating statistical models for use with RooFit and RooStats, Report No. CERN-OPEN-2012-016, 2012, http://cdsweb.cern.ch/record/1456844.

[143] G. Cowan, K. Cranmer, E. Gross, and O. Vitells, Asymptotic formulae for likelihood-based tests of new physics, Eur. Phys. J. C **71,** 1554 (2011); Erratum, Eur. Phys. J. C **73,** 2501 (2013).

[144] A. L. Read, Presentation of search results: the CLs technique, J. Phys. G **28,** 2693 (2002).

[145] ATLAS Collaboration, Measurements of the Higgs boson production and decay rates and coupling strengths using pp collision data at $\sqrt{s} = 7$ and 8 TeV in the ATLAS experiment, Eur. Phys. J. C **76,** 6 (2016).

[146] ATLAS Collaboration, Evaluation of theoretical uncertainties for simplified template cross section measurements of V-associated production of the Higgs boson, Report No. ATL-PHYS-PUB-2018-035, 2018, https://cds.cern.ch/record/2649241.

[147] ATLAS Collaboration, Constraints on the off-shell Higgs boson signal strength in the high-mass ZZ and WW final

states with the ATLAS detector, Eur. Phys. J. C **75**, 335 (2015).

[148] C. Englert, M. McCullough, and M. Spannowsky, Gluon-initiated associated production boosts Higgs physics, Phys. Rev. D **89**, 013013 (2014).

[149] ALEPH, CDF, D0, DELPHI, L3, OPAL, SLD Collaborations, LEP and Tevatron Electroweak Working Group, and SLD Electroweak and Heavy Flavour Groups, Precision electroweak measurements and constraints on the standard model, arXiv:1012.2367.

[150] T. D. Lee, A theory of spontaneous *T* violation, Phys. Rev. D **8**, 1226 (1973).

[151] J. F. Gunion and H. E. Haber, The *CP* conserving two Higgs doublet model: The approach to the decoupling limit, Phys. Rev. D **67**, 075019 (2003).

[152] G. C. Branco, P. M. Ferreira, L. Lavoura, M. N. Rebelo, M. Sher, and J. P. Silva, Theory and phenomenology of two-Higgs-doublet models, Phys. Rep. **516**, 1 (2012).

[153] Y. A. Gol'fand and E. P. Likhtman, Extension of the algebra of poincare group generators and violation of *p* invariance, Pis'ma Zh. Eksp. Teor. Fiz. **13**, 452 (1971) [JETP Lett. **13**, 323 (1971)].

[154] D. V. Volkov and V. P. Akulov, Is the neutrino a Goldstone particle?, Phys. Lett. **46B**, 109 (1973).

[155] J. Wess and B. Zumino, Supergauge transformations in four-dimensions, Nucl. Phys. **B70**, 39 (1974).

[156] J. Wess and B. Zumino, Supergauge invariant extension of quantum electrodynamics, Nucl. Phys. **B78**, 1 (1974).

[157] S. Ferrara and B. Zumino, Supergauge invariant Yang-Mills theories, Nucl. Phys. **B79**, 413 (1974).

[158] A. Salam and J. A. Strathdee, Supersymmetry and non-abelian gauges, Phys. Lett. **51B**, 353 (1974).

[159] S. L. Glashow and S. Weinberg, Natural conservation laws for neutral currents, Phys. Rev. D **15**, 1958 (1977).

[160] E. A. Paschos, Diagonal neutral currents, Phys. Rev. D **15**, 1966 (1977).

[161] P. Fayet, Supergauge invariant extension of the higgs mechanism and a model for the electron and its neutrino, Nucl. Phys. **B90**, 104 (1975).

[162] P. Fayet, Supersymmetry and weak, electromagnetic and strong interactions, Phys. Lett. **64B**, 159 (1976).

[163] P. Fayet, Spontaneously broken supersymmetric theories of weak, electromagnetic and strong interactions, Phys. Lett. **69B**, 489 (1977).

[164] L. Maiani, A. D. Polosa, and V. Riquer, Bounds to the higgs sector masses in minimal supersymmetry from LHC data, Phys. Lett. B **724**, 274 (2013).

[165] A. Djouadi, L. Maiani, G. Moreau, A. Polosa, J. Quevillon, and V. Riquer, The post-Higgs MSSM scenario: Habemus MSSM?, Eur. Phys. J. C **73**, 2650 (2013).

[166] A. Djouadi, L. Maiani, A. Polosa, J. Quevillon, and V. Riquer, Fully covering the MSSM Higgs sector at the LHC, J. High Energy Phys. 06 (2015) 168.

[167] ATLAS Collaboration, ATLAS computing acknowledgements, Report No. ATL-GEN-PUB-2016-002, https://cds.cern.ch/record/2202407.

G. Aad,[101] B. Abbott,[128] D. C. Abbott,[102] O. Abdinov,[13,a] A. Abed Abud,[70a,70b] K. Abeling,[53] D. K. Abhayasinghe,[93] S. H. Abidi,[167] O. S. AbouZeid,[40] N. L. Abraham,[156] H. Abramowicz,[161] H. Abreu,[160] Y. Abulaiti,[6] B. S. Acharya,[66a,66b,b] B. Achkar,[53] S. Adachi,[163] L. Adam,[99] C. Adam Bourdarios,[132] L. Adamczyk,[83a] L. Adamek,[167] J. Adelman,[120] M. Adersberger,[113] A. Adiguzel,[12c,c] S. Adorni,[54] T. Adye,[144] A. A. Affolder,[146] Y. Afik,[160] C. Agapopoulou,[132] M. N. Agaras,[38] A. Aggarwal,[118] C. Agheorghiesei,[27c] J. A. Aguilar-Saavedra,[140f,140a,d] F. Ahmadov,[79] W. S. Ahmed,[103] X. Ai,[15a] G. Aielli,[73a,73b] S. Akatsuka,[85] T. P. A. Åkesson,[96] E. Akilli,[54] A. V. Akimov,[110] K. Al Khoury,[132] G. L. Alberghi,[23b,23a] J. Albert,[176] M. J. Alconada Verzini,[161] S. Alderweireldt,[36] M. Aleksa,[36] I. N. Aleksandrov,[79] C. Alexa,[27b] D. Alexandre,[19] T. Alexopoulos,[10] A. Alfonsi,[119] M. Alhroob,[128] B. Ali,[142] G. Alimonti,[68a] J. Alison,[37] S. P. Alkire,[148] C. Allaire,[132] B. M. M. Allbrooke,[156] B. W. Allen,[131] P. P. Allport,[21] A. Aloisio,[69a,69b] A. Alonso,[40] F. Alonso,[88] C. Alpigiani,[148] A. A. Alshehri,[57] M. Alvarez Estevez,[98] D. Álvarez Piqueras,[174] M. G. Alviggi,[69a,69b] Y. Amaral Coutinho,[80b] A. Ambler,[103] L. Ambroz,[135] C. Amelung,[26] D. Amidei,[105] S. P. Amor Dos Santos,[140a] S. Amoroso,[46] C. S. Amrouche,[54] F. An,[78] C. Anastopoulos,[149] N. Andari,[145] T. Andeen,[11] C. F. Anders,[61b] J. K. Anders,[20] A. Andreazza,[68a,68b] V. Andrei,[61a] C. R. Anelli,[176] S. Angelidakis,[38] A. Angerami,[39] A. V. Anisenkov,[121b,121a] A. Annovi,[71a] C. Antel,[61a] M. T. Anthony,[149] M. Antonelli,[51] D. J. A. Antrim,[171] F. Anulli,[72a] M. Aoki,[81] J. A. Aparisi Pozo,[174] L. Aperio Bella,[36] G. Arabidze,[106] J. P. Araque,[140a] V. Araujo Ferraz,[80b] R. Araujo Pereira,[80b] C. Arcangeletti,[51] A. T. H. Arce,[49] F. A. Arduh,[88] J-F. Arguin,[109] S. Argyropoulos,[77] J.-H. Arling,[46] A. J. Armbruster,[36] L. J. Armitage,[92] A. Armstrong,[171] O. Arnaez,[167] H. Arnold,[119] A. Artamonov,[123,a] G. Artoni,[135] S. Artz,[99] S. Asai,[163] N. Asbah,[59] E. M. Asimakopoulou,[172] L. Asquith,[156] K. Assamagan,[29] R. Astalos,[28a] R. J. Atkin,[33a] M. Atkinson,[173] N. B. Atlay,[151] H. Atmani,[132] K. Augsten,[142] G. Avolio,[36] R. Avramidou,[60a] M. K. Ayoub,[15a] A. M. Azoulay,[168b] G. Azuelos,[109,e] M. J. Baca,[21] H. Bachacou,[145] K. Bachas,[67a,67b] M. Backes,[135] F. Backman,[45a,45b] P. Bagnaia,[72a,72b] M. Bahmani,[84] H. Bahrasemani,[152] A. J. Bailey,[174] V. R. Bailey,[173] J. T. Baines,[144] M. Bajic,[40] C. Bakalis,[10] O. K. Baker,[183] P. J. Bakker,[119] D. Bakshi Gupta,[8] S. Balaji,[157] E. M. Baldin,[121b,121a] P. Balek,[180] F. Balli,[145] W. K. Balunas,[135] J. Balz,[99] E. Banas,[84] A. Bandyopadhyay,[24] Sw. Banerjee,[181,f] A. A. E. Bannoura,[182] L. Barak,[161] W. M. Barbe,[38] E. L. Barberio,[104]

D. Barberis,[55b,55a] M. Barbero,[101] T. Barillari,[114] M-S. Barisits,[36] J. Barkeloo,[131] T. Barklow,[153] R. Barnea,[160] S. L. Barnes,[60c] B. M. Barnett,[144] R. M. Barnett,[18] Z. Barnovska-Blenessy,[60a] A. Baroncelli,[60a] G. Barone,[29] A. J. Barr,[135] L. Barranco Navarro,[45a,45b] F. Barreiro,[98] J. Barreiro Guimarães da Costa,[15a] S. Barsov,[138] R. Bartoldus,[153] G. Bartolini,[101] A. E. Barton,[89] P. Bartos,[28a] A. Basalaev,[46] A. Bassalat,[132,g] R. L. Bates,[57] S. J. Batista,[167] S. Batlamous,[35e] J. R. Batley,[32] B. Batool,[151] M. Battaglia,[146] M. Bauce,[72a,72b] F. Bauer,[145] K. T. Bauer,[171] H. S. Bawa,[31,h] J. B. Beacham,[49] T. Beau,[136] P. H. Beauchemin,[170] F. Becherer,[52] P. Bechtle,[24] H. C. Beck,[53] H. P. Beck,[20,i] K. Becker,[52] M. Becker,[99] C. Becot,[46] A. Beddall,[12d] A. J. Beddall,[12a] V. A. Bednyakov,[79] M. Bedognetti,[119] C. P. Bee,[155] T. A. Beermann,[76] M. Begalli,[80b] M. Begel,[29] A. Behera,[155] J. K. Behr,[46] F. Beisiegel,[24] A. S. Bell,[94] G. Bella,[161] L. Bellagamba,[23b] A. Bellerive,[34] P. Bellos,[9] K. Beloborodov,[121b,121a] K. Belotskiy,[111] N. L. Belyaev,[111] D. Benchekroun,[35a] N. Benekos,[10] Y. Benhammou,[161] D. P. Benjamin,[6] M. Benoit,[54] J. R. Bensinger,[26] S. Bentvelsen,[119] L. Beresford,[135] M. Beretta,[51] D. Berge,[46] E. Bergeaas Kuutmann,[172] N. Berger,[5] B. Bergmann,[142] L. J. Bergsten,[26] J. Beringer,[18] S. Berlendis,[7] N. R. Bernard,[102] G. Bernardi,[136] C. Bernius,[153] T. Berry,[93] P. Berta,[99] C. Bertella,[15a] I. A. Bertram,[89] G. J. Besjes,[40] O. Bessidskaia Bylund,[182] N. Besson,[145] A. Bethani,[100] S. Bethke,[114] A. Betti,[24] A. J. Bevan,[92] J. Beyer,[114] R. Bi,[139] R. M. Bianchi,[139] O. Biebel,[113] D. Biedermann,[19] R. Bielski,[36] K. Bierwagen,[99] N. V. Biesuz,[71a,71b] M. Biglietti,[74a] T. R. V. Billoud,[109] M. Bindi,[53] A. Bingul,[12d] C. Bini,[72a,72b] S. Biondi,[23b,23a] M. Birman,[180] T. Bisanz,[53] J. P. Biswal,[161] A. Bitadze,[100] C. Bittrich,[48] K. Bjørke,[134] K. M. Black,[25] T. Blazek,[28a] I. Bloch,[46] C. Blocker,[26] A. Blue,[57] U. Blumenschein,[92] G. J. Bobbink,[119] V. S. Bobrovnikov,[121b,121a] S. S. Bocchetta,[96] A. Bocci,[49] D. Boerner,[46] D. Bogavac,[14] A. G. Bogdanchikov,[121b,121a] C. Bohm,[45a] V. Boisvert,[93] P. Bokan,[53,172] T. Bold,[83a] A. S. Boldyrev,[112] A. E. Bolz,[61b] M. Bomben,[136] M. Bona,[92] J. S. Bonilla,[131] M. Boonekamp,[145] H. M. Borecka-Bielska,[90] A. Borisov,[122] G. Borissov,[89] J. Bortfeldt,[36] D. Bortoletto,[135] V. Bortolotto,[73a,73b] D. Boscherini,[23b] M. Bosman,[14] J. D. Bossio Sola,[103] K. Bouaouda,[35a] J. Boudreau,[139] E. V. Bouhova-Thacker,[89] D. Boumediene,[38] S. K. Boutle,[57] A. Boveia,[126] J. Boyd,[36] D. Boye,[33b,j] I. R. Boyko,[79] A. J. Bozson,[93] J. Bracinik,[21] N. Brahimi,[101] G. Brandt,[182] O. Brandt,[61a] F. Braren,[46] B. Brau,[102] J. E. Brau,[131] W. D. Breaden Madden,[57] K. Brendlinger,[46] L. Brenner,[46] R. Brenner,[172] S. Bressler,[180] B. Brickwedde,[99] D. L. Briglin,[21] D. Britton,[57] D. Britzger,[114] I. Brock,[24] R. Brock,[106] G. Brooijmans,[39] W. K. Brooks,[147c] E. Brost,[120] J. H. Broughton,[21] P. A. Bruckman de Renstrom,[84] D. Bruncko,[28b] A. Bruni,[23b] G. Bruni,[23b] L. S. Bruni,[119] S. Bruno,[73a,73b] B. H. Brunt,[32] M. Bruschi,[23b] N. Bruscino,[139] P. Bryant,[37] L. Bryngemark,[96] T. Buanes,[17] Q. Buat,[36] P. Buchholz,[151] A. G. Buckley,[57] I. A. Budagov,[79] M. K. Bugge,[134] F. Bührer,[52] O. Bulekov,[111] T. J. Burch,[120] S. Burdin,[90] C. D. Burgard,[119] A. M. Burger,[129] B. Burghgrave,[8] J. T. P. Burr,[46] J. C. Burzynski,[102] V. Büscher,[99] E. Buschmann,[53] P. J. Bussey,[57] J. M. Butler,[25] C. M. Buttar,[57] J. M. Butterworth,[94] P. Butti,[36] W. Buttinger,[36] A. Buzatu,[158] A. R. Buzykaev,[121b,121a] G. Cabras,[23b,23a] S. Cabrera Urbán,[174] D. Caforio,[56] H. Cai,[173] V. M. M. Cairo,[153] O. Cakir,[4a] N. Calace,[36] P. Calafiura,[18] A. Calandri,[101] G. Calderini,[136] P. Calfayan,[65] G. Callea,[57] L. P. Caloba,[80b] S. Calvente Lopez,[98] D. Calvet,[38] S. Calvet,[38] T. P. Calvet,[155] M. Calvetti,[71a,71b] R. Camacho Toro,[136] S. Camarda,[36] D. Camarero Munoz,[98] P. Camarri,[73a,73b] D. Cameron,[134] R. Caminal Armadans,[102] C. Camincher,[36] S. Campana,[36] M. Campanelli,[94] A. Camplani,[40] A. Campoverde,[151] V. Canale,[69a,69b] A. Canesse,[103] M. Cano Bret,[60c] J. Cantero,[129] T. Cao,[161] Y. Cao,[173] M. D. M. Capeans Garrido,[36] M. Capua,[41b,41a] R. Cardarelli,[73a] F. Cardillo,[149] G. Carducci,[41b,41a] I. Carli,[143] T. Carli,[36] G. Carlino,[69a] B. T. Carlson,[139] L. Carminati,[68a,68b] R. M. D. Carney,[45a,45b] S. Caron,[118] E. Carquin,[147c] S. Carrá,[46] J. W. S. Carter,[167] M. P. Casado,[14,k] A. F. Casha,[167] D. W. Casper,[171] R. Castelijn,[119] F. L. Castillo,[174] V. Castillo Gimenez,[174] N. F. Castro,[140a,140e] A. Catinaccio,[36] J. R. Catmore,[134] A. Cattai,[36] J. Caudron,[24] V. Cavaliere,[29] E. Cavallaro,[14] M. Cavalli-Sforza,[14] V. Cavasinni,[71a,71b] E. Celebi,[12b] F. Ceradini,[74a,74b] L. Cerda Alberich,[174] K. Cerny,[130] A. S. Cerqueira,[80a] A. Cerri,[156] L. Cerrito,[73a,73b] F. Cerutti,[18] A. Cervelli,[23b,23a] S. A. Cetin,[12b] D. Chakraborty,[120] S. K. Chan,[59] W. S. Chan,[119] W. Y. Chan,[90] J. D. Chapman,[32] B. Chargeishvili,[159b] D. G. Charlton,[21] T. P. Charman,[92] C. C. Chau,[34] S. Che,[126] A. Chegwidden,[106] S. Chekanov,[6] S. V. Chekulaev,[168a] G. A. Chelkov,[79,l] M. A. Chelstowska,[36] B. Chen,[78] C. Chen,[60a] C. H. Chen,[78] H. Chen,[29] J. Chen,[60a] J. Chen,[39] S. Chen,[137] S. J. Chen,[15c] X. Chen,[15b,m] Y. Chen,[82] Y-H. Chen,[46] H. C. Cheng,[63a] H. J. Cheng,[15a,15d] A. Cheplakov,[79] E. Cheremushkina,[122] R. Cherkaoui El Moursli,[35e] E. Cheu,[7] K. Cheung,[64] T. J. A. Chevalérias,[145] L. Chevalier,[145] V. Chiarella,[51] G. Chiarelli,[71a] G. Chiodini,[67a] A. S. Chisholm,[36,21] A. Chitan,[27b] I. Chiu,[163] Y. H. Chiu,[176] M. V. Chizhov,[79] K. Choi,[65] A. R. Chomont,[72a,72b] S. Chouridou,[162] Y. S. Chow,[119] M. C. Chu,[63a] X. Chu,[15a] J. Chudoba,[141] A. J. Chuinard,[103] J. J. Chwastowski,[84] L. Chytka,[130] K. M. Ciesla,[84] D. Cinca,[47] V. Cindro,[91] I. A. Cioară,[27b] A. Ciocio,[18] F. Cirotto,[69a,69b] Z. H. Citron,[180,n] M. Citterio,[68a] D. A. Ciubotaru,[27b] B. M. Ciungu,[167] A. Clark,[54] M. R. Clark,[39] P. J. Clark,[50] C. Clement,[45a,45b] Y. Coadou,[101] M. Cobal,[66a,66c] A. Coccaro,[55b] J. Cochran,[78] H. Cohen,[161] A. E. C. Coimbra,[36]

L. Colasurdo,[118] B. Cole,[39] A. P. Colijn,[119] J. Collot,[58] P. Conde Muiño,[140a,o] E. Coniavitis,[52] S. H. Connell,[33b] I. A. Connelly,[57] S. Constantinescu,[27b] F. Conventi,[69a,p] A. M. Cooper-Sarkar,[135] F. Cormier,[175] K. J. R. Cormier,[167] L. D. Corpe,[94] M. Corradi,[72a,72b] E. E. Corrigan,[96] F. Corriveau,[103,q] A. Cortes-Gonzalez,[36] M. J. Costa,[174] F. Costanza,[5] D. Costanzo,[149] G. Cowan,[93] J. W. Cowley,[32] J. Crane,[100] K. Cranmer,[124] S. J. Crawley,[57] R. A. Creager,[137] S. Crépé-Renaudin,[58] F. Crescioli,[136] M. Cristinziani,[24] V. Croft,[119] G. Crosetti,[41b,41a] A. Cueto,[5] T. Cuhadar Donszelmann,[149] A. R. Cukierman,[153] S. Czekierda,[84] P. Czodrowski,[36] M. J. Da Cunha Sargedas De Sousa,[60b] J. V. Da Fonseca Pinto,[80b] C. Da Via,[100] W. Dabrowski,[83a] T. Dado,[28a] S. Dahbi,[35e] T. Dai,[105] C. Dallapiccola,[102] M. Dam,[40] G. D'amen,[23b,23a] V. D'Amico,[74a,74b] J. Damp,[99] J. R. Dandoy,[137] M. F. Daneri,[30] N. P. Dang,[181,f] N. S. Dann,[100] M. Danninger,[175] V. Dao,[36] G. Darbo,[55b] O. Dartsi,[5] A. Dattagupta,[131] T. Daubney,[46] S. D'Auria,[68a,68b] W. Davey,[24] C. David,[46] T. Davidek,[143] D. R. Davis,[49] I. Dawson,[149] K. De,[8] R. De Asmundis,[69a] M. De Beurs,[119] S. De Castro,[23b,23a] S. De Cecco,[72a,72b] N. De Groot,[118] P. de Jong,[119] H. De la Torre,[106] A. De Maria,[15c] D. De Pedis,[72a] A. De Salvo,[72a] U. De Sanctis,[73a,73b] M. De Santis,[73a,73b] A. De Santo,[156] K. De Vasconcelos Corga,[101] J. B. De Vivie De Regie,[132] C. Debenedetti,[146] D. V. Dedovich,[79] A. M. Deiana,[42] M. Del Gaudio,[41b,41a] J. Del Peso,[98] Y. Delabat Diaz,[46] D. Delgove,[132] F. Deliot,[145,r] C. M. Delitzsch,[7] M. Della Pietra,[69a,69b] D. Della Volpe,[54] A. Dell'Acqua,[36] L. Dell'Asta,[73a,73b] M. Delmastro,[5] C. Delporte,[132] P. A. Delsart,[58] D. A. DeMarco,[167] S. Demers,[183] M. Demichev,[79] G. Demontigny,[109] S. P. Denisov,[122] D. Denysiuk,[119] L. D'Eramo,[136] D. Derendarz,[84] J. E. Derkaoui,[35d] F. Derue,[136] P. Dervan,[90] K. Desch,[24] C. Deterre,[46] K. Dette,[167] C. Deutsch,[24] M. R. Devesa,[30] P. O. Deviveiros,[36] A. Dewhurst,[144] S. Dhaliwal,[26] F. A. Di Bello,[54] A. Di Ciaccio,[73a,73b] L. Di Ciaccio,[5] W. K. Di Clemente,[137] C. Di Donato,[69a,69b] A. Di Girolamo,[36] G. Di Gregorio,[71a,71b] B. Di Micco,[74a,74b] R. Di Nardo,[102] K. F. Di Petrillo,[59] R. Di Sipio,[167] D. Di Valentino,[34] C. Diaconu,[101] F. A. Dias,[40] T. Dias Do Vale,[140a] M. A. Diaz,[147a] J. Dickinson,[18] E. B. Diehl,[105] J. Dietrich,[19] S. Díez Cornell,[46] A. Dimitrievska,[18] W. Ding,[15b] J. Dingfelder,[24] F. Dittus,[36] F. Djama,[101] T. Djobava,[159b] J. I. Djuvsland,[17] M. A. B. Do Vale,[80c] M. Dobre,[27b] D. Dodsworth,[26] C. Doglioni,[96] J. Dolejsi,[143] Z. Dolezal,[143] M. Donadelli,[80d] B. Dong,[60c] J. Donini,[38] A. D'onofrio,[92] M. D'Onofrio,[90] J. Dopke,[144] A. Doria,[69a] M. T. Dova,[88] A. T. Doyle,[57] E. Drechsler,[152] E. Dreyer,[152] T. Dreyer,[53] A. S. Drobac,[170] Y. Duan,[60b] F. Dubinin,[110] M. Dubovsky,[28a] A. Dubreuil,[54] E. Duchovni,[180] G. Duckeck,[113] A. Ducourthial,[136] O. A. Ducu,[109] D. Duda,[114] A. Dudarev,[36] A. C. Dudder,[99] E. M. Duffield,[18] L. Duflot,[132] M. Dührssen,[36] C. Dülsen,[182] M. Dumancic,[180] A. E. Dumitriu,[27b] A. K. Duncan,[57] M. Dunford,[61a] A. Duperrin,[101] H. Duran Yildiz,[4a] M. Düren,[56] A. Durglishvili,[159b] D. Duschinger,[48] B. Dutta,[46] D. Duvnjak,[1] G. I. Dyckes,[137] M. Dyndal,[36] S. Dysch,[100] B. S. Dziedzic,[84] K. M. Ecker,[114] R. C. Edgar,[105] T. Eifert,[36] G. Eigen,[17] K. Einsweiler,[18] T. Ekelof,[172] H. El Jarrari,[35e] M. El Kacimi,[35c] R. El Kosseifi,[101] V. Ellajosyula,[172] M. Ellert,[172] F. Ellinghaus,[182] A. A. Elliot,[92] N. Ellis,[36] J. Elmsheuser,[29] M. Elsing,[36] D. Emeliyanov,[144] A. Emerman,[39] Y. Enari,[163] J. S. Ennis,[178] M. B. Epland,[49] J. Erdmann,[47] A. Ereditato,[20] M. Errenst,[36] M. Escalier,[132] C. Escobar,[174] O. Estrada Pastor,[174] E. Etzion,[161] H. Evans,[65] A. Ezhilov,[138] F. Fabbri,[57] L. Fabbri,[23b,23a] V. Fabiani,[118] G. Facini,[94] R. M. Faisca Rodrigues Pereira,[140a] R. M. Fakhrutdinov,[122] S. Falciano,[72a] P. J. Falke,[5] S. Falke,[5] J. Faltova,[143] Y. Fang,[15a] Y. Fang,[15a] G. Fanourakis,[44] M. Fanti,[68a,68b] A. Farbin,[8] A. Farilla,[74a] E. M. Farina,[70a,70b] T. Farooque,[106] S. Farrell,[18] S. M. Farrington,[50] P. Farthouat,[36] F. Fassi,[35e] P. Fassnacht,[36] D. Fassouliotis,[9] M. Faucci Giannelli,[50] W. J. Fawcett,[32] L. Fayard,[132] O. L. Fedin,[138,s] W. Fedorko,[175] M. Feickert,[42] S. Feigl,[134] L. Feligioni,[101] A. Fell,[149] C. Feng,[60b] E. J. Feng,[36] M. Feng,[49] M. J. Fenton,[57] A. B. Fenyuk,[122] J. Ferrando,[46] A. Ferrante,[173] A. Ferrari,[172] P. Ferrari,[119] R. Ferrari,[70a] D. E. Ferreira de Lima,[61b] A. Ferrer,[174] D. Ferrere,[54] C. Ferretti,[105] F. Fiedler,[99] A. Filipčič,[91] F. Filthaut,[118] K. D. Finelli,[25] M. C. N. Fiolhais,[140a,140c,t] L. Fiorini,[174] F. Fischer,[113] W. C. Fisher,[106] I. Fleck,[151] P. Fleischmann,[105] R. R. M. Fletcher,[137] T. Flick,[182] B. M. Flierl,[113] L. Flores,[137] L. R. Flores Castillo,[63a] F. M. Follega,[75a,75b] N. Fomin,[17] J. H. Foo,[167] G. T. Forcolin,[75a,75b] A. Formica,[145] F. A. Förster,[14] A. C. Forti,[100] A. G. Foster,[21] M. G. Foti,[135] D. Fournier,[132] H. Fox,[89] P. Francavilla,[71a,71b] S. Francescato,[72a,72b] M. Franchini,[23b,23a] S. Franchino,[61a] D. Francis,[36] L. Franconi,[20] M. Franklin,[59] A. N. Fray,[92] B. Freund,[109] W. S. Freund,[80b] E. M. Freundlich,[47] D. C. Frizzell,[128] D. Froidevaux,[36] J. A. Frost,[135] C. Fukunaga,[164] E. Fullana Torregrosa,[174] E. Fumagalli,[55b,55a] T. Fusayasu,[115] J. Fuster,[174] A. Gabrielli,[23b,23a] A. Gabrielli,[18] G. P. Gach,[83a] S. Gadatsch,[54] P. Gadow,[114] G. Gagliardi,[55b,55a] L. G. Gagnon,[109] C. Galea,[27b] B. Galhardo,[140a] G. E. Gallardo,[135] E. J. Gallas,[135] B. J. Gallop,[144] P. Gallus,[142] G. Galster,[40] R. Gamboa Goni,[92] K. K. Gan,[126] S. Ganguly,[180] J. Gao,[60a] Y. Gao,[90] Y. S. Gao,[31,h] C. García,[174] J. E. García Navarro,[174] J. A. García Pascual,[15a] C. Garcia-Argos,[52] M. Garcia-Sciveres,[18] R. W. Gardner,[37] N. Garelli,[153] S. Gargiulo,[52] V. Garonne,[134] A. Gaudiello,[55b,55a] G. Gaudio,[70a] I. L. Gavrilenko,[110] A. Gavrilyuk,[123] C. Gay,[175] G. Gaycken,[24] E. N. Gazis,[10] A. A. Geanta,[27b] C. N. P. Gee,[144] J. Geisen,[53] M. Geisen,[99] M. P. Geisler,[61a] C. Gemme,[55b]

M. H. Genest,[58] C. Geng,[105] S. Gentile,[72a,72b] S. George,[93] T. Geralis,[44] L. O. Gerlach,[53] P. Gessinger-Befurt,[99] G. Gessner,[47] S. Ghasemi,[151] M. Ghasemi Bostanabad,[176] A. Ghosh,[132] A. Ghosh,[77] B. Giacobbe,[23b] S. Giagu,[72a,72b] N. Giangiacomi,[23b,23a] P. Giannetti,[71a] A. Giannini,[69a,69b] S. M. Gibson,[93] M. Gignac,[146] D. Gillberg,[34] G. Gilles,[182] D. M. Gingrich,[3,e] M. P. Giordani,[66a,66c] F. M. Giorgi,[23b] P. F. Giraud,[145] G. Giugliarelli,[66a,66c] D. Giugni,[68a] F. Giuli,[73a,73b] S. Gkaitatzis,[162] I. Gkialas,[9,u] E. L. Gkougkousis,[14] P. Gkountoumis,[10] L. K. Gladilin,[112] C. Glasman,[98] J. Glatzer,[14] P. C. F. Glaysher,[46] A. Glazov,[46] M. Goblirsch-Kolb,[26] S. Goldfarb,[104] T. Golling,[54] D. Golubkov,[122] A. Gomes,[140a,140b] R. Goncalves Gama,[53] R. Gonçalo,[140a,140b] G. Gonella,[52] L. Gonella,[21] A. Gongadze,[79] F. Gonnella,[21] J. L. Gonski,[59] S. González de la Hoz,[174] S. Gonzalez-Sevilla,[54] G. R. Gonzalvo Rodriguez,[174] L. Goossens,[36] P. A. Gorbounov,[123] H. A. Gordon,[29] B. Gorini,[36] E. Gorini,[67a,67b] A. Gorišek,[91] A. T. Goshaw,[49] M. I. Gostkin,[79] C. A. Gottardo,[24] M. Gouighri,[35b] D. Goujdami,[35c] A. G. Goussiou,[148] N. Govender,[33b,v] C. Goy,[5] E. Gozani,[160] I. Grabowska-Bold,[83a] E. C. Graham,[90] J. Gramling,[171] E. Gramstad,[134] S. Grancagnolo,[19] M. Grandi,[156] V. Gratchev,[138] P. M. Gravila,[27f] F. G. Gravili,[67a,67b] C. Gray,[57] H. M. Gray,[18] C. Grefe,[24] K. Gregersen,[96] I. M. Gregor,[46] P. Grenier,[153] K. Grevtsov,[46] C. Grieco,[14] N. A. Grieser,[128] J. Griffiths,[8] A. A. Grillo,[146] K. Grimm,[31,w] S. Grinstein,[14,x] J.-F. Grivaz,[132] S. Groh,[99] E. Gross,[180] J. Grosse-Knetter,[53] Z. J. Grout,[94] C. Grud,[105] A. Grummer,[117] L. Guan,[105] W. Guan,[181] J. Guenther,[36] A. Guerguichon,[132] J. G. R. Guerrero Rojas,[174] F. Guescini,[114] D. Guest,[171] R. Gugel,[52] T. Guillemin,[5] S. Guindon,[36] U. Gul,[57] J. Guo,[60c] W. Guo,[105] Y. Guo,[60a,y] Z. Guo,[101] R. Gupta,[46] S. Gurbuz,[12c] G. Gustavino,[128] P. Gutierrez,[128] C. Gutschow,[94] C. Guyot,[145] M. P. Guzik,[83a] C. Gwenlan,[135] C. B. Gwilliam,[90] A. Haas,[124] C. Haber,[18] H. K. Hadavand,[8] N. Haddad,[35e] A. Hadef,[60a] S. Hageböck,[36] M. Hagihara,[169] M. Haleem,[177] J. Haley,[129] G. Halladjian,[106] G. D. Hallewell,[101] K. Hamacher,[182] P. Hamal,[130] K. Hamano,[176] H. Hamdaoui,[35e] G. N. Hamity,[149] K. Han,[60a,z] L. Han,[60a] S. Han,[15a,15d] K. Hanagaki,[81,aa] M. Hance,[146] D. M. Handl,[113] B. Haney,[137] R. Hankache,[136] E. Hansen,[96] J. B. Hansen,[40] J. D. Hansen,[40] M. C. Hansen,[24] P. H. Hansen,[40] E. C. Hanson,[100] K. Hara,[169] A. S. Hard,[181] T. Harenberg,[182] S. Harkusha,[107] P. F. Harrison,[178] N. M. Hartmann,[113] Y. Hasegawa,[150] A. Hasib,[50] S. Hassani,[145] S. Haug,[20] R. Hauser,[106] L. B. Havener,[39] M. Havranek,[142] C. M. Hawkes,[21] R. J. Hawkings,[36] D. Hayden,[106] C. Hayes,[155] R. L. Hayes,[175] C. P. Hays,[135] J. M. Hays,[92] H. S. Hayward,[90] S. J. Haywood,[144] F. He,[60a] M. P. Heath,[50] V. Hedberg,[96] L. Heelan,[8] S. Heer,[24] K. K. Heidegger,[52] W. D. Heidorn,[78] J. Heilman,[34] S. Heim,[46] T. Heim,[18] B. Heinemann,[46,bb] J. J. Heinrich,[131] L. Heinrich,[36] C. Heinz,[56] J. Hejbal,[141] L. Helary,[61b] A. Held,[175] S. Hellesund,[134] C. M. Helling,[146] S. Hellman,[45a,45b] C. Helsens,[36] R. C. W. Henderson,[89] Y. Heng,[181] S. Henkelmann,[175] A. M. Henriques Correia,[36] G. H. Herbert,[19] H. Herde,[26] V. Herget,[177] Y. Hernández Jiménez,[33c] H. Herr,[99] M. G. Herrmann,[113] T. Herrmann,[48] G. Herten,[52] R. Hertenberger,[113] L. Hervas,[36] T. C. Herwig,[137] G. G. Hesketh,[94] N. P. Hessey,[168a] A. Higashida,[163] S. Higashino,[81] E. Higón-Rodriguez,[174] K. Hildebrand,[37] E. Hill,[176] J. C. Hill,[32] K. K. Hill,[29] K. H. Hiller,[46] S. J. Hillier,[21] M. Hils,[48] I. Hinchliffe,[18] F. Hinterkeuser,[24] M. Hirose,[133] S. Hirose,[52] D. Hirschbuehl,[182] B. Hiti,[91] O. Hladik,[141] D. R. Hlaluku,[33c] X. Hoad,[50] J. Hobbs,[155] N. Hod,[180] M. C. Hodgkinson,[149] A. Hoecker,[36] F. Hoenig,[113] D. Hohn,[52] D. Hohov,[132] T. R. Holmes,[37] M. Holzbock,[113] L. B. A. H Hommels,[32] S. Honda,[169] T. Honda,[81] T. M. Hong,[139] A. Hönle,[114] B. H. Hooberman,[173] W. H. Hopkins,[6] Y. Horii,[116] P. Horn,[48] L. A. Horyn,[37] J-Y. Hostachy,[58] A. Hostiuc,[148] S. Hou,[158] A. Hoummada,[35a] J. Howarth,[100] J. Hoya,[88] M. Hrabovsky,[130] J. Hrdinka,[76] I. Hristova,[19] J. Hrivnac,[132] A. Hrynevich,[108] T. Hryn'ova,[5] P. J. Hsu,[64] S.-C. Hsu,[148] Q. Hu,[29] S. Hu,[60c] Y. Huang,[15a] Z. Hubacek,[142] F. Hubaut,[101] M. Huebner,[24] F. Huegging,[24] T. B. Huffman,[135] M. Huhtinen,[36] R. F. H. Hunter,[34] P. Huo,[155] A. M. Hupe,[34] N. Huseynov,[79,cc] J. Huston,[106] J. Huth,[59] R. Hyneman,[105] S. Hyrych,[28a] G. Iacobucci,[54] G. Iakovidis,[29] I. Ibragimov,[151] L. Iconomidou-Fayard,[132] Z. Idrissi,[35e] P. Iengo,[36] R. Ignazzi,[40] O. Igonkina,[119,a,dd] R. Iguchi,[163] T. Iizawa,[54] Y. Ikegami,[81] M. Ikeno,[81] D. Iliadis,[162] N. Ilic,[118] F. Iltzsche,[48] G. Introzzi,[70a,70b] M. Iodice,[74a] K. Iordanidou,[168a] V. Ippolito,[72a,72b] M. F. Isacson,[172] M. Ishino,[163] M. Ishitsuka,[165] W. Islam,[129] C. Issever,[135] S. Istin,[160] F. Ito,[169] J. M. Iturbe Ponce,[63a] R. Iuppa,[75a,75b] A. Ivina,[180] H. Iwasaki,[81] J. M. Izen,[43] V. Izzo,[69a] P. Jacka,[141] P. Jackson,[1] R. M. Jacobs,[24] B. P. Jaeger,[152] V. Jain,[2] G. Jäkel,[182] K. B. Jakobi,[99] K. Jakobs,[52] S. Jakobsen,[76] T. Jakoubek,[141] J. Jamieson,[57] K. W. Janas,[83a] R. Jansky,[54] J. Janssen,[24] M. Janus,[53] P. A. Janus,[83a] G. Jarlskog,[96] N. Javadov,[79,cc] T. Javůrek,[36] M. Javurkova,[52] F. Jeanneau,[145] L. Jeanty,[131] J. Jejelava,[159a,ee] A. Jelinskas,[178] P. Jenni,[52,ff] J. Jeong,[46] N. Jeong,[46] S. Jézéquel,[5] H. Ji,[181] J. Jia,[155] H. Jiang,[78] Y. Jiang,[60a] Z. Jiang,[153,gg] S. Jiggins,[52] F. A. Jimenez Morales,[38] J. Jimenez Pena,[174] S. Jin,[15c] A. Jinaru,[27b] O. Jinnouchi,[165] H. Jivan,[33c] P. Johansson,[149] K. A. Johns,[7] C. A. Johnson,[65] K. Jon-And,[45a,45b] R. W. L. Jones,[89] S. D. Jones,[156] S. Jones,[7] T. J. Jones,[90] J. Jongmanns,[61a] P. M. Jorge,[140a] J. Jovicevic,[36] X. Ju,[18] J. J. Junggeburth,[114] A. Juste Rozas,[14,x] A. Kaczmarska,[84] M. Kado,[72a,72b] H. Kagan,[126] M. Kagan,[153] C. Kahra,[99] T. Kaji,[179] E. Kajomovitz,[160] C. W. Kalderon,[96] A. Kaluza,[99] A. Kamenshchikov,[122] L. Kanjir,[91] Y. Kano,[163]

V. A. Kantserov,[111] J. Kanzaki,[81] L. S. Kaplan,[181] D. Kar,[33c] M. J. Kareem,[168b] E. Karentzos,[10] S. N. Karpov,[79] Z. M. Karpova,[79] V. Kartvelishvili,[89] A. N. Karyukhin,[122] L. Kashif,[181] R. D. Kass,[126] A. Kastanas,[45a,45b] Y. Kataoka,[163] C. Kato,[60d,60c] J. Katzy,[46] K. Kawade,[82] K. Kawagoe,[87] T. Kawaguchi,[116] T. Kawamoto,[163] G. Kawamura,[53] E. F. Kay,[176] V. F. Kazanin,[121b,121a] R. Keeler,[176] R. Kehoe,[42] J. S. Keller,[34] E. Kellermann,[96] D. Kelsey,[156] J. J. Kempster,[21] J. Kendrick,[21] O. Kepka,[141] S. Kersten,[182] B. P. Kerševan,[91] S. Ketabchi Haghighat,[167] M. Khader,[173] F. Khalil-Zada,[13] M. Khandoga,[145] A. Khanov,[129] A. G. Kharlamov,[121b,121a] T. Kharlamova,[121b,121a] E. E. Khoda,[175] A. Khodinov,[166] T. J. Khoo,[54] E. Khramov,[79] J. Khubua,[159b] S. Kido,[82] M. Kiehn,[54] C. R. Kilby,[93] Y. K. Kim,[37] N. Kimura,[66a,66c] O. M. Kind,[19] B. T. King,[90,a] D. Kirchmeier,[48] J. Kirk,[144] A. E. Kiryunin,[114] T. Kishimoto,[163] D. P. Kisliuk,[167] V. Kitali,[46] O. Kivernyk,[5] E. Kladiva,[28b,a] T. Klapdor-Kleingrothaus,[52] M. Klassen,[61a] M. H. Klein,[105] M. Klein,[90] U. Klein,[90] K. Kleinknecht,[99] P. Klimek,[120] A. Klimentov,[29] T. Klingl,[24] T. Klioutchnikova,[36] F. F. Klitzner,[113] P. Kluit,[119] S. Kluth,[114] E. Kneringer,[76] E. B. F. G. Knoops,[101] A. Knue,[52] D. Kobayashi,[87] T. Kobayashi,[163] M. Kobel,[48] M. Kocian,[153] P. Kodys,[143] P. T. Koenig,[24] T. Koffas,[34] N. M. Köhler,[114] T. Koi,[153] M. Kolb,[61b] I. Koletsou,[5] T. Komarek,[130] T. Kondo,[81] N. Kondrashova,[60c] K. Köneke,[52] A. C. König,[118] T. Kono,[125] R. Konoplich,[124,hh] V. Konstantinides,[94] N. Konstantinidis,[94] B. Konya,[96] R. Kopeliansky,[65] S. Koperny,[83a] K. Korcyl,[84] K. Kordas,[162] G. Koren,[161] A. Korn,[94] I. Korolkov,[14] E. V. Korolkova,[149] N. Korotkova,[112] O. Kortner,[114] S. Kortner,[114] T. Kosek,[143] V. V. Kostyukhin,[24] A. Kotwal,[49] A. Koulouris,[10] A. Kourkoumeli-Charalampidi,[70a,70b] C. Kourkoumelis,[9] E. Kourlitis,[149] V. Kouskoura,[29] A. B. Kowalewska,[84] R. Kowalewski,[176] C. Kozakai,[163] W. Kozanecki,[145] A. S. Kozhin,[122] V. A. Kramarenko,[112] G. Kramberger,[91] D. Krasnopevtsev,[60a] M. W. Krasny,[136] A. Krasznahorkay,[36] D. Krauss,[114] J. A. Kremer,[83a] J. Kretzschmar,[90] P. Krieger,[167] F. Krieter,[113] A. Krishnan,[61b] K. Krizka,[18] K. Kroeninger,[47] H. Kroha,[114] J. Kroll,[141] J. Kroll,[137] J. Krstic,[16] U. Kruchonak,[79] H. Krüger,[24] N. Krumnack,[78] M. C. Kruse,[49] J. A. Krzysiak,[84] T. Kubota,[104] O. Kuchinskaia,[166] S. Kuday,[4b] J. T. Kuechler,[46] S. Kuehn,[36] A. Kugel,[61a] T. Kuhl,[46] V. Kukhtin,[79] R. Kukla,[101] Y. Kulchitsky,[107,ii] S. Kuleshov,[147c] Y. P. Kulinich,[173] M. Kuna,[58] T. Kunigo,[85] A. Kupco,[141] T. Kupfer,[47] O. Kuprash,[52] H. Kurashige,[82] L. L. Kurchaninov,[168a] Y. A. Kurochkin,[107] A. Kurova,[111] M. G. Kurth,[15a,15d] E. S. Kuwertz,[36] M. Kuze,[165] A. K. Kvam,[148] J. Kvita,[130] T. Kwan,[103] A. La Rosa,[114] L. La Rotonda,[41b,41a] F. La Ruffa,[41b,41a] C. Lacasta,[174] F. Lacava,[72a,72b] D. P. J. Lack,[100] H. Lacker,[19] D. Lacour,[136] E. Ladygin,[79] R. Lafaye,[5] B. Laforge,[136] T. Lagouri,[33c] S. Lai,[53] S. Lammers,[65] W. Lampl,[7] C. Lampoudis,[162] E. Lançon,[29] U. Landgraf,[52] M. P. J. Landon,[92] M. C. Lanfermann,[54] V. S. Lang,[46] J. C. Lange,[53] R. J. Langenberg,[36] A. J. Lankford,[171] F. Lanni,[29] K. Lantzsch,[24] A. Lanza,[70a] A. Lapertosa,[55b,55a] S. Laplace,[136] J. F. Laporte,[145] T. Lari,[68a] F. Lasagni Manghi,[23b,23a] M. Lassnig,[36] T. S. Lau,[63a] A. Laudrain,[132] A. Laurier,[34] M. Lavorgna,[69a,69b] M. Lazzaroni,[68a,68b] B. Le,[104] E. Le Guirriec,[101] M. LeBlanc,[7] T. LeCompte,[6] F. Ledroit-Guillon,[58] C. A. Lee,[29] G. R. Lee,[17] L. Lee,[59] S. C. Lee,[158] S. J. Lee,[34] B. Lefebvre,[168a] M. Lefebvre,[176] F. Legger,[113] C. Leggett,[18] K. Lehmann,[152] N. Lehmann,[182] G. Lehmann Miotto,[36] W. A. Leight,[46] A. Leisos,[162,jj] M. A. L. Leite,[80d] C. E. Leitgeb,[113] R. Leitner,[143] D. Lellouch,[180,a] K. J. C. Leney,[42] T. Lenz,[24] B. Lenzi,[36] R. Leone,[7] S. Leone,[71a] C. Leonidopoulos,[50] A. Leopold,[136] G. Lerner,[156] C. Leroy,[109] R. Les,[167] C. G. Lester,[32] M. Levchenko,[138] J. Levêque,[5] D. Levin,[105] L. J. Levinson,[180] D. J. Lewis,[21] B. Li,[15b] B. Li,[105] C-Q. Li,[60a] F. Li,[60c] H. Li,[60a] H. Li,[60b] J. Li,[60c] K. Li,[153] L. Li,[60c] M. Li,[15a] Q. Li,[15a,15d] Q. Y. Li,[60a] S. Li,[60d,60c] X. Li,[46] Y. Li,[46] Z. Li,[60b] Z. Liang,[15a] B. Liberti,[73a] A. Liblong,[167] K. Lie,[63c] S. Liem,[119] C. Y. Lin,[32] K. Lin,[106] T. H. Lin,[99] R. A. Linck,[65] J. H. Lindon,[21] A. L. Lionti,[54] E. Lipeles,[137] A. Lipniacka,[17] M. Lisovyi,[61b] T. M. Liss,[173,kk] A. Lister,[175] A. M. Litke,[146] J. D. Little,[8] B. Liu,[78,ll] B. L. Liu,[6] H. B. Liu,[29] H. Liu,[105] J. B. Liu,[60a] J. K. K. Liu,[135] K. Liu,[136] M. Liu,[60a] P. Liu,[18] Y. Liu,[15a,15d] Y. L. Liu,[105] Y. W. Liu,[60a] M. Livan,[70a,70b] A. Lleres,[58] J. Llorente Merino,[15a] S. L. Lloyd,[92] C. Y. Lo,[63b] F. Lo Sterzo,[42] E. M. Lobodzinska,[46] P. Loch,[7] S. Loffredo,[73a,73b] T. Lohse,[19] K. Lohwasser,[149] M. Lokajicek,[141] J. D. Long,[173] R. E. Long,[89] L. Longo,[36] K. A. Looper,[126] J. A. Lopez,[147c] I. Lopez Paz,[100] A. Lopez Solis,[149] J. Lorenz,[113] N. Lorenzo Martinez,[5] M. Losada,[22] P. J. Lösel,[113] A. Lösle,[52] X. Lou,[46] X. Lou,[15a] A. Lounis,[132] J. Love,[6] P. A. Love,[89] J. J. Lozano Bahilo,[174] M. Lu,[60a] Y. J. Lu,[64] H. J. Lubatti,[148] C. Luci,[72a,72b] A. Lucotte,[58] C. Luedtke,[52] F. Luehring,[65] I. Luise,[136] L. Luminari,[72a] B. Lund-Jensen,[154] M. S. Lutz,[102] D. Lynn,[29] R. Lysak,[141] E. Lytken,[96] F. Lyu,[15a] V. Lyubushkin,[79] T. Lyubushkina,[79] H. Ma,[29] L. L. Ma,[60b] Y. Ma,[60b] G. Maccarrone,[51] A. Macchiolo,[114] C. M. Macdonald,[149] J. Machado Miguens,[137] D. Madaffari,[174] R. Madar,[38] W. F. Mader,[48] N. Madysa,[48] J. Maeda,[82] K. Maekawa,[163] S. Maeland,[17] T. Maeno,[29] M. Maerker,[48] A. S. Maevskiy,[112] V. Magerl,[52] N. Magini,[78] D. J. Mahon,[39] C. Maidantchik,[80b] T. Maier,[113] A. Maio,[140a,140b,140d] K. Maj,[84] O. Majersky,[28a] S. Majewski,[131] Y. Makida,[81] N. Makovec,[132] B. Malaescu,[136] Pa. Malecki,[84] V. P. Maleev,[138] F. Malek,[58] U. Mallik,[77] D. Malon,[6] C. Malone,[32] S. Maltezos,[10] S. Malyukov,[79] J. Mamuzic,[174] G. Mancini,[51] I. Mandić,[91] L. Manhaes de Andrade Filho,[80a] I. M. Maniatis,[162]

J. Manjarres Ramos,[48] K. H. Mankinen,[96] A. Mann,[113] A. Manousos,[76] B. Mansoulie,[145] I. Manthos,[162] S. Manzoni,[119] A. Marantis,[162] G. Marceca,[30] L. Marchese,[135] G. Marchiori,[136] M. Marcisovsky,[141] C. Marcon,[96] C. A. Marin Tobon,[36] M. Marjanovic,[38] Z. Marshall,[18] M. U. F. Martensson,[172] S. Marti-Garcia,[174] C. B. Martin,[126] T. A. Martin,[178] V. J. Martin,[50] B. Martin dit Latour,[17] L. Martinelli,[74a,74b] M. Martinez,[14,x] V. I. Martinez Outschoorn,[102] S. Martin-Haugh,[144] V. S. Martoiu,[27b] A. C. Martyniuk,[94] A. Marzin,[36] S. R. Maschek,[114] L. Masetti,[99] T. Mashimo,[163] R. Mashinistov,[110] J. Masik,[100] A. L. Maslennikov,[121b,121a] L. H. Mason,[104] L. Massa,[73a,73b] P. Massarotti,[69a,69b] P. Mastrandrea,[71a,71b] A. Mastroberardino,[41b,41a] T. Masubuchi,[163] A. Matic,[113] P. Mättig,[24] J. Maurer,[27b] B. Maček,[91] D. A. Maximov,[121b,121a] R. Mazini,[158] I. Maznas,[162] S. M. Mazza,[146] S. P. Mc Kee,[105] T. G. McCarthy,[114] L. I. McClymont,[94] W. P. McCormack,[18] E. F. McDonald,[104] J. A. Mcfayden,[36] M. A. McKay,[42] K. D. McLean,[176] S. J. McMahon,[144] P. C. McNamara,[104] C. J. McNicol,[178] R. A. McPherson,[176,q] J. E. Mdhluli,[33c] Z. A. Meadows,[102] S. Meehan,[148] T. Megy,[52] S. Mehlhase,[113] A. Mehta,[90] T. Meideck,[58] B. Meirose,[43] D. Melini,[174] B. R. Mellado Garcia,[33c] J. D. Mellenthin,[53] M. Melo,[28a] F. Meloni,[46] A. Melzer,[24] S. B. Menary,[100] E. D. Mendes Gouveia,[140a,140e] L. Meng,[36] X. T. Meng,[105] S. Menke,[114] E. Meoni,[41b,41a] S. Mergelmeyer,[19] S. A. M. Merkt,[139] C. Merlassino,[20] P. Mermod,[54] L. Merola,[69a,69b] C. Meroni,[68a] O. Meshkov,[112,110] J. K. R. Meshreki,[151] A. Messina,[72a,72b] J. Metcalfe,[6] A. S. Mete,[171] C. Meyer,[65] J. Meyer,[160] J-P. Meyer,[145] H. Meyer Zu Theenhausen,[61a] F. Miano,[156] M. Michetti,[19] R. P. Middleton,[144] L. Mijović,[50] G. Mikenberg,[180] M. Mikestikova,[141] M. Mikuž,[91] H. Mildner,[149] M. Milesi,[104] A. Milic,[167] D. A. Millar,[92] D. W. Miller,[37] A. Milov,[180] D. A. Milstead,[45a,45b] R. A. Mina,[153,gg] A. A. Minaenko,[122] M. Miñano Moya,[174] I. A. Minashvili,[159b] A. I. Mincer,[124] B. Mindur,[83a] M. Mineev,[79] Y. Minegishi,[163] Y. Ming,[181] L. M. Mir,[14] A. Mirto,[67a,67b] K. P. Mistry,[137] T. Mitani,[179] J. Mitrevski,[113] V. A. Mitsou,[174] M. Mittal,[60c] A. Miucci,[20] P. S. Miyagawa,[149] A. Mizukami,[81] J. U. Mjörnmark,[96] T. Mkrtchyan,[184] M. Mlynarikova,[143] T. Moa,[45a,45b] K. Mochizuki,[109] P. Mogg,[52] S. Mohapatra,[39] R. Moles-Valls,[24] M. C. Mondragon,[106] K. Mönig,[46] J. Monk,[40] E. Monnier,[101] A. Montalbano,[152] J. Montejo Berlingen,[36] M. Montella,[94] F. Monticelli,[88] S. Monzani,[68a] N. Morange,[132] D. Moreno,[22] M. Moreno Llácer,[36] C. Moreno Martinez,[14] P. Morettini,[55b] M. Morgenstern,[119] S. Morgenstern,[48] D. Mori,[152] M. Morii,[59] M. Morinaga,[179] V. Morisbak,[134] A. K. Morley,[36] G. Mornacchi,[36] A. P. Morris,[94] L. Morvaj,[155] P. Moschovakos,[36] B. Moser,[119] M. Mosidze,[159b] T. Moskalets,[145] H. J. Moss,[149] J. Moss,[31,mm] K. Motohashi,[165] E. Mountricha,[36] E. J. W. Moyse,[102] S. Muanza,[101] J. Mueller,[139] R. S. P. Mueller,[113] D. Muenstermann,[89] G. A. Mullier,[96] J. L. Munoz Martinez,[14] F. J. Munoz Sanchez,[100] P. Murin,[28b] W. J. Murray,[178,144] A. Murrone,[68a,68b] M. Muškinja,[18] C. Mwewa,[33a] A. G. Myagkov,[122,nn] J. Myers,[131] M. Myska,[142] B. P. Nachman,[18] O. Nackenhorst,[47] A. Nag Nag,[48] K. Nagai,[135] K. Nagano,[81] Y. Nagasaka,[62] M. Nagel,[52] E. Nagy,[101] A. M. Nairz,[36] Y. Nakahama,[116] K. Nakamura,[81] T. Nakamura,[163] I. Nakano,[127] H. Nanjo,[133] F. Napolitano,[61a] R. F. Naranjo Garcia,[46] R. Narayan,[42] D. I. Narrias Villar,[61a] I. Naryshkin,[138] T. Naumann,[46] G. Navarro,[22] H. A. Neal,[105,a] P. Y. Nechaeva,[110] F. Nechansky,[46] T. J. Neep,[21] A. Negri,[70a,70b] M. Negrini,[23b] C. Nellist,[53] M. E. Nelson,[135] S. Nemecek,[141] P. Nemethy,[124] M. Nessi,[36,oo] M. S. Neubauer,[173] M. Neumann,[182] P. R. Newman,[21] Y. S. Ng,[19] Y. W. Y. Ng,[171] H. D. N. Nguyen,[101] T. Nguyen Manh,[109] E. Nibigira,[38] R. B. Nickerson,[135] R. Nicolaidou,[145] D. S. Nielsen,[40] J. Nielsen,[146] N. Nikiforou,[11] V. Nikolaenko,[122,nn] I. Nikolic-Audit,[136] K. Nikolopoulos,[21] P. Nilsson,[29] H. R. Nindhito,[54] Y. Ninomiya,[81] A. Nisati,[72a] N. Nishu,[60c] R. Nisius,[114] I. Nitsche,[47] T. Nitta,[179] T. Nobe,[163] Y. Noguchi,[85] I. Nomidis,[136] M. A. Nomura,[29] M. Nordberg,[36] N. Norjoharuddeen,[135] T. Novak,[91] O. Novgorodova,[48] R. Novotny,[142] L. Nozka,[130] K. Ntekas,[171] E. Nurse,[94] F. G. Oakham,[34,e] H. Oberlack,[114] J. Ocariz,[136] A. Ochi,[82] I. Ochoa,[39] J. P. Ochoa-Ricoux,[147a] K. O'Connor,[26] S. Oda,[87] S. Odaka,[81] S. Oerdek,[53] A. Ogrodnik,[83a] A. Oh,[100] S. H. Oh,[49] C. C. Ohm,[154] H. Oide,[55b,55a] M. L. Ojeda,[167] H. Okawa,[169] Y. Okazaki,[85] Y. Okumura,[163] T. Okuyama,[81] A. Olariu,[27b] L. F. Oleiro Seabra,[140a] S. A. Olivares Pino,[147a] D. Oliveira Damazio,[29] J. L. Oliver,[1] M. J. R. Olsson,[171] A. Olszewski,[84] J. Olszowska,[84] D. C. O'Neil,[152] A. Onofre,[140a,140e] K. Onogi,[116] P. U. E. Onyisi,[11] H. Oppen,[134] M. J. Oreglia,[37] G. E. Orellana,[88] D. Orestano,[74a,74b] N. Orlando,[14] R. S. Orr,[167] V. O'Shea,[57] R. Ospanov,[60a] G. Otero y Garzon,[30] H. Otono,[87] M. Ouchrif,[35d] J. Ouellette,[29] F. Ould-Saada,[134] A. Ouraou,[145] Q. Ouyang,[15a] M. Owen,[57] R. E. Owen,[21] V. E. Ozcan,[12c] N. Ozturk,[8] J. Pacalt,[130] H. A. Pacey,[32] K. Pachal,[49] A. Pacheco Pages,[14] C. Padilla Aranda,[14] S. Pagan Griso,[18] M. Paganini,[183] G. Palacino,[65] S. Palazzo,[50] S. Palestini,[36] M. Palka,[83b] D. Pallin,[38] I. Panagoulias,[10] C. E. Pandini,[36] J. G. Panduro Vazquez,[93] P. Pani,[46] G. Panizzo,[66a,66c] L. Paolozzi,[54] C. Papadatos,[109] K. Papageorgiou,[9,u] A. Paramonov,[6] D. Paredes Hernandez,[63b] S. R. Paredes Saenz,[135] B. Parida,[166] T. H. Park,[167] A. J. Parker,[89] M. A. Parker,[32] F. Parodi,[55b,55a] E. W. Parrish,[120] J. A. Parsons,[39] U. Parzefall,[52] L. Pascual Dominguez,[136] V. R. Pascuzzi,[167] J. M. P. Pasner,[146] E. Pasqualucci,[72a] S. Passaggio,[55b] F. Pastore,[93] P. Pasuwan,[45a,45b] S. Pataraia,[99] J. R. Pater,[100] A. Pathak,[181] T. Pauly,[36] B. Pearson,[114] M. Pedersen,[134] L. Pedraza Diaz,[118]

R. Pedro,[140a] T. Peiffer,[53] S. V. Peleganchuk,[121b,121a] O. Penc,[141] H. Peng,[60a] B. S. Peralva,[80a] M. M. Perego,[132] A. P. Pereira Peixoto,[140a] D. V. Perepelitsa,[29] F. Peri,[19] L. Perini,[68a,68b] H. Pernegger,[36] S. Perrella,[69a,69b] K. Peters,[46] R. F. Y. Peters,[100] B. A. Petersen,[36] T. C. Petersen,[40] E. Petit,[101] A. Petridis,[1] C. Petridou,[162] P. Petroff,[132] M. Petrov,[135] F. Petrucci,[74a,74b] M. Pettee,[183] N. E. Pettersson,[102] K. Petukhova,[143] A. Peyaud,[145] R. Pezoa,[147c] L. Pezzotti,[70a,70b] T. Pham,[104] F. H. Phillips,[106] P. W. Phillips,[144] M. W. Phipps,[173] G. Piacquadio,[155] E. Pianori,[18] A. Picazio,[102] R. H. Pickles,[100] R. Piegaia,[30] D. Pietreanu,[27b] J. E. Pilcher,[37] A. D. Pilkington,[100] M. Pinamonti,[73a,73b] J. L. Pinfold,[3] M. Pitt,[180] L. Pizzimento,[73a,73b] M.-A. Pleier,[29] V. Pleskot,[143] E. Plotnikova,[79] D. Pluth,[78] P. Podberezko,[121b,121a] R. Poettgen,[96] R. Poggi,[54] L. Poggioli,[132] I. Pogrebnyak,[106] D. Pohl,[24] I. Pokharel,[53] G. Polesello,[70a] A. Poley,[18] A. Policicchio,[72a,72b] R. Polifka,[143] A. Polini,[23b] C. S. Pollard,[46] V. Polychronakos,[29] D. Ponomarenko,[111] L. Pontecorvo,[36] S. Popa,[27a] G. A. Popeneciu,[27d] D. M. Portillo Quintero,[58] S. Pospisil,[142] K. Potamianos,[46] I. N. Potrap,[79] C. J. Potter,[32] H. Potti,[11] T. Poulsen,[96] J. Poveda,[36] T. D. Powell,[149] G. Pownall,[46] M. E. Pozo Astigarraga,[36] P. Pralavorio,[101] S. Prell,[78] D. Price,[100] M. Primavera,[67a] S. Prince,[103] M. L. Proffitt,[148] N. Proklova,[111] K. Prokofiev,[63c] F. Prokoshin,[79] S. Protopopescu,[29] J. Proudfoot,[6] M. Przybycien,[83a] D. Pudzha,[138] A. Puri,[173] P. Puzo,[132] J. Qian,[105] Y. Qin,[100] A. Quadt,[53] M. Queitsch-Maitland,[46] A. Qureshi,[1] P. Rados,[104] F. Ragusa,[68a,68b] G. Rahal,[97] J. A. Raine,[54] S. Rajagopalan,[29] A. Ramirez Morales,[92] K. Ran,[15a,15d] T. Rashid,[132] S. Raspopov,[5] M. G. Ratti,[68a,68b] D. M. Rauch,[46] F. Rauscher,[113] S. Rave,[99] B. Ravina,[149] I. Ravinovich,[180] J. H. Rawling,[100] M. Raymond,[36] A. L. Read,[134] N. P. Readioff,[58] M. Reale,[67a,67b] D. M. Rebuzzi,[70a,70b] A. Redelbach,[177] G. Redlinger,[29] K. Reeves,[43] L. Rehnisch,[19] J. Reichert,[137] D. Reikher,[161] A. Reiss,[99] A. Rej,[151] C. Rembser,[36] M. Renda,[27b] M. Rescigno,[72a] S. Resconi,[68a] E. D. Resseguie,[137] S. Rettie,[175] E. Reynolds,[21] O. L. Rezanova,[121b,121a] P. Reznicek,[143] E. Ricci,[75a,75b] R. Richter,[114] S. Richter,[46] E. Richter-Was,[83b] O. Ricken,[24] M. Ridel,[136] P. Rieck,[114] C. J. Riegel,[182] O. Rifki,[46] M. Rijssenbeek,[155] A. Rimoldi,[70a,70b] M. Rimoldi,[46] L. Rinaldi,[23b] G. Ripellino,[154] B. Ristić,[89] E. Ritsch,[36] I. Riu,[14] J. C. Rivera Vergara,[176] F. Rizatdinova,[129] E. Rizvi,[92] C. Rizzi,[36] R. T. Roberts,[100] S. H. Robertson,[103,q] M. Robin,[46] D. Robinson,[32] J. E. M. Robinson,[46] C. M. Robles Gajardo,[147c] A. Robson,[57] E. Rocco,[99] C. Roda,[71a,71b] S. Rodriguez Bosca,[174] A. Rodriguez Perez,[14] D. Rodriguez Rodriguez,[174] A. M. Rodríguez Vera,[168b] S. Roe,[36] O. Røhne,[134] R. Röhrig,[114] C. P. A. Roland,[65] J. Roloff,[59] A. Romaniouk,[111] M. Romano,[23b,23a] N. Rompotis,[90] M. Ronzani,[124] L. Roos,[136] S. Rosati,[72a] K. Rosbach,[52] G. Rosin,[102] B. J. Rosser,[137] E. Rossi,[46] E. Rossi,[74a,74b] E. Rossi,[69a,69b] L. P. Rossi,[55b] L. Rossini,[68a,68b] R. Rosten,[14] M. Rotaru,[27b] J. Rothberg,[148] D. Rousseau,[132] G. Rovelli,[70a,70b] A. Roy,[11] D. Roy,[33c] A. Rozanov,[101] Y. Rozen,[160] X. Ruan,[33c] F. Rubbo,[153] F. Rühr,[52] A. Ruiz-Martinez,[174] A. Rummler,[36] Z. Rurikova,[52] N. A. Rusakovich,[79] H. L. Russell,[103] L. Rustige,[38,47] J. P. Rutherfoord,[7] E. M. Rüttinger,[46,pp] M. Rybar,[39] G. Rybkin,[132] A. Ryzhov,[122] G. F. Rzehorz,[53] P. Sabatini,[53] G. Sabato,[119] S. Sacerdoti,[132] H. F-W. Sadrozinski,[146] R. Sadykov,[79] F. Safai Tehrani,[72a] B. Safarzadeh Samani,[156] P. Saha,[120] S. Saha,[103] M. Sahinsoy,[61a] A. Sahu,[182] M. Saimpert,[46] M. Saito,[163] T. Saito,[163] H. Sakamoto,[163] A. Sakharov,[124,hh] D. Salamani,[54] G. Salamanna,[74a,74b] J. E. Salazar Loyola,[147c] P. H. Sales De Bruin,[172] A. Salnikov,[153] J. Salt,[174] D. Salvatore,[41b,41a] F. Salvatore,[156] A. Salvucci,[63a,63b,63c] A. Salzburger,[36] J. Samarati,[36] D. Sammel,[52] D. Sampsonidis,[162] D. Sampsonidou,[162] J. Sánchez,[174] A. Sanchez Pineda,[66a,66c] H. Sandaker,[134] C. O. Sander,[46] I. G. Sanderswood,[89] M. Sandhoff,[182] C. Sandoval,[22] D. P. C. Sankey,[144] M. Sannino,[55b,55a] Y. Sano,[116] A. Sansoni,[51] C. Santoni,[38] H. Santos,[140a,140b] S. N. Santpur,[18] A. Santra,[174] A. Sapronov,[79] J. G. Saraiva,[140a,140d] O. Sasaki,[81] K. Sato,[169] E. Sauvan,[5] P. Savard,[167,e] N. Savic,[114] R. Sawada,[163] C. Sawyer,[144] L. Sawyer,[95,qq] C. Sbarra,[23b] A. Sbrizzi,[23a] T. Scanlon,[94] J. Schaarschmidt,[148] P. Schacht,[114] B. M. Schachtner,[113] D. Schaefer,[37] L. Schaefer,[137] J. Schaeffer,[99] S. Schaepe,[36] U. Schäfer,[99] A. C. Schaffer,[132] D. Schaile,[113] R. D. Schamberger,[155] N. Scharmberg,[100] V. A. Schegelsky,[138] D. Scheirich,[143] F. Schenck,[19] M. Schernau,[171] C. Schiavi,[55b,55a] S. Schier,[146] L. K. Schildgen,[24] Z. M. Schillaci,[26] E. J. Schioppa,[36] M. Schioppa,[41b,41a] K. E. Schleicher,[52] S. Schlenker,[36] K. R. Schmidt-Sommerfeld,[114] K. Schmieden,[36] C. Schmitt,[99] S. Schmitt,[46] S. Schmitz,[99] J. C. Schmoeckel,[46] U. Schnoor,[52] L. Schoeffel,[145] A. Schoening,[61b] P. G. Scholer,[52] E. Schopf,[135] M. Schott,[99] J. F. P. Schouwenberg,[118] J. Schovancova,[36] S. Schramm,[54] F. Schroeder,[182] A. Schulte,[99] H-C. Schultz-Coulon,[61a] M. Schumacher,[52] B. A. Schumm,[146] Ph. Schune,[145] A. Schwartzman,[153] T. A. Schwarz,[105] Ph. Schwemling,[145] R. Schwienhorst,[106] A. Sciandra,[146] G. Sciolla,[26] M. Scodeggio,[46] M. Scornajenghi,[41b,41a] F. Scuri,[71a] F. Scutti,[104] L. M. Scyboz,[114] C. D. Sebastiani,[72a,72b] P. Seema,[19] S. C. Seidel,[117] A. Seiden,[146] T. Seiss,[37] J. M. Seixas,[80b] G. Sekhniaidze,[69a] K. Sekhon,[105] S. J. Sekula,[42] N. Semprini-Cesari,[23b,23a] S. Sen,[49] S. Senkin,[38] C. Serfon,[76] L. Serin,[132] L. Serkin,[66a,66b] M. Sessa,[60a] H. Severini,[128] T. Šfiligoj,[91] F. Sforza,[170] A. Sfyrla,[54] E. Shabalina,[53] J. D. Shahinian,[146] N. W. Shaikh,[45a,45b] D. Shaked Renous,[180] L. Y. Shan,[15a] R. Shang,[173] J. T. Shank,[25] M. Shapiro,[18] A. Sharma,[135]

A. S. Sharma,[1] P. B. Shatalov,[123] K. Shaw,[156] S. M. Shaw,[100] A. Shcherbakova,[138] Y. Shen,[128] N. Sherafati,[34] A. D. Sherman,[25] P. Sherwood,[94] L. Shi,[158,rr] S. Shimizu,[81] C. O. Shimmin,[183] Y. Shimogama,[179] M. Shimojima,[115] I. P. J. Shipsey,[135] S. Shirabe,[87] M. Shiyakova,[79,ss] J. Shlomi,[180] A. Shmeleva,[110] M. J. Shochet,[37] J. Shojaii,[104] D. R. Shope,[128] S. Shrestha,[126] E. M. Shrif,[33c] E. Shulga,[180] P. Sicho,[141] A. M. Sickles,[173] P. E. Sidebo,[154] E. Sideras Haddad,[33c] O. Sidiropoulou,[36] A. Sidoti,[23b,23a] F. Siegert,[48] Dj. Sijacki,[16] M. Silva Jr.,[181] M. V. Silva Oliveira,[80a] S. B. Silverstein,[45a] S. Simion,[132] E. Simioni,[99] R. Simoniello,[99] S. Simsek,[12b] P. Sinervo,[167] V. Sinetckii,[112,110] N. B. Sinev,[131] M. Sioli,[23b,23a] I. Siral,[105] S. Yu. Sivoklokov,[112] J. Sjölin,[45a,45b] E. Skorda,[96] P. Skubic,[128] M. Slawinska,[84] K. Sliwa,[170] R. Slovak,[143] V. Smakhtin,[180] B. H. Smart,[144] J. Smiesko,[28a] N. Smirnov,[111] S. Yu. Smirnov,[111] Y. Smirnov,[111] L. N. Smirnova,[112,tt] O. Smirnova,[96] J. W. Smith,[53] M. Smizanska,[89] K. Smolek,[142] A. Smykiewicz,[84] A. A. Snesarev,[110] H. L. Snoek,[119] I. M. Snyder,[131] S. Snyder,[29] R. Sobie,[176,q] A. M. Soffa,[171] A. Soffer,[161] A. Søgaard,[50] F. Sohns,[53] C. A. Solans Sanchez,[36] E. Yu. Soldatov,[111] U. Soldevila,[174] A. A. Solodkov,[122] A. Soloshenko,[79] O. V. Solovyanov,[122] V. Solovyev,[138] P. Sommer,[149] H. Son,[170] W. Song,[144] W. Y. Song,[168b] A. Sopczak,[142] F. Sopkova,[28b] C. L. Sotiropoulou,[71a,71b] S. Sottocornola,[70a,70b] R. Soualah,[66a,66c,uu] A. M. Soukharev,[121b,121a] D. South,[46] S. Spagnolo,[67a,67b] M. Spalla,[114] M. Spangenberg,[178] F. Spanò,[93] D. Sperlich,[52] T. M. Spieker,[61a] R. Spighi,[23b] G. Spigo,[36] M. Spina,[156] D. P. Spiteri,[57] M. Spousta,[143] A. Stabile,[68a,68b] B. L. Stamas,[120] R. Stamen,[61a] M. Stamenkovic,[119] E. Stanecka,[84] R. W. Stanek,[6] B. Stanislaus,[135] M. M. Stanitzki,[46] M. Stankaityte,[135] B. Stapf,[119] E. A. Starchenko,[122] G. H. Stark,[146] J. Stark,[58] S. H. Stark,[40] P. Staroba,[141] P. Starovoitov,[61a] S. Stärz,[103] R. Staszewski,[84] G. Stavropoulos,[44] M. Stegler,[46] P. Steinberg,[29] A. L. Steinhebel,[131] B. Stelzer,[152] H. J. Stelzer,[139] O. Stelzer-Chilton,[168a] H. Stenzel,[56] T. J. Stevenson,[156] G. A. Stewart,[36] M. C. Stockton,[36] G. Stoicea,[27b] M. Stolarski,[140a] P. Stolte,[53] S. Stonjek,[114] A. Straessner,[48] J. Strandberg,[154] S. Strandberg,[45a,45b] M. Strauss,[128] P. Strizenec,[28b] R. Ströhmer,[177] D. M. Strom,[131] R. Stroynowski,[42] A. Strubig,[50] S. A. Stucci,[29] B. Stugu,[17] J. Stupak,[128] N. A. Styles,[46] D. Su,[153] S. Suchek,[61a] V. V. Sulin,[110] M. J. Sullivan,[90] D. M. S. Sultan,[54] S. Sultansoy,[4c] T. Sumida,[85] S. Sun,[105] X. Sun,[3] K. Suruliz,[156] C. J. E. Suster,[157] M. R. Sutton,[156] S. Suzuki,[81] M. Svatos,[141] M. Swiatlowski,[37] S. P. Swift,[2] T. Swirski,[177] A. Sydorenko,[99] I. Sykora,[28a] M. Sykora,[143] T. Sykora,[143] D. Ta,[99] K. Tackmann,[46,vv] J. Taenzer,[161] A. Taffard,[171] R. Tafirout,[168a] H. Takai,[29] R. Takashima,[86] K. Takeda,[82] T. Takeshita,[150] E. P. Takeva,[50] Y. Takubo,[81] M. Talby,[101] A. A. Talyshev,[121b,121a] N. M. Tamir,[161] J. Tanaka,[163] M. Tanaka,[165] R. Tanaka,[132] S. Tapia Araya,[173] S. Tapprogge,[99] A. Tarek Abouelfadl Mohamed,[136] S. Tarem,[160] G. Tarna,[27b,ww] G. F. Tartarelli,[68a] P. Tas,[143] M. Tasevsky,[141] T. Tashiro,[85] E. Tassi,[41b,41a] A. Tavares Delgado,[140a,140b] Y. Tayalati,[35e] A. J. Taylor,[50] G. N. Taylor,[104] W. Taylor,[168b] A. S. Tee,[89] R. Teixeira De Lima,[153] P. Teixeira-Dias,[93] H. Ten Kate,[36] J. J. Teoh,[119] S. Terada,[81] K. Terashi,[163] J. Terron,[98] S. Terzo,[14] M. Testa,[51] R. J. Teuscher,[167,q] S. J. Thais,[183] T. Theveneaux-Pelzer,[46] F. Thiele,[40] D. W. Thomas,[93] J. O. Thomas,[42] J. P. Thomas,[21] A. S. Thompson,[57] P. D. Thompson,[21] L. A. Thomsen,[183] E. Thomson,[137] Y. Tian,[39] R. E. Ticse Torres,[53] V. O. Tikhomirov,[110,xx] Yu. A. Tikhonov,[121b,121a] S. Timoshenko,[111] P. Tipton,[183] S. Tisserant,[101] K. Todome,[23b,23a] S. Todorova-Nova,[5] S. Todt,[48] J. Tojo,[87] S. Tokár,[28a] K. Tokushuku,[81] E. Tolley,[126] K. G. Tomiwa,[33c] M. Tomoto,[116] L. Tompkins,[153,gg] B. Tong,[59] P. Tornambe,[102] E. Torrence,[131] H. Torres,[48] E. Torró Pastor,[148] C. Tosciri,[135] J. Toth,[101,yy] D. R. Tovey,[149] A. Traeet,[17] C. J. Treado,[124] T. Trefzger,[177] F. Tresoldi,[156] A. Tricoli,[29] I. M. Trigger,[168a] S. Trincaz-Duvoid,[136] W. Trischuk,[167] B. Trocmé,[58] A. Trofymov,[145] C. Troncon,[68a] M. Trovatelli,[176] F. Trovato,[156] L. Truong,[33b] M. Trzebinski,[84] A. Trzupek,[84] F. Tsai,[46] J. C-L. Tseng,[135] P. V. Tsiareshka,[107,ii] A. Tsirigotis,[162] N. Tsirintanis,[9] V. Tsiskaridze,[155] E. G. Tskhadadze,[159a] M. Tsopoulou,[162] I. I. Tsukerman,[123] V. Tsulaia,[18] S. Tsuno,[81] D. Tsybychev,[155] Y. Tu,[63b] A. Tudorache,[27b] V. Tudorache,[27b] T. T. Tulbure,[27a] A. N. Tuna,[59] S. Turchikhin,[79] D. Turgeman,[180] I. Turk Cakir,[4b,zz] R. J. Turner,[21] R. T. Turra,[68a] P. M. Tuts,[39] S. Tzamarias,[162] E. Tzovara,[99] G. Ucchielli,[47] K. Uchida,[163] I. Ueda,[81] F. Ukegawa,[169] G. Unal,[36] A. Undrus,[29] G. Unel,[171] F. C. Ungaro,[104] Y. Unno,[81] K. Uno,[163] J. Urban,[28b] P. Urquijo,[104] G. Usai,[8] J. Usui,[81] Z. Uysal,[12d] L. Vacavant,[101] V. Vacek,[142] B. Vachon,[103] K. O. H. Vadla,[134] A. Vaidya,[94] C. Valderanis,[113] E. Valdes Santurio,[45a,45b] M. Valente,[54] S. Valentinetti,[23b,23a] A. Valero,[174] L. Valéry,[46] R. A. Vallance,[21] A. Vallier,[36] J. A. Valls Ferrer,[174] T. R. Van Daalen,[14] P. Van Gemmeren,[6] I. Van Vulpen,[119] M. Vanadia,[73a,73b] W. Vandelli,[36] A. Vaniachine,[166] D. Vannicola,[72a,72b] R. Vari,[72a] E. W. Varnes,[7] C. Varni,[55b,55a] T. Varol,[42] D. Varouchas,[132] K. E. Varvell,[157] M. E. Vasile,[27b] G. A. Vasquez,[176] J. G. Vasquez,[183] F. Vazeille,[38] D. Vazquez Furelos,[14] T. Vazquez Schroeder,[36] J. Veatch,[53] V. Vecchio,[74a,74b] M. J. Veen,[119] L. M. Veloce,[167] F. Veloso,[140a,140c] S. Veneziano,[72a] A. Ventura,[67a,67b] N. Venturi,[36] A. Verbytskyi,[114] V. Vercesi,[70a] M. Verducci,[74a,74b] C. M. Vergel Infante,[78] C. Vergis,[24] W. Verkerke,[119] A. T. Vermeulen,[119] J. C. Vermeulen,[119] M. C. Vetterli,[152,e] N. Viaux Maira,[147c] M. Vicente Barreto Pinto,[54] T. Vickey,[149] O. E. Vickey Boeriu,[149]

G. H. A. Viehhauser,[135] L. Vigani,[135] M. Villa,[23b,23a] M. Villaplana Perez,[68a,68b] E. Vilucchi,[51] M. G. Vincter,[34] V. B. Vinogradov,[79] A. Vishwakarma,[46] C. Vittori,[23b,23a] I. Vivarelli,[156] M. Vogel,[182] P. Vokac,[142] S. E. von Buddenbrock,[33c] E. Von Toerne,[24] V. Vorobel,[143] K. Vorobev,[111] M. Vos,[174] J. H. Vossebeld,[90] M. Vozak,[100] N. Vranjes,[16] M. Vranjes Milosavljevic,[16] V. Vrba,[142] M. Vreeswijk,[119] R. Vuillermet,[36] I. Vukotic,[37] P. Wagner,[24] W. Wagner,[182] J. Wagner-Kuhr,[113] S. Wahdan,[182] H. Wahlberg,[88] K. Wakamiya,[82] V. M. Walbrecht,[114] J. Walder,[89] R. Walker,[113] S. D. Walker,[93] W. Walkowiak,[151] V. Wallangen,[45a,45b] A. M. Wang,[59] C. Wang,[60b] F. Wang,[181] H. Wang,[18] H. Wang,[3] J. Wang,[157] J. Wang,[61b] P. Wang,[42] Q. Wang,[128] R.-J. Wang,[99] R. Wang,[60a] R. Wang,[6] S. M. Wang,[158] W. T. Wang,[60a] W. Wang,[15c,aaa] W. X. Wang,[60a,aaa] Y. Wang,[60a,bbb] Z. Wang,[60c] C. Wanotayaroj,[46] A. Warburton,[103] C. P. Ward,[32] D. R. Wardrope,[94] N. Warrack,[57] A. Washbrook,[50] A. T. Watson,[21] M. F. Watson,[21] G. Watts,[148] B. M. Waugh,[94] A. F. Webb,[11] S. Webb,[99] C. Weber,[183] M. S. Weber,[20] S. A. Weber,[34] S. M. Weber,[61a] A. R. Weidberg,[135] J. Weingarten,[47] M. Weirich,[99] C. Weiser,[52] P. S. Wells,[36] T. Wenaus,[29] T. Wengler,[36] S. Wenig,[36] N. Wermes,[24] M. D. Werner,[78] M. Wessels,[61a] T. D. Weston,[20] K. Whalen,[131] N. L. Whallon,[148] A. M. Wharton,[89] A. S. White,[105] A. White,[8] M. J. White,[1] D. Whiteson,[171] B. W. Whitmore,[89] F. J. Wickens,[144] W. Wiedenmann,[181] M. Wielers,[144] N. Wieseotte,[99] C. Wiglesworth,[40] L. A. M. Wiik-Fuchs,[52] F. Wilk,[100] H. G. Wilkens,[36] L. J. Wilkins,[93] H. H. Williams,[137] S. Williams,[32] C. Willis,[106] S. Willocq,[102] J. A. Wilson,[21] I. Wingerter-Seez,[5] E. Winkels,[156] F. Winklmeier,[131] O. J. Winston,[156] B. T. Winter,[52] M. Wittgen,[153] M. Wobisch,[95] A. Wolf,[99] T. M. H. Wolf,[119] R. Wolff,[101] R. W. Wölker,[135] J. Wollrath,[52] M. W. Wolter,[84] H. Wolters,[140a,140c] V. W. S. Wong,[175] N. L. Woods,[146] S. D. Worm,[21] B. K. Wosiek,[84] K. W. Woźniak,[84] K. Wraight,[57] S. L. Wu,[181] X. Wu,[54] Y. Wu,[60a] T. R. Wyatt,[100] B. M. Wynne,[50] S. Xella,[40] Z. Xi,[105] L. Xia,[178] D. Xu,[15a] H. Xu,[60a,ww] L. Xu,[29] T. Xu,[145] W. Xu,[105] Z. Xu,[60b] Z. Xu,[153] B. Yabsley,[157] S. Yacoob,[33a] K. Yajima,[133] D. P. Yallup,[94] D. Yamaguchi,[165] Y. Yamaguchi,[165] A. Yamamoto,[81] T. Yamanaka,[163] F. Yamane,[82] M. Yamatani,[163] T. Yamazaki,[163] Y. Yamazaki,[82] Z. Yan,[25] H. J. Yang,[60c,60d] H. T. Yang,[18] S. Yang,[77] X. Yang,[60b,58] Y. Yang,[163] W-M. Yao,[18] Y. C. Yap,[46] Y. Yasu,[81] E. Yatsenko,[60c,60d] J. Ye,[42] S. Ye,[29] I. Yeletskikh,[79] M. R. Yexley,[89] E. Yigitbasi,[25] K. Yorita,[179] K. Yoshihara,[137] C. J. S. Young,[36] C. Young,[153] J. Yu,[78] R. Yuan,[60b,ccc] X. Yue,[61a] S. P. Y. Yuen,[24] B. Zabinski,[84] G. Zacharis,[10] E. Zaffaroni,[54] J. Zahreddine,[136] A. M. Zaitsev,[122,nn] T. Zakareishvili,[159b] N. Zakharchuk,[34] S. Zambito,[59] D. Zanzi,[36] D. R. Zaripovas,[57] S. V. Zeißner,[47] C. Zeitnitz,[182] G. Zemaityte,[135] J. C. Zeng,[173] O. Zenin,[122] T. Ženiš,[28a] D. Zerwas,[132] M. Zgubič,[135] D. F. Zhang,[15b] F. Zhang,[181] G. Zhang,[60a] G. Zhang,[15b] H. Zhang,[15c] J. Zhang,[6] L. Zhang,[15c] L. Zhang,[60a] M. Zhang,[173] R. Zhang,[60a] R. Zhang,[24] X. Zhang,[60b] Y. Zhang,[15a,15d] Z. Zhang,[63a] Z. Zhang,[132] P. Zhao,[49] Y. Zhao,[60b] Z. Zhao,[60a] A. Zhemchugov,[79] Z. Zheng,[105] D. Zhong,[173] B. Zhou,[105] C. Zhou,[181] M. S. Zhou,[15a,15d] M. Zhou,[155] N. Zhou,[60c] Y. Zhou,[7] C. G. Zhu,[60b] H. L. Zhu,[60a] H. Zhu,[15a] J. Zhu,[105] Y. Zhu,[60a] X. Zhuang,[15a] K. Zhukov,[110] V. Zhulanov,[121b,121a] D. Zieminska,[65] N. I. Zimine,[79] S. Zimmermann,[52] Z. Zinonos,[114] M. Ziolkowski,[151] L. Živković,[16] G. Zobernig,[181] A. Zoccoli,[23b,23a] K. Zoch,[53] T. G. Zorbas,[149] R. Zou,[37] and L. Zwalinski[36]

(ATLAS Collaboration)

[1]*Department of Physics, University of Adelaide, Adelaide, Australia*
[2]*Physics Department, SUNY Albany, Albany, New York, USA*
[3]*Department of Physics, University of Alberta, Edmonton, Alberta, Canada*
[4a]*Department of Physics, Ankara University, Ankara, Turkey*
[4b]*Istanbul Aydin University, Istanbul, Turkey*
[4c]*Division of Physics, TOBB University of Economics and Technology, Ankara, Turkey*
[5]*LAPP, Université Grenoble Alpes, Université Savoie Mont Blanc, CNRS/IN2P3, Annecy, France*
[6]*High Energy Physics Division, Argonne National Laboratory, Argonne, Illinois, USA*
[7]*Department of Physics, University of Arizona, Tucson, Arizona, USA*
[8]*Department of Physics, University of Texas at Arlington, Arlington, Texas, USA*
[9]*Physics Department, National and Kapodistrian University of Athens, Athens, Greece*
[10]*Physics Department, National Technical University of Athens, Zografou, Greece*
[11]*Department of Physics, University of Texas at Austin, Austin, Texas, USA*
[12a]*Bahcesehir University, Faculty of Engineering and Natural Sciences, Istanbul, Turkey*
[12b]*Istanbul Bilgi University, Faculty of Engineering and Natural Sciences, Istanbul, Turkey*
[12c]*Department of Physics, Bogazici University, Istanbul, Turkey*
[12d]*Department of Physics Engineering, Gaziantep University, Gaziantep, Turkey*
[13]*Institute of Physics, Azerbaijan Academy of Sciences, Baku, Azerbaijan*

[14]*Institut de Física d'Altes Energies (IFAE), Barcelona Institute of Science and Technology, Barcelona, Spain*

[15a]*Institute of High Energy Physics, Chinese Academy of Sciences, Beijing, China*

[15b]*Physics Department, Tsinghua University, Beijing, China*

[15c]*Department of Physics, Nanjing University, Nanjing, China*

[15d]*University of Chinese Academy of Science (UCAS), Beijing, China*

[16]*Institute of Physics, University of Belgrade, Belgrade, Serbia*

[17]*Department for Physics and Technology, University of Bergen, Bergen, Norway*

[18]*Physics Division, Lawrence Berkeley National Laboratory and University of California, Berkeley, California, USA*

[19]*Institut für Physik, Humboldt Universität zu Berlin, Berlin, Germany*

[20]*Albert Einstein Center for Fundamental Physics and Laboratory for High Energy Physics, University of Bern, Bern, Switzerland*

[21]*School of Physics and Astronomy, University of Birmingham, Birmingham, United Kingdom*

[22]*Facultad de Ciencias y Centro de Investigaciónes, Universidad Antonio Nariño, Bogota, Colombia*

[23a]*INFN Bologna and Universita' di Bologna, Dipartimento di Fisica, Italy*

[23b]*INFN Sezione di Bologna, Italy*

[24]*Physikalisches Institut, Universität Bonn, Bonn, Germany*

[25]*Department of Physics, Boston University, Boston, Massachusetts, USA*

[26]*Department of Physics, Brandeis University, Waltham, Massachusetts, USA*

[27a]*Transilvania University of Brasov, Brasov, Romania*

[27b]*Horia Hulubei National Institute of Physics and Nuclear Engineering, Bucharest, Romania*

[27c]*Department of Physics, Alexandru Ioan Cuza University of Iasi, Iasi, Romania*

[27d]*National Institute for Research and Development of Isotopic and Molecular Technologies, Physics Department, Cluj-Napoca, Romania*

[27e]*University Politehnica Bucharest, Bucharest, Romania*

[27f]*West University in Timisoara, Timisoara, Romania*

[28a]*Faculty of Mathematics, Physics and Informatics, Comenius University, Bratislava, Slovak Republic*

[28b]*Department of Subnuclear Physics, Institute of Experimental Physics of the Slovak Academy of Sciences, Kosice, Slovak Republic*

[29]*Physics Department, Brookhaven National Laboratory, Upton, New York, USA*

[30]*Departamento de Física, Universidad de Buenos Aires, Buenos Aires, Argentina*

[31]*California State University, California, USA*

[32]*Cavendish Laboratory, University of Cambridge, Cambridge, United Kingdom*

[33a]*Department of Physics, University of Cape Town, Cape Town, South Africa*

[33b]*Department of Mechanical Engineering Science, University of Johannesburg, Johannesburg, South Africa*

[33c]*School of Physics, University of the Witwatersrand, Johannesburg, South Africa*

[34]*Department of Physics, Carleton University, Ottawa, Ontario, Canada*

[35a]*Faculté des Sciences Ain Chock, Réseau Universitaire de Physique des Hautes Energies—Université Hassan II, Casablanca, Morocco*

[35b]*Faculté des Sciences, Université Ibn-Tofail, Kénitra, Morocco*

[35c]*Faculté des Sciences Semlalia, Université Cadi Ayyad, LPHEA-Marrakech, Morocco*

[35d]*Faculté des Sciences, Université Mohamed Premier and LPTPM, Oujda, Morocco*

[35e]*Faculté des sciences, Université Mohammed V, Rabat, Morocco*

[36]*CERN, Geneva, Switzerland*

[37]*Enrico Fermi Institute, University of Chicago, Chicago, Illinois, USA*

[38]*LPC, Université Clermont Auvergne, CNRS/IN2P3, Clermont-Ferrand, France*

[39]*Nevis Laboratory, Columbia University, Irvington, New York, USA*

[40]*Niels Bohr Institute, University of Copenhagen, Copenhagen, Denmark*

[41a]*Dipartimento di Fisica, Università della Calabria, Rende, Italy*

[41b]*INFN Gruppo Collegato di Cosenza, Laboratori Nazionali di Frascati, Italy*

[42]*Physics Department, Southern Methodist University, Dallas, Texas, USA*

[43]*Physics Department, University of Texas at Dallas, Richardson, Texas, USA*

[44]*National Centre for Scientific Research "Demokritos", Agia Paraskevi, Greece*

[45a]*Department of Physics, Stockholm University, Sweden*

[45b]*Oskar Klein Centre, Stockholm, Sweden*

[46]*Deutsches Elektronen-Synchrotron DESY, Hamburg and Zeuthen, Germany*

[47]*Lehrstuhl für Experimentelle Physik IV, Technische Universität Dortmund, Dortmund, Germany*

[48]*Institut für Kern- und Teilchenphysik, Technische Universität Dresden, Dresden, Germany*

[49]Department of Physics, Duke University, Durham, North Carolina, USA
[50]SUPA—School of Physics and Astronomy, University of Edinburgh, Edinburgh, United Kingdom
[51]INFN e Laboratori Nazionali di Frascati, Frascati, Italy
[52]Physikalisches Institut, Albert-Ludwigs-Universität Freiburg, Freiburg, Germany
[53]II. Physikalisches Institut, Georg-August-Universität Göttingen, Göttingen, Germany
[54]Département de Physique Nucléaire et Corpusculaire, Université de Genève, Genève, Switzerland
[55a]Dipartimento di Fisica, Università di Genova, Genova, Italy
[55b]INFN Sezione di Genova, Italy
[56]II. Physikalisches Institut, Justus-Liebig-Universität Giessen, Giessen, Germany
[57]SUPA—School of Physics and Astronomy, University of Glasgow, Glasgow, United Kingdom
[58]LPSC, Université Grenoble Alpes, CNRS/IN2P3, Grenoble INP, Grenoble, France
[59]Laboratory for Particle Physics and Cosmology, Harvard University, Cambridge, Massachusetts, USA
[60a]Department of Modern Physics and State Key Laboratory of Particle Detection and Electronics,
University of Science and Technology of China, Hefei, China
[60b]Institute of Frontier and Interdisciplinary Science and Key Laboratory of Particle Physics and Particle
Irradiation (MOE), Shandong University, Qingdao, China
[60c]School of Physics and Astronomy, Shanghai Jiao Tong University,
KLPPAC-MoE, SKLPPC, Shanghai, China
[60d]Tsung-Dao Lee Institute, Shanghai, China
[61a]Kirchhoff-Institut für Physik, Ruprecht-Karls-Universität Heidelberg, Heidelberg, Germany
[61b]Physikalisches Institut, Ruprecht-Karls-Universität Heidelberg, Heidelberg, Germany
[62]Faculty of Applied Information Science, Hiroshima Institute of Technology, Hiroshima, Japan
[63a]Department of Physics, Chinese University of Hong Kong, Shatin, New Territories, Hong Kong, China
[63b]Department of Physics, University of Hong Kong, Hong Kong, China
[63c]Department of Physics and Institute for Advanced Study, Hong Kong University of Science and
Technology, Clear Water Bay, Kowloon, Hong Kong, China
[64]Department of Physics, National Tsing Hua University, Hsinchu, Taiwan
[65]Department of Physics, Indiana University, Bloomington, Indiana, USA
[66a]INFN Gruppo Collegato di Udine, Sezione di Trieste, Udine, Italy
[66b]ICTP, Trieste, Italy
[66c]Dipartimento Politecnico di Ingegneria e Architettura, Università di Udine, Udine, Italy
[67a]INFN Sezione di Lecce, Italy
[67b]Dipartimento di Matematica e Fisica, Università del Salento, Lecce, Italy
[68a]INFN Sezione di Milano, Italy
[68b]Dipartimento di Fisica, Università di Milano, Milano, Italy
[69a]INFN Sezione di Napoli, Italy
[69b]Dipartimento di Fisica, Università di Napoli, Napoli, Italy
[70a]INFN Sezione di Pavia, Italy
[70b]Dipartimento di Fisica, Università di Pavia, Pavia, Italy
[71a]INFN Sezione di Pisa, Italy
[71b]Dipartimento di Fisica E. Fermi, Università di Pisa, Pisa, Italy
[72a]INFN Sezione di Roma, Italy
[72b]Dipartimento di Fisica, Sapienza Università di Roma, Roma, Italy
[73a]INFN Sezione di Roma Tor Vergata, Italy
[73b]Dipartimento di Fisica, Università di Roma Tor Vergata, Roma, Italy
[74a]INFN Sezione di Roma Tre, Italy
[74b]Dipartimento di Matematica e Fisica, Università Roma Tre, Roma, Italy
[75a]INFN-TIFPA, Italy
[75b]Università degli Studi di Trento, Trento, Italy
[76]Institut für Astro- und Teilchenphysik, Leopold-Franzens-Universität, Innsbruck, Austria
[77]University of Iowa, Iowa City, Iowa, USA
[78]Department of Physics and Astronomy, Iowa State University, Ames, Iowa, USA
[79]Joint Institute for Nuclear Research, Dubna, Russia
[80a]Departamento de Engenharia Elétrica, Universidade Federal de Juiz de Fora (UFJF),
Juiz de Fora, Brazil
[80b]Universidade Federal do Rio De Janeiro COPPE/EE/IF, Rio de Janeiro, Brazil
[80c]Universidade Federal de São João del Rei (UFSJ), São João del Rei, Brazil
[80d]Instituto de Física, Universidade de São Paulo, São Paulo, Brazil
[81]KEK, High Energy Accelerator Research Organization, Tsukuba, Japan
[82]Graduate School of Science, Kobe University, Kobe, Japan

[83a]*AGH University of Science and Technology, Faculty of Physics and Applied Computer Science, Krakow, Poland*

[83b]*Marian Smoluchowski Institute of Physics, Jagiellonian University, Krakow, Poland*

[84]*Institute of Nuclear Physics Polish Academy of Sciences, Krakow, Poland*

[85]*Faculty of Science, Kyoto University, Kyoto, Japan*

[86]*Kyoto University of Education, Kyoto, Japan*

[87]*Research Center for Advanced Particle Physics and Department of Physics, Kyushu University, Fukuoka, Japan*

[88]*Instituto de Física La Plata, Universidad Nacional de La Plata and CONICET, La Plata, Argentina*

[89]*Physics Department, Lancaster University, Lancaster, United Kingdom*

[90]*Oliver Lodge Laboratory, University of Liverpool, Liverpool, United Kingdom*

[91]*Department of Experimental Particle Physics, Jožef Stefan Institute and Department of Physics, University of Ljubljana, Ljubljana, Slovenia*

[92]*School of Physics and Astronomy, Queen Mary University of London, London, United Kingdom*

[93]*Department of Physics, Royal Holloway University of London, Egham, United Kingdom*

[94]*Department of Physics and Astronomy, University College London, London, United Kingdom*

[95]*Louisiana Tech University, Ruston, Louisiana, USA*

[96]*Fysiska institutionen, Lunds universitet, Lund, Sweden*

[97]*Centre de Calcul de l'Institut National de Physique Nucléaire et de Physique des Particules (IN2P3), Villeurbanne, France*

[98]*Departamento de Física Teorica C-15 and CIAFF, Universidad Autónoma de Madrid, Madrid, Spain*

[99]*Institut für Physik, Universität Mainz, Mainz, Germany*

[100]*School of Physics and Astronomy, University of Manchester, Manchester, United Kingdom*

[101]*CPPM, Aix-Marseille Université, CNRS/IN2P3, Marseille, France*

[102]*Department of Physics, University of Massachusetts, Amherst, Massachusetts, USA*

[103]*Department of Physics, McGill University, Montreal, Québec, Canada*

[104]*School of Physics, University of Melbourne, Victoria, Australia*

[105]*Department of Physics, University of Michigan, Ann Arbor, Michigan, USA*

[106]*Department of Physics and Astronomy, Michigan State University, East Lansing, Michigan, USA*

[107]*B.I. Stepanov Institute of Physics, National Academy of Sciences of Belarus, Minsk, Belarus*

[108]*Research Institute for Nuclear Problems of Byelorussian State University, Minsk, Belarus*

[109]*Group of Particle Physics, University of Montreal, Montreal, Québec, Canada*

[110]*P.N. Lebedev Physical Institute of the Russian Academy of Sciences, Moscow, Russia*

[111]*National Research Nuclear University MEPhI, Moscow, Russia*

[112]*D.V. Skobeltsyn Institute of Nuclear Physics, M.V. Lomonosov Moscow State University, Moscow, Russia*

[113]*Fakultät für Physik, Ludwig-Maximilians-Universität München, München, Germany*

[114]*Max-Planck-Institut für Physik (Werner-Heisenberg-Institut), München, Germany*

[115]*Nagasaki Institute of Applied Science, Nagasaki, Japan*

[116]*Graduate School of Science and Kobayashi-Maskawa Institute, Nagoya University, Nagoya, Japan*

[117]*Department of Physics and Astronomy, University of New Mexico, Albuquerque, New Mexico, USA*

[118]*Institute for Mathematics, Astrophysics and Particle Physics, Radboud University Nijmegen/Nikhef, Nijmegen, Netherlands*

[119]*Nikhef National Institute for Subatomic Physics and University of Amsterdam, Amsterdam, Netherlands*

[120]*Department of Physics, Northern Illinois University, DeKalb, Illinois, USA*

[121a]*Budker Institute of Nuclear Physics and NSU, SB RAS, Novosibirsk, Russia*

[121b]*Novosibirsk State University Novosibirsk, Russia*

[122]*Institute for High Energy Physics of the National Research Centre Kurchatov Institute, Protvino, Russia*

[123]*Institute for Theoretical and Experimental Physics named by A.I. Alikhanov of National Research Centre "Kurchatov Institute", Moscow, Russia*

[124]*Department of Physics, New York University, New York, New York, USA*

[125]*Ochanomizu University, Otsuka, Bunkyo-ku, Tokyo, Japan*

[126]*Ohio State University, Columbus, Ohio, USA*

[127]*Faculty of Science, Okayama University, Okayama, Japan*

[128]*Homer L. Dodge Department of Physics and Astronomy, University of Oklahoma, Norman, Oklahoma, USA*

[129]*Department of Physics, Oklahoma State University, Stillwater, Oklahoma, USA*

[130]*Palacký University, RCPTM, Joint Laboratory of Optics, Olomouc, Czech Republic*

[131]*Center for High Energy Physics, University of Oregon, Eugene, Oregon, USA*

[132]*LAL, Université Paris-Sud, CNRS/IN2P3, Université Paris-Saclay, Orsay, France*

[133]*Graduate School of Science, Osaka University, Osaka, Japan*
[134]*Department of Physics, University of Oslo, Oslo, Norway*
[135]*Department of Physics, Oxford University, Oxford, United Kingdom*
[136]*LPNHE, Sorbonne Université, Université de Paris, CNRS/IN2P3, Paris, France*
[137]*Department of Physics, University of Pennsylvania, Philadelphia, Pennsylvania, USA*
[138]*Konstantinov Nuclear Physics Institute of National Research Centre "Kurchatov Institute",*
PNPI, St. Petersburg, Russia
[139]*Department of Physics and Astronomy, University of Pittsburgh, Pittsburgh, Pennsylvania, USA*
[140a]*Laboratório de Instrumentação e Física Experimental de Partículas—LIP, Lisboa, Portugal*
[140b]*Departamento de Física, Faculdade de Ciências, Universidade de Lisboa, Lisboa, Portugal*
[140c]*Departamento de Física, Universidade de Coimbra, Coimbra, Portugal*
[140d]*Centro de Física Nuclear da Universidade de Lisboa, Lisboa, Portugal*
[140e]*Departamento de Física, Universidade do Minho, Braga, Portugal*
[140f]*Departamento de Física Teórica y del Cosmos, Universidad de Granada, Granada (Spain), Spain*
[140g]*Dep Física and CEFITEC of Faculdade de Ciências e Tecnologia,*
Universidade Nova de Lisboa, Caparica, Portugal
[140h]*Instituto Superior Técnico, Universidade de Lisboa, Lisboa, Portugal*
[141]*Institute of Physics of the Czech Academy of Sciences, Prague, Czech Republic*
[142]*Czech Technical University in Prague, Prague, Czech Republic*
[143]*Charles University, Faculty of Mathematics and Physics, Prague, Czech Republic*
[144]*Particle Physics Department, Rutherford Appleton Laboratory, Didcot, United Kingdom*
[145]*IRFU, CEA, Université Paris-Saclay, Gif-sur-Yvette, France*
[146]*Santa Cruz Institute for Particle Physics, University of California Santa Cruz,*
Santa Cruz, California, USA
[147a]*Departamento de Física, Pontificia Universidad Católica de Chile, Santiago, Chile*
[147b]*Universidad Andres Bello, Department of Physics, Santiago, Chile*
[147c]*Departamento de Física, Universidad Técnica Federico Santa María, Valparaíso, Chile*
[148]*Department of Physics, University of Washington, Seattle, Washington, USA*
[149]*Department of Physics and Astronomy, University of Sheffield, Sheffield, United Kingdom*
[150]*Department of Physics, Shinshu University, Nagano, Japan*
[151]*Department Physik, Universität Siegen, Siegen, Germany*
[152]*Department of Physics, Simon Fraser University, Burnaby, British Columbia, Canada*
[153]*SLAC National Accelerator Laboratory, Stanford, California, USA*
[154]*Physics Department, Royal Institute of Technology, Stockholm, Sweden*
[155]*Departments of Physics and Astronomy, Stony Brook University, Stony Brook, New York, USA*
[156]*Department of Physics and Astronomy, University of Sussex, Brighton, United Kingdom*
[157]*School of Physics, University of Sydney, Sydney, Australia*
[158]*Institute of Physics, Academia Sinica, Taipei, Taiwan*
[159a]*E. Andronikashvili Institute of Physics, Iv. Javakhishvili Tbilisi State University, Tbilisi, Georgia*
[159b]*High Energy Physics Institute, Tbilisi State University, Tbilisi, Georgia*
[160]*Department of Physics, Technion, Israel Institute of Technology, Haifa, Israel*
[161]*Raymond and Beverly Sackler School of Physics and Astronomy, Tel Aviv University, Tel Aviv, Israel*
[162]*Department of Physics, Aristotle University of Thessaloniki, Thessaloniki, Greece*
[163]*International Center for Elementary Particle Physics and Department of Physics,*
University of Tokyo, Tokyo, Japan
[164]*Graduate School of Science and Technology, Tokyo Metropolitan University, Tokyo, Japan*
[165]*Department of Physics, Tokyo Institute of Technology, Tokyo, Japan*
[166]*Tomsk State University, Tomsk, Russia*
[167]*Department of Physics, University of Toronto, Toronto, Ontario, Canada*
[168a]*TRIUMF, Vancouver, British Columbia, Canada*
[168b]*Department of Physics and Astronomy, York University, Toronto, Ontario, Canada*
[169]*Division of Physics and Tomonaga Center for the History of the Universe, Faculty of Pure and Applied*
Sciences, University of Tsukuba, Tsukuba, Japan
[170]*Department of Physics and Astronomy, Tufts University, Medford, Massachusetts, USA*
[171]*Department of Physics and Astronomy, University of California Irvine, Irvine, California, USA*
[172]*Department of Physics and Astronomy, University of Uppsala, Uppsala, Sweden*
[173]*Department of Physics, University of Illinois, Urbana, Illinois, USA*
[174]*Instituto de Física Corpuscular (IFIC), Centro Mixto Universidad de Valencia—CSIC, Valencia, Spain*
[175]*Department of Physics, University of British Columbia, Vancouver, British Columbia, Canada*
[176]*Department of Physics and Astronomy, University of Victoria, Victoria, British Columbia, Canada*

[177]Fakultät für Physik und Astronomie, Julius-Maximilians-Universität Würzburg, Würzburg, Germany
[178]Department of Physics, University of Warwick, Coventry, United Kingdom
[179]Waseda University, Tokyo, Japan
[180]Department of Particle Physics, Weizmann Institute of Science, Rehovot, Israel
[181]Department of Physics, University of Wisconsin, Madison, Wisconsin, USA
[182]Fakultät für Mathematik und Naturwissenschaften, Fachgruppe Physik,
Bergische Universität Wuppertal, Wuppertal, Germany
[183]Department of Physics, Yale University, New Haven, Connecticut, USA
[184]Yerevan Physics Institute, Yerevan, Armenia

[a]Deceased.
[b]Also at Department of Physics, King's College London, London, United Kingdom.
[c]Also at Istanbul University, Dept. of Physics, Istanbul, Turkey.
[d]Also at Instituto de Fisica Teorica, IFT-UAM/CSIC, Madrid, Spain.
[e]Also at TRIUMF, Vancouver, Brirish Columbia, Canada.
[f]Also at Department of Physics and Astronomy, University of Louisville, Louisville, Kentucky, USA.
[g]Also at Physics Department, An-Najah National University, Nablus, Palestine.
[h]Also at Department of Physics, California State University, Fresno, USA.
[i]Also at Department of Physics, University of Fribourg, Fribourg, Switzerland.
[j]Also at Physics Dept, University of South Africa, Pretoria, South Africa.
[k]Also at Departament de Fisica de la Universitat Autonoma de Barcelona, Barcelona, Spain.
[l]Also at Tomsk State University, Tomsk, and Moscow Institute of Physics and Technology State University, Dolgoprudny, Russia.
[m]Also at The Collaborative Innovation Center of Quantum Matter (CICQM), Beijing, China.
[n]Also at Department of Physics, Ben Gurion University of the Negev, Beer Sheva, Israel.
[o]Also at Departamento de Física, Instituto Superior Técnico, Universidade de Lisboa, Lisboa, Portugal.
[p]Also at Universita di Napoli Parthenope, Napoli, Italy.
[q]Also at Institute of Particle Physics (IPP), Vancouver, Canada.
[r]Also at Department of Physics, University of Adelaide, Adelaide, Australia.
[s]Also at Department of Physics, St. Petersburg State Polytechnical University, St. Petersburg, Russia.
[t]Also at Borough of Manhattan Community College, City University of New York, New York, New York, USA.
[u]Also at Department of Financial and Management Engineering, University of the Aegean, Chios, Greece.
[v]Also at Centre for High Performance Computing, CSIR Campus, Rosebank, Cape Town, South Africa.
[w]Also at Department of Physics, California State University, East Bay, USA.
[x]Also at Institucio Catalana de Recerca i Estudis Avancats, ICREA, Barcelona, Spain.
[y]Also at Department of Physics, University of Michigan, Ann Arbor, Michigan, USA.
[z]Also at LAL, Université Paris-Sud, CNRS/IN2P3, Université Paris-Saclay, Orsay, France.
[aa]Also at Graduate School of Science, Osaka University, Osaka, Japan.
[bb]Also at Physikalisches Institut, Albert-Ludwigs-Universität Freiburg, Freiburg, Germany.
[cc]Also at Institute of Physics, Azerbaijan Academy of Sciences, Baku, Azerbaijan.
[dd]Also at Institute for Mathematics, Astrophysics and Particle Physics, Radboud University Nijmegen/Nikhef, Nijmegen, Netherlands.
[ee]Also at Institute of Theoretical Physics, Ilia State University, Tbilisi, Georgia.
[ff]Also at CERN, Geneva, Switzerland.
[gg]Also at Department of Physics, Stanford University, Stanford, California, USA.
[hh]Also at Manhattan College, New York, New York, USA.
[ii]Also at Joint Institute for Nuclear Research, Dubna, Russia.
[jj]Also at Hellenic Open University, Patras, Greece.
[kk]Also at The City College of New York, New York, New York, USA.
[ll]Also at Institute of High Energy Physics, Chinese Academy of Sciences, Beijing, China.
[mm]Also at Department of Physics, California State University, Sacramento, USA.
[nn]Also at Moscow Institute of Physics and Technology State University, Dolgoprudny, Russia.
[oo]Also at Département de Physique Nucléaire et Corpusculaire, Université de Genève, Genève, Switzerland.
[pp]Also at Department of Physics and Astronomy, University of Sheffield, Sheffield, United Kingdom.
[qq]Also at Louisiana Tech University, Ruston, Los Angeles, USA.
[rr]Also at School of Physics, Sun Yat-sen University, Guangzhou, China.
[ss]Also at Institute for Nuclear Research and Nuclear Energy (INRNE) of the Bulgarian Academy of Sciences, Sofia, Bulgaria.
[tt]Also at Faculty of Physics, M.V. Lomonosov Moscow State University, Moscow, Russia.
[uu]Also at Department of Applied Physics and Astronomy, University of Sharjah, Sharjah, United Arab Emirates.
[vv]Also at Institut für Experimentalphysik, Universität Hamburg, Hamburg, Germany.
[ww]Also at CPPM, Aix-Marseille Université, CNRS/IN2P3, Marseille, France.

[xx]Also at National Research Nuclear University MEPhI, Moscow, Russia.

[yy]Also at Institute for Particle and Nuclear Physics, Wigner Research Centre for Physics, Budapest, Hungary.

[zz]Also at Giresun University, Faculty of Engineering, Giresun, Turkey.

[aaa]Also at Institute of Physics, Academia Sinica, Taipei, Taiwan.

[bbb]Also at LPNHE, Sorbonne Université, Université de Paris, CNRS/IN2P3, Paris, France.

[ccc]Also at Department of Physics and Astronomy, Michigan State University, East Lansing, Michigan, USA.